ION TRANSPORT BEHAVIOR OF POLYPYRROLE DURING REDOX SWITCHING

By

MYOUNGHO PYO

A DISSERTATION PRESENTED TO THE GRADUATE SCHOOL
OF THE UNIVERSITY OF FLORIDA IN PARTIAL FULFILLMENT
OF THE REQUIREMENTS FOR THE DEGREE OF
DOCTOR OF PHILOSOPHY

UNIVERSITY OF FLORIDA

1994

I dedicate this work and dissertation to my family, who have given me continuous, unconditional support.

ACKNOWLEDGMENTS

I would like to thank sincerely my research advisor, Dr. John R. Reynolds, for his encouragement and support. He has been a tremendous source of knowledge and ideas while at the same time encouraging the development of individual ideas and solutions to scientific problems. He has always been there to provide focus and guidance.

I would also like to thank all my friends and colleagues, especially Greg Sotzing, Fernando Larmat, Seungho Kim, Andrew Child, Bala Sankaran, Peter Balanda, Don Cameron, Tony Pullen, and Michael DiVerdi, for their help and support.

I would also like to thank Dr. Gabrielle Maeder and Professor Robert T. Kennedy for collaboration.

This research was funded by grants from the DARPA University Research Initiative (monitored by ONR), Rockwell International, the Naval Air Warfare Center, China Lake, Califonia, the University of Florida, Division of Sponsored Research, and the National Science Foundation (CHE 9307732).

TABLE OF CONTENTS

LIST OF FIGURES

Abstract of Dissertation Presented to the Graduate School
of the University of Florida in Partial Fulfillment of the
Requirements for the Degree of Doctor of Philosophy

ION TRANSPORT BEHAVIOR OF POLYPYRROLE DURING REDOX SWITCHING

by

Myoungho Pyo

April 1994

Chairperson: John R. Reynolds
Major Department: Chemistry

The long-term stability of polypyrrole (PP) subjected to different electrochemical switching conditions has been investigated. The effects of solvents and dopant ions on the polymer's electroactivity were monitored with time to find the most stable systems for further studies.

The ion transport properties of PP/poly(styrene sulfonate) (PP/PSS) have been extensively studied by utilizing electrochemical, electrogravimetric and spectroscopic methods. Frequency responses of electrogravimetric results and fluorescent probe method showed that initial oxidation of PP/PSS leads to cation incorporation for charge neutrality resulting from immobility of PSS^- anions.

Fast electrochemically stimulated adenosine 5'-triphosphate (ATP) release (onset < 0.1 second) from PP-ATP films was found relative to no spontaneous ATP exchange at open circuit. The potential dependence of ATP release, monitored at different reduction potentials, indicates that ATP release was not perceptible above -0.4 V on a reasonable time scale (~ one day) and fast ATP release was observed at -0.5 V (vs. Ag

wire). The stability of ATP subjected to these potential switches was confirmed by capillary zone electrophoresis (CZE).

The potential dependent dual ion transport concept of PP/PSS was extended to bilayer films. Potential dependent dual ion transport behaviors of PP/PSS : poly(*N*-methylpyrrole chloride) (PP/PSS : PNMP-Cl) bilayers were investigated by the electrochemical quartz crystal microbalance (EQCM). This bilayer showed cation dominant transport behavior at low potential resulting from PP/PSS oxidation. Subsequent oxidation of the outer film resulted in anion dominant transport due to PNMP oxidation, along with continued oxidation of PP/PSS at high potentials.

In order to avoid monomer diffusion into the inner film during electropolymerization of the outer film, PP/PSS : poly(vinyl ferrocene) (PP/PSS : PVFc) bilayers, in which PVFc is solvent cast on the top of the inner layer, were prepared and their polymer-polymer interfacial structures were analyzed along with a study of the ion transport properties. As expected, PP/PSS controlled cation dominant transport was observed at low potentials and PVFc controlled anion dominant transport at high potentials. Potential scanning results showed reduced net ion movement between the redox potentials of PP/PSS and PVFc films.

The dual ion transport concept through bilayer construction was combined with ATP release from PP-ATP. Ion transport properties of bilayers which consist of PP-ATP inner films and PNMP outer films with various dopant anions were examined. PNMP/heparin (PNMP/HPN) outer films were studied for biocompatibility improvement along with ATP release. UV spectroscopy was utilized to compare the amount and rate of ATP release upon varying the thickness of each layer.

CHAPTER 1
INTRODUCTION

The modern era of conducting polymers began at the end of the 1970s when Chiang et al. discovered that polyacetylene, $((CH)_x)$, synthesized by Shirakawa's method [1], could obtain a 12 order of magnitude increase of conductivity upon oxidative doping [2]. The essential structural characteristics of conducting polymers are their conjugated π system extending over a large number of polymer repeating units. Polyacetylene is the simplest model of this class of materials and, despite its environmental instability which constitutes a major obstacle along with poor processibility to practical applications, $(CH)_x$ remains the prototype of conducting polymers and is still subject to much theoretical and experimental work [3].

Polyheterocycles can be viewed as a sp^2 carbon chain in which the structure analogous to s-cis $(CH)_x$ is stabilized by the heteroatom as shown in Figure 1-1. These conducting polymers differ from $(CH)_x$ in several aspects. First, their ground state is nondegenerate, which is related to the energetic inequivalence of their two limiting forms, i.e., aromatic and quinoidal [4]. Second, in general, polyheterocycles show higher environmental stability. Third, it is facile to modulate their electronic and electrochemical properties by manipulation of the monomer structure [5].

An important step in the development of conjugated polyheterocycles occurred in 1979 when it was shown that highly conducting and homogeneous free standing films of polypyrrole could be produced by oxidative electropolymerization of pyrrole in

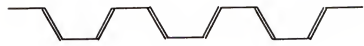

(a) s-cis $(CH)_x$

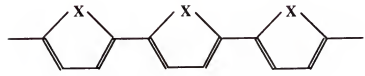

(b) polyheterocycle

Figure 1-1 Comparison of polyheterocycles and polyacetylene structures.
X can be NH for polypyrrole, S for polythiophene, and O for polyfurane.

acetonitrile containing 1 % water [6]. The electrochemical synthesis of polypyrrole from aqueous H_2SO_4 solutions had been initially reported 10 years before but the poor mechanical and electrical properties of the obtained material did not give rise to further developments [7].

The electrochemical polymerization has been rapidly extended to other aromatic compounds such as thiophene [8], furan [9], indole [9], carbazole [10], azulene [11], pyrene [12], benzene [13], and fluorene [14]. These pioneering works have also triggered a renewal of interest for electrogenerated polyaniline [15].

These conducting polymers can be prepared chemically as well as electrochemically. For example, chemical oxidation of pyrrole results in the formation of polypyrrole [16]. In order to oxidize pyrrole, the oxidizing agent has to be carefully chosen so that its formal potential matches the oxidation potential of the monomer. This sometimes requires the use of toxic compounds such as Br_2 and AsF_5 [17]. Moreover, most chemical oxidations produce polypyrrole powders [18] instead of well defined shapes such as a film. Although films can be chemically produced by oxidizing pyrrole at a solid-liquid interface, these films are of poor quality [19] and sometimes

even nonconductive [20]. It was also showed that chemically polymerized polypyrrole has a higher degree of disorder than the electrochemically synthesized polymer by x-ray diffraction [21].

On the other hand, in electropolymerization, an adhering polymer film is formed on the electrode and can be peeled off as a free standing film in most cases. The electrode supported films are characterized with a variety of electrochemical techniques.

1-1 Electropolymerization

The electropolymerization of heterocycles on a conducting or semiconducting (Au, Pt, stainless steel) electrode surface is performed by applying a potential across an electrochemical cell containing a solution of electrolyte and monomer. This potential must be high enough to oxidize the monomer in the solution, and can be driven using a potential sweep (cyclic voltammetry), potential step (constant potential), or galvanostatic (constant current) method.

1-1-1 Mechanism of Electropolymerization

The mechanism of electropolymerization has been a main focus of study but still remains controversial. In early studies, it was suggested that a neutral monomer was adsorbed onto the electrode surface prior to oxidation, and the subsequent polymerization then occurred on the electrode surface [22]. However, more recent studies using in situ differential ellipsometry [23], rotating ring-disk electrodes [24], and microelectrodes [25] have supported the hypothesis that the first step in polymer deposition involves solution polymerization with subsequent precipitation of oligomers onto the electrode surface. These studies all confirm the presence of soluble intermediates prior to polymer formation, including the identification of the radical cation [24A] and the bipyrrole moiety [24B]. The solution used for polymer film formation was also analyzed by UV-Vis spectroscopy after chromatographic separation

[26] to reveal that pyrrole oligomers consisting of up to about nine monomer units are present. H^+ release during electropolymerization has been detected, using rotating ring-disk electrodes, by Bruckenstein and Sharkey [27] who observed the cathodic current at the ring due to H^+ reduction while pyrrole is polymerized on the disk electrode. The pH changes in a two-compartment cell connected by a glass frit were also investigated by Bose et al. [28], supporting H^+ release during electropolymerization.

There are still several different views regarding the coupling of monomer units. When we symbolize the monomer with two hydrogens in the 2,5-positions as H-M-H, then the initial anodic formation of a radical cation can be simply written as

$$H\text{-}M\text{-}H \text{ ---> } [H\text{-}M\text{-}H]^{\cdot +} + e^-.$$

The next step will be a dimerization, and two possibilities arise. The α,α'-coupling of two radical cations (I) has been suggested, resulting in dicationic adducts from which two protons are expelled to form neutral species [29].

$$2[H\text{-}M\text{-}H]^{\cdot +} \text{ ---> } H\text{-}M\text{-}M\text{-}H + 2H^+ \qquad (I)$$

The other possible mechanism (II) considers dimerization resulting from couplings between radical cations and neutral monomer molecules [30].

$$[H\text{-}M\text{-}H]^{\cdot +} + H\text{-}M\text{-}H \text{ ---> } H\text{-}M\text{-}M\text{-}H + e^- + 2H^+ \qquad (II)$$

It was also proposed [31] that electrochemically initiated radical cations can be polymerized by a chain growth mechanism at the early stage in the presence of ClO_4^-, BF_4^-, and PF_6^- electrolytes, indicating that the electropolymerization mechanism can be subjected to a change during film growth in some cases. The continued growth reaction leads eventually to the formation of oligomeric chains that surpass the solubility limit, resulting in a supersaturation at the electrode/solution interface, which is the driving force for the nucleation [32] and deposition of polypyrrole on the electrode surface. Although the radical cation-monomer coupling mechanism is based on the fact that strong coulombic repulsion between radical cations would

prevent the radical cation-radical cation coupling [33], the latter has been favored by most authors since Genies et al. [34] found that the growth of a polymer is terminated as soon as the electrode potential is lowered below the oxidation potential of the monomer. Based on the fact that growing polymer chain ends can continue to react with the monomer in the solution in the case of the radical cation-monomer coupling mechanism, they suggested the mechanism in Figure 1-2 which is generally accepted for the electropolymerization of heterocycles. Further evidence from MO calculations supports this view [35].

1-1-2 Electrolytic Conditions

Various factors such as solvents, electrolytes, nature of working electrodes, oxidation potentials, etc. can have an influence on the physical properties of the polymer formed. For the electrochemical reactions of heterocycles, a wide variety of aprotic solvents can be used as long as the nucleophilic character of the solvent is poor [36]. If the nucleophilic character of the solvent is enhanced, film formation is minimized and instead soluble products are produced which color the reaction solutions. This is because the nucleophile reacts efficiently with the electrochemically generated radical cations. For this reason, many of the reported studies have been performed in acetonitrile. Water, which is also a commonly used solvent, can also be used at a neutral or acidic pH.

The working electrode material which is used as the substrate for the polymer growth affects film properties. It is important that the electrode does not oxidize concurrently with the monomer [37]. For this reason, electrodes made from inert conducting metals (Pt, Au) and semiconducting materials (glassy carbon, indium tin oxide glass) are commonly used due to their high electrochemical stability [38].

Variation of the identity of the anions used during electropolymerization also has a profound influence on the film formation and physical properties such as densities and

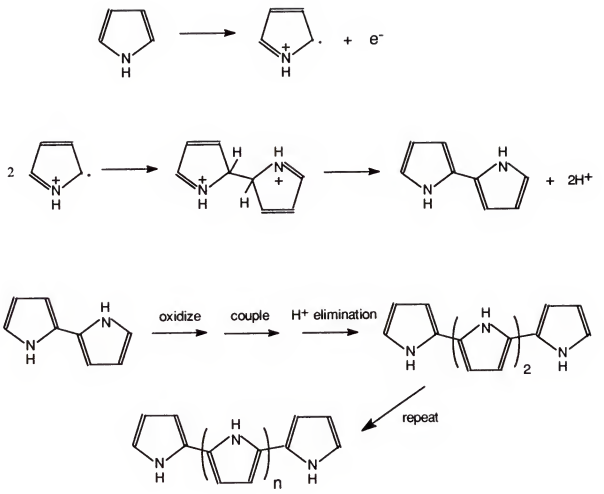

Figure 1-2 Suggested electropolymerization mechanism of pyrrole

conductivities [39]. The anion serves as dopant and is incorporated into the polymer during electrosynthesis. The nucleophilicity of dopant anions should be low so that the radical cation-radical cation coupling process is not prevented as just mentioned. This effect can be seen by examining the film formation with pH changes of the electrolyte solution. Several authors [40] showed that the electropolymerization is suppressed at a high pH and the critical pH, below which the film produced is smooth and homogeneous, depends on the identity of the electrolyte solution. Qian et al. [40C] claimed that this is due to fast H^+ removal as well as the abundance of nucleophiles (OH^-) present at high pH as H^+ is known to play an important role during electropolymerization [41]. Investigations of the impact of electrolyte on the properties of polypyrrole, using a series of sodium sulfonate salts, revealed that larger aromatic sulfonate anions tend to yield higher conductivity and better mechanical properties [42]. Attempts to improve the mechanical properties of polyheterocycles have led to the development of conducting polymer molecular composites [43], including polypyrrole/poly(styrene sulfonate) [44] in which the polyanion chains are electrostatically and physically bound to the polyheterocycle chains, serving as a reinforcing matrix to impart mechanical strength.

The electrode potential should be adjusted to minimize overoxidation [45], which breaks the conjugated π system of the polymer backbone, resulting in the loss of conductivity [46]. This irreversible oxidation is attributed to nucleophilic attack by anions and/or water on the cationic pyrrole in the polymer and occurs at potentials higher than +0.8 V (vs. Ag/AgCl) in the case of polypyrrole. There have been several attempts [47], however, to prepare permselective electrodes by overoxidizing polypyrrole films since redox reactions at the underlying electrode still occur in spite of the loss of conductivity, indicating that the film is porous enough to allow diffusion of analyte to underlying electrode surface.

Since the oxidation potential of the monomer is higher than the polymer redox potential, as grown film is always in the oxidized state. As shown in Figure 1-2 above, 2 electrons for the coupling reaction and, on the average, ca. 0.3 electron for the oxidation of the polymer are consumed per one polymer repeating unit. This fact leads to the relative estimate of the film thickness from the total charge consumed during electropolymerization [48]. Using profilometry, the film thickness of poly(pyrrole naphthalene sulfonate) has been compared with the charge consumed and the linear dependence was reported [49]. Their results showed that the slope of the plot yields a factor of 5.7 $\mu m\ C^{-1}\ cm^2$, indicating that ca. 180 $mC\ cm^{-2}$ passed during electropolymerization produces 1 μm thick films. Other direct measurements of the film thickness are made by using scanning electron microscopy [50] and ellipsometry [51]. The film thickness of poly(pyrrole *p*-toluene sulfonate), examined by scanning electron microscopy [50], also showed that ca. 200 - 240 $mC\ cm^{-2}$ is required to prepare 1 μm thick films. Although the film thicknesses slightly depend on dopant anions incoporated, these results indicate well related proportionality of ca. 200 $mC\ cm^{-2}\ \mu m^{-1}$ between the charge and the film thickness.

1-2 Ion Transport

A number of interesting properties of the conducting polymer come from reversible switches between insulating (neutral, undoped) and conducting (charged, doped) states within certain potential ranges [52]. During redox switches of the conducting polymer, electrons are withdrawn from, or added into, the π system of the polymer backbone reversibly, which makes the conducting polymer retain its electroactivity. While polyacetylene and poly(*p*-phenylene) can carry positive or negative charges through the backbone which leads to so-called p-doped or n-doped states respectively [53], polyheterocycles are commonly only p-doped due to their low

reduction potentials. Therefore, the conducting state of polyheterocycles usually includes only the positively charged (oxidized) state.

The redox polymers, where the redox active species is part of the polymer backbone and the electron transfer occur solely by hopping between the discrete redox centers (electroactive polymers include both electronically conducting polymers and redox polymers) such as poly(vinyl ferrocene) [54] and pyridine complexes of ruthenium [55], also show varied ion transport behaviors during redox switches. The difference between the conducting and redox polymer is that the latter is not conducting in the oxidized state since no charge carrier exists after complete oxidation of every discrete redox center.

1-2-1 Dominant Ion Transport Behavior

As grown conducting polymer films are in the oxidized state, containing charge balancing anions since the oxidation potential of the polymer is always lower than that of the monomer. Therefore, reduction of these polymers may lead either to the diffusion of anions out of the polymer film, or to the incorporation of cations into the polymer film to compensate the negative charge on the anions which no longer serve as dopant ions. Since these processes are reversible, switching of conducting polymers between the oxidized state and the reduced state induces the movement of ionic species within the polymer and at the polymer/solution interface [56].

The control of these ionic species is possible by changing dopant anions used during electropolymerization. As shown in Figure 1-3, an anion exchange film [57] can be produced by using the electrolyte solution containing small anions such as Cl^- and ClO_4^-, while a cation exchange film [58] is prepared by entrapping anionic polyelectrolyte such as poly(styrene sulfonate) and poly(vinyl sulfonate) during electropolymerization. Medium-sized anions such as *p*-toluenesulfonate show both apparent anion and cation movement during the redox process [59].

Anion Specific Transport

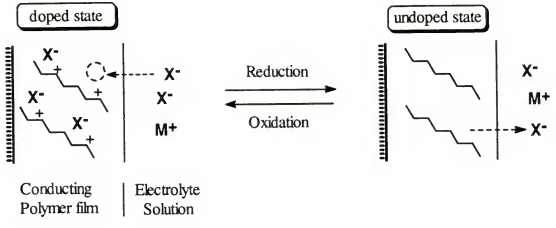

Cation Specific Transport

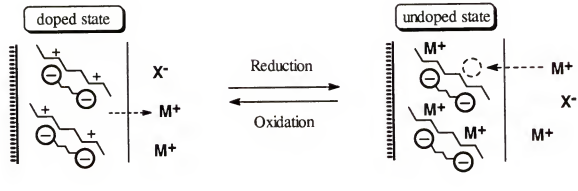

Figure 1-3 Specific ion transport during redox switching of conducting polymer films.

The rate of the charging process of the conducting polymer is affected by the size of the moving species. The investigation of the electroactivity retention with potential scan rate changes (scan rate dependence of cyclic voltammograms) is commonly performed for this study. Shimidzu et al. [60] reported that the redox process of polypyrrole using a large anionic electrolyte (but, still mobile) is diffusion controlled while polypyrrole doped with small-sized anions behaves as a surface bound mode [61]. This fact suggests that the charge balance by relatively large dopant ions is controlled by the diffusion in the switching medium and/or polymer matrix. The apparent diffusion coefficients of moving species were obtained from the charge and mass responses of the conducting polymer during potential steps and in general, are in the range of 10^{-9} and 10^{-11} cm^2 s^{-1} [49, 58, 60, 62].

The dopant anions can be spontaneously exchanged with anions in an external electrolyte solution. Curtin et al. [63] investigated the diffusive anion self-exchange in polypyrrole by ESCA/Auger. Their results show that ClO_4^- incorporated into polypyrrole during electropolymerization is replaced by a variety of anions in solution. The exchanged anions are uniformly distributed throughout the film, not limited to the film surface. The ion exchange takes more time to complete in a thicker film. Tsai et al. [64] have investigated the anion exchange behavior of poly(pyrrole *p*-toluenesulfonate) films, employing spectrophotometry. They found that the apparent diffusion coefficients of the *p*-toluenesulfonate exchange process spans the 10^{-10} - 10^{-12} cm^{-2} s^{-1} range. Schlenoff and Chien [65] studied spontaneous ClO_4^- exchange by using isotope labeling and found strong solvent dependence of the diffusion process, implying that solvent swelling plays an important role in the ion transport.

1-2-2 Complex Ion Transport Behavior

The classification of the ion transport mechanism of the conducting polymer by a certain ion specific type (specific ion transport) is not always the case. Kaufmann et al.

[66] and Genies and Pernaut [67] have first reported that when a ClO_4^- incorporated PP is reduced, electrolyte cations (Li^+) penetrate into the PP matrix to compensate the incomplete release of ClO_4^-. Since their pioneering works, the cation involvement during redox switches of small anion doped PP have been extensively studied [68-76]. Several authors [69] reported that reduction of polypyrrole doped with $Fe(CN)_6^{3-}$ counter ion in aqueous NaCl results in a polymer free of ferricyanide, i.e. the iron complex is expelled when the cationic backbone is neutralized. In contrast, reduction of PP^+-$Fe(CN)_6^{3-}$ in aqueous CsCl produces a polymer containing $Fe(CN)_6^{3-}$ and Cs^+.

PP^+-$Fe(CN)_6^{3-}$ ----> PP^0 + $Fe(CN)_6^{4-}$ in aq. NaCl

PP^+-$Fe(CN)_6^{3-}$ ----> PP^0-$Fe(CN)_6^{4-}$-Cs^+ in aq. CsCl

Cation incorporation during reduction of a polypyrrole doped with Cl^-, ClO_4^-, and *p*-toluenesulfonate was also studied by using atomic absorption spectroscopy and X-ray photoelectron spectroscopy [70]. It was revealed that, during reduction in aqueous electrolyte solutions, poly(pyrrole chloride) (PP^+-Cl^-) and poly(pyrrole *p*-toluenesulfonate) (PP^+-TOS^-) incorporate significant amount of cations while no cation is present in reduced poly(pyrrole perchlorate) (PP^+-ClO_4^-). After soaking the reduced PP^0-TOS^--Na^+ in water for 30 minutes, PP^0-TOS^--Na^+ release TOS^--Na^+ to become PP^0. Their results suggest that the cation involvement depends on the identity of initially incorporated anions, cation size of the switching electrolyte, and solvent used. The solvent effect is evident since cations (Li^+) are incorporated during PP^+-ClO_4^- reduction in organic electrolyte solutions [66] while no Li^+ is detected in the polymer after reduction in aqueous electrolyte solutions [70]. The charge balance by cation movement into PP^+-ClO_4^- in acetonitrile was further confirmed by using radioactive $^{24}NaClO_4$ solutions [71]. Most recently, John and Wallace [72] applied cyclic voltammetry to investigate this and concluded that the identity of the mobile ion is a function of the electrode potentials.

The H^+ and OH^- contribution to ion transport in aqueous electrolyte was also elucidated, which make the ion transport mechanism complicated. Shinohara et al. [73] utilized a rotating ring-disk electrode to examine the discrepancy between the amount of Br^- incorporated into a polypyrrole matrix and the anodic charge at the disk electrode. The difference was attributed to simultaneous doping by OH^- and this fact was supported by the large pH changes near the polypyrrole film. Bose et al. [28], employing ion selective electrodes and microgravimetric method, claimed that ca. 15 % to 25 % of the ion transport for the charge balance of poly(pyrrole chloride) in KCl electrolyte is partitioned between H^+ and K^+ depending on the pH of the aqueous KCl solution.

The effect of electrolyte solution pH on the ion transport mechanism was extensively studied with a multi-valent conjugate acid by Reynolds et al. [74]. For example, while HPO_4^{2-} implanted in the polymer matrix is not mobile over a certain pH range of electrolyte solutions, it moves out in the form of $H_2PO_4^-$ as the polypyrrole is cycled in electrolyte solutions of low pH.

Solvent molecules also participate in these complex ion transport mechanisms [75]. In general, there are two extreme cases for solvent flux during switching. In one extreme, the solvent can move into the polymer film to fill the void volume created by ions which are moving out of the film. This causes the solvent molecules and mobile ions to move in opposite directions and has been reported for a nickel ferrocyanide film [76]. On the other hand, solvent motion can be associated with the mobile ions due to ion solvation. This results in a unidirectional movement of ion and solvent.

Similar complex ion transport behavior was found in cation exchange conducting polymers. Lien and Smyrl [77] carried out microgravimetric measurements during redox cycling of polypyrrole/poly(styrene sulfonate) which is known to be cation dominant at $E \leq -0.1$ V vs. Ag/AgCl. They showed cation dominant transport at low potentials and anion dominant transport at high potentials, indicating that the ion

transport mechanism is potential dependent. Anion incorporation into poly(pyrrole dodecylsulfate) was examined by several authors. Owing to the long aliphatic chain, the mobility of the dodecylsulfate ions in the polymer matrix is small enough that anionic sites can be considered to be fixed. Zhong and Doblhofer [78] investigated this system in detail by electrochemical and EDAX measurements, showing that continued oxidation at high potentials requires anion incorporation. In situ FTIR results [79] indicate the electrolyte anion dependence on the ion transport mechanism, that the film is charge-balanced partly by anions in aqueous carbonate solutions while cation dominant in aqueous ClO_4^- solutions.

Several other analytical probes have been used to elucidate the ion transport behaviors. Spectroscopy, such as UV-VIS or fluorescence [56B,80], would be the most general and convenient method. In this technique, spectroscopically active probe molecules are dissolved in the polymerization or switching medium and electrochemical release or spontaneous exchange of these molecules are investigated in spectroscopically inactive electrolyte solutions. Therefore, this method is limited to spectroscopically active electrolytes.

By using concentration gradients occurring at the polymer/solution interface during ion transport, probe beam deflection has been used to elucidate the direction of ion flux [81]. In this experiment, the refractive index profile gives rise to a deflection of a probing laser beam aligned parallel and close to a flat electrode surface. For example, when poly(pyrrole chloride) is reduced in NaCl solutions, the generation of Cl^- ions leads to an increased refractive index at the electrode surface, which decays into the bulk of the solution. The probing laser beam is deflected toward the region of the higher refractive index, i.e., toward the electrode. The interpretation of results is complicated by the possibility of simultaneous counter flux of co-ions as deflection angles depend only on the concentration profile and are insensitive to the solvent flow.

1-3 Electrochemical Quartz Crystal Microbalance

The quartz crystal microbalance (QCM), a mass sensitive detector, has been combined with electrochemical techniques and adapted for use in solution. This method has become known as the electrochemical quartz crystal microbalance (EQCM). The EQCM technique has been applied to conducting polymer studies, which allows direct, in situ measurement of mass changes on the electrode surface, providing information about mass transport which would be difficult to obtain with other methods. The EQCM has been proven a powerful tool in many research fields including metal deposition and dissolution [82], electrocrystallization [83], various adsorption phenomena [84], mechanistic study of electropolymerization [29B] and ion transport in electroactive polymers.

1-3-1 Fundamentals of the QCM

In 1880, Jacques and Pierre Curie discovered that a mechanical stress applied to the surfaces of various crystals afforded an electrical potential across the crystal whose magnitude was proportional to the applied stress [85]. This piezoelectric property only exists in crystals that have a non-centrosymmetric space group. Shortly after their initial discovery, the Curies experimentally verified the converse piezoelectric effect in which application of a voltage across these crystals afforded a corresponding mechanical strain. The converse piezoelectric effect is the basis of the QCM. This was illustrated well by Buttry and Ward [86] and is reproduced in Figure 1-4. The shear motion of the Au coated AT-cut quartz resonator, which consists of a thin quartz wafer prepared by slicing through a quartz rod at an angle of ca. 35° with respect to the x-axis, is generated by application of an alternating potential across the crystal. This causes a vibrational motion in the quartz crystal with amplitude parallel to the surface of the crystal.

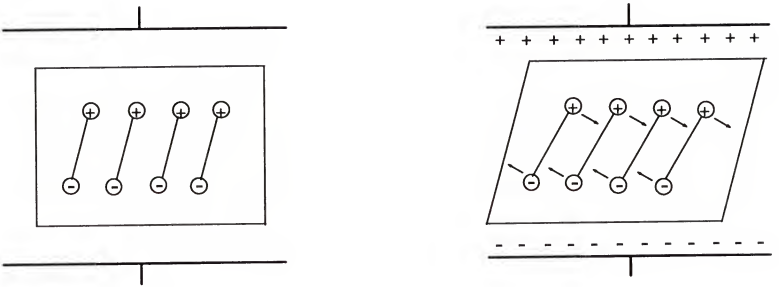

Figure 1-4 Schematic representation of the converse piezoelectric effect for shear motion.

The result of the vibrational motion of the quartz crystal is the establishment of a transverse acoustic wave that propagates across the thickness of the crystal (t), reflecting back into the crystal at the surfaces. A standing wave condition can therefore be established when the acoustic wavelength is equal to 2t, as shown in Figure 1-5.

$$f_0 = v_{tr} / 2t = (\mu / \rho)^{1/2} / 2t \quad (1\text{-}1)$$

f_0 : resonance frequency

v_{tr} : transverse velocity of sound

μ : shear modulus of quartz (2.947×10^{11} g cm^{-1} s^{-2})

ρ : density of quartz (2.648 g cm^{-3})

If the assumption is made that the acoustic properties of the foreign layer (e.g. polymer) are identical to those of quartz, this system can be treated as a composite resonator in which the change in thickness due to the foreign layer is treated as equal to a change in the quartz crystal thickness. A fractional change in thickness (Δt) then results in a fractional change in frequency (Δf). This is shown in Equation (1-2) through (1-5).

$$f_1 = v_{tr} / 2(t + \Delta t) \quad (1\text{-}2)$$

$$\Delta f = f_1 - f_0 = v_{tr} / 2(t + \Delta t) - v_{tr} / 2t = (v_{tr} / 2t) (\{t / (t + \Delta t)\} - 1) \quad (1\text{-}3)$$

$$= f_0 (\{t / (t + \Delta t)\} - 1) = f_0 (-\Delta t / (t + \Delta t)) \sim f_0 (-\Delta t / t) \quad (1\text{-}4)$$

$$= -2f_0^2 \Delta t / v_{tr} \quad (1\text{-}5)$$

Δt is related to the mass change (Δm) as shown in Equation (1-6) and v_{tr} is substituted by $(\mu / \rho)^{1/2}$ to obtain a frequency-mass relationship in Equation (1-8).

Since $\Delta m = A \times \Delta t \times \rho$, $\Delta t = \Delta m / A\rho$ (1–6)

Δm : mass change

A : electrode area

$$\Delta f = -2f_0^2 \Delta m / A\rho v_{tr} \quad (1\text{-}7)$$

$$= -2f_0^2 \Delta m / A(\mu\rho)^{1/2} : \text{Sauerbrey relationship} \quad (1\text{-}8)$$

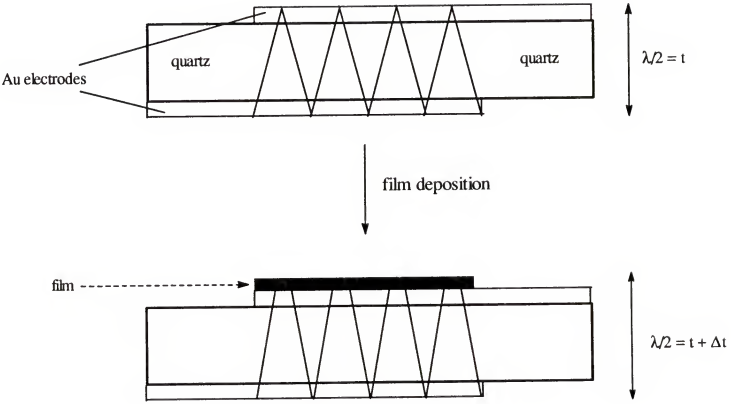

Figure 1-5 Schematic representation of the transverse wave in the quartz crystal and a foreign material.

The Sauerbrey equation indicates that mass gain on a Au electrode results in the frequency decrease and vice versa [87].

This relationship is based on several implicit assumptions. First, it is assumed that the density and the transverse velocity associated with a foreign layer are identical to those of quartz. Second, the frequency response is considered uniform over the entire active region of the resonator. Studies of evaporation and sputtering of metal deposits onto localized areas of a QCM have indicated that sensitivity is highest at the center of the QCM and decreases monotonically in a Gaussian mode, becoming negligible at the electrode boundary [88]. Third, viscoelasticity changes of polymer films during measurements can lead to erroneous conclusions about mass transport in the film [89]. In general, impedence analysis combined with the EQCM measurements is performed to study this behavior [86]. In the absence of impedence analysis, EQCM investigations are carried out for a range of film thicknesses. Linearity of response over the chosen range can be taken as evidence of rigid layer behavior. However, a number of cases have been documented, showing that thin polymer films behave as a rigid film [29B,76,86]. In addition to these, sensitivity changes due to high mass loading [86], microscopic roughness of the QCM electrode surface [90], and interfacial slippage between the deposited polymer and quartz crystal [86], can also affect the frequency response of the QCM. Therefore, care should be taken for quantitative interpretation of EQCM results.

1-3-2 Application of the EQCM to Electroactive Polymers

The EQCM can be distinguished from the QCM in that one side of the Au coated quartz crystal is exposed to an electrolyte solution and serves as a working electrode during redox processes. Thus, the EQCM is a combination of the QCM and electrochemical techniques and allows us to examine mass changes during electrochemical events. Although QCM techniques had been applied to various fields

before, the first interesting report of a polymer film on an EQCM electrode was by Kaufmann et al. [66] in 1984 who observed the transport of both ionic species in polypyrrole during doping and undoping. Their work spurred a great deal of activity in similar studies of a wide variety of redox and conducting polymers.

Various redox polymers have been studied by using EQCM methods, including poly(vinyl ferrocene) [75C,91], poly(thionine) [75B,92], and Prussian blue [93]. Poly(vinyl ferrocene) was the first and the most extensively studied redox polymer by EQCM. Buttry and Varineau [94] prepared solvent cast films of poly(vinyl ferrocene) on Au electrodes and cycled electrochemically in several separate aqueous supporting electrolytes. Comparison of the charge with the frequency change revealed that, under conditions in which ClO_4^- or PF_6^- is the anion of the supporting electrolyte, one anion is inserted into the film for extraction of each electron from the film during oxidation with little accompanying solvent. Hillman et al. have also reported on the film deposition of poly(vinyl ferrocene) [95]. They studied the electrodeposition of films by oxidation in CH_2Cl_2 solutions and found the initiation of the deposition occurs immediately after the potential step to oxidizing potentials, but that the mass change inferred from the initial frequency change suggested deposition of considerably more mass than expected based on deposition of one polymer repeat unit per electron extracted during the oxidation. This was suggested to be due to deposition of polymer chains which were only partially oxidized and possibly to simultaneous solvent and/or supporting electrolyte entrapment inside of the deposited film. The EQCM was also utilized for the kinetic study during chemical oxidation of poly(vinyl ferrocene) [96] and redox switches [97]. Since the initial EQCM work on polypyrrole by Kaufmann et al. [66], the electropolymerization and ion transport of various conducting polymers have been studied, including polypyrrole, polyaniline [98], and polythiophene [99]. For polypyrrole which is the most widely studied conducting polyheterocycle, a study on the electropolymerization mechanism was reported by Baker and Reynolds [29B,100].

They were able to quantitatively analyze the relationship between electropolymerization rate and pyrrole concentration, revealing a second order dependence of the electropolymerization rate on the pyrrole concentration, suggesting that the rate limiting step is the bimolecular coupling of radical cations. Also, ion transport behaviors during redox switches of polyheterocycles have been investigated by various workers, to elucidate simultaneous movement of counter ions, solvent molecules, co-ions and etc. and is documented above in section 1-2.

1-4 Mathematical Models of Ion Transport

There have been several attempts [101] to predict electrochemical behaviors of electroactive polymers using mathematical models. Feldberg [102] suggested a mathematical model including a substantial capacitive current during the electrochemical switching of the polymer films, but failed to include the transport effects of counter ions. Pickup and Osteryoung [103] developed a mathematical model for potential step chronoamperometry and concluded that a polymer film could be modeled as a porous electrode. The porous electrode model they used is not satisfactory since it is based on the assumption that faradaic reactions are negligible.

The most extensive works of potential step chronoamperometry were carried out by Saveant [104]. He developed a mathematical formula for electroneutrality coupling of electron hopping between localized sites with electroinactive counter ions. They assumed that electron hopping follows a second-order law deriving from the bimolecular character, while counter ion transport obeys the classical Nernst-Planck law. For an A + ne = B, couple the rate laws they used are as below.

Electron hopping:

$$(\partial C_A/\partial t) = D_E(\partial/\partial x)\left[(\partial C_A/\partial x) + (nF/RT)C_A(1 - C_A/C^0_E)(\partial\Phi/\partial x)\right] \qquad (1\text{-}9)$$

Counter ion (C) transport:

$$(\partial C_C/\partial t) = D_I(\partial/\partial x)\left[(\partial C_C/\partial x) + z_C(F/RT)C_C(\partial\Phi/\partial x)\right] \qquad (1\text{-}10)$$

where t, time; C_i, concentration of species i; x, distance; z_C, is charge number; Φ, potential; D_I, diffusion coefficient of electroinactive counter ions.

From these mathematical models, they suggested that steady state currents resulting from electroneutrality coupling of electron hopping between localized sites with electroinactive counter ion transport do not depend on the mobility of the electroinactive counter ions. On the other hand, as the mobility of the electroinactive counter ions decreases, the transient current response increases as a consequence of migration. However, these studies are limited to redox polymers since the electron transport of conducting polymers through interchain hopping and intrachain displacement makes a mathematical prediction complicated.

A mathematical model to simulate cyclic voltammograms of polypyrrole on a rotating disk electrode was presented by Yeu et al. [105]. The model was based on the conservation of mass and charged species. The equations included migration of charged species in an electric field, diffusion of charged and uncharged species, and the electrochemical reaction that occurs within the porous polypyrrole film. Simulated cyclic voltammograms were compared with experimental results and they concluded that the current responses can be decomposed into a capacitive current due to the double layer charging and a faradaic current due to an electrochemical reaction. Various kinetic parameters were estimated by comparing with experimental data.

1-5 Applications of Conducting Polymers

Due to the relatively high electrical conductivity and good environmental stability of polyheterocycles, great efforts have been made in the use of these materials in novel electronic and chemical applications, including rechargeable battery electrodes [106], drug release devices [107], biosensors [108], electrochromic devices [109], EMI shielding [110], conducting polymer fibers [111], light-emitting diodes [112], and molecular transistors [113]. Also, using the volume change of conducting polymers

during redox switches, potential artificial muscle construction has been proposed [114]. Of these, applications for rechargeable battery electrodes, drug release devices, and biosensors utilize ion transport behaviors during redox switches and further explained below.

1-5-1 Rechargeable Batteries

A variety of conducting polymers have been investigated with regard to their possible application in rechargeable batteries, including polyacetylene [106A,B], poly(*p*-phenylene) [106C], polypyrrole [106D,E], polyaniline [106F-H], and polythiophene [106I]. The reason why conducting polymers are investigated for this purpose is that their specific weight is lower than that of ordinary inorganic materials. Based on the same reason, most authors have used Li, which has the highest charge to mass ratio and very low E, as the electrode coupled with the conducting polymer electrode.

Various cell configurations have been reported, depending on the moving species and ion movement directions during charging and discharging of batteries. When Li is used as an anode and the polymer as a cathode, the conducting polymer is reduced during discharging. The use of anion dominant conducting polymer films results in anion release and cation dominant films incorporate cations (Li^+) to keep the ion concentration constant during charging and discharging processes. The other cell configuration studied is the use of Li as a cathode and n-type dopable conducting polymers as an anode. In this cell, cations and anions are released from the anode and cathode during discharging, respectively.

Although these studies described plausible discharge voltage and high energy density, there are still some limitations from an industrial point of view, such as their dimensional limitation, the lack of mechanical strength and flexibility, and long term charge-discharge stability.

1-5-2 Drug Release Devices

The first plausible application of the conducting polymer for a drug release device was reported by Zinger and Miller [107A] in 1984. They incorporated glutamate anions into polypyrrole-ClO_4^- films by potential-cycling in sodium glutamate solutions and showed that glutamate is released cathodically. Similar results were obtained with poly(3-methoxythiophene) [107B]. Cationic drug release such as dopamine, which is an intermediate for a human hormone system and is of importance in the treatment of Parkinson's disease, was also studied using poly(*N*-methylpyrrole)/ poly(styrene sulfonate) films [107C] and the electrochemically controlled dopamine release was proved by UV absorbance changes in electrolyte during film oxidation. Although these results triggered investigation of the electrochemically controlled release of various biologically active molecules [107D], spontaneous release by ion exchange with external electrolyte or electrode potential drift still appears to be a problem.

1-5-3 Biosensors

Various biosensors designed for specific biological molecules have been reported, including olfactory [108A,B], penicillin [108C], methoxitin [108D], and glucose sensors [108E-G]. In these studies, a specific enzyme is immobilized in the conducting polymer matrix during electropolymerization. For example, polypyrrole glucose oxidase (PP/GOD) electrodes, which is a prototype biosensor, are prepared electrochemically in solutions of pyrrole and glucose oxidase. Since the isoelectric point of GOD is 4.3, GOD functions as dopant anions in an electrochemical synthesis.

When these enzyme immobilized electrodes are exposed to solutions containing enzymatic reactants, current or conductivity changes occur due to spontaneous reactions. In the case of PP/GOD, the reaction is

glucose + O_2 + GOD ------> gluconic acid + GOD(H_2) + H_2O_2

and formation of H_2O_2 is detected by the amperometric current method during electrode oxidation

H_2O_2 -----> $O_2 + 2H^+ + 2e^-$.

The change of the conductivity is considered to be due to the decrease of pH, resulting from the gluconic acid formation, as it is known that the electronic conductivity is a function of pH [115]. The glucose sensor prepared in this way showed a linear response to the glucose concentration in a range of 10^{-5} - 10^{-3} M. Recently, a bilayer electrode consisting of a PP/GOD film as an inner layer and a poly(pyrrole horseradish peroxidase) (PP/HRP) film as an outer layer and a PP/GOD/HRP homogeneous single electrode were fabricated [116] to reduce polypyrrole degradation due to H_2O_2 reduction at high potentials. This bilayer glucose sensor has a higher signal transfer efficiency, while exhibiting a lower sensitivity than PP/GOD/HRP owing to the outer layer inhibiting the glucose supply to the inner layer.

1-6 Scope of this Work

This dissertation will focus on ion transport in electroactive polymers, which is crucial to many of their applications. The EQCM as well as various other analytical methods was utilized for this study. Attempts have first been made to investigate long term stability of polypyrrole in various electrolyte/solvent systems and to understand fundamental ion transport behaviors of polypyrrole/poly(styrene sulfonate) (PP/PSS) which was proven to be one of the most stable conducting polymers.

Bilayers, consisting of PP/PSS and poly(*N*-methylpyrrole chloride) have been electrochemically constructed and their independent ion transport at well separated potentials (dual ion transport) was examined. This concept was extended to PP/PSS : poly(vinyl ferrocene) bilayers, in which outer layers were prepared by solvent casting and their ion movement during redox switching was elucidated.

Electrochemically stimulated adenosine 5'-triphosphate (ATP) release from PP-ATP films has been studied and compared with spontaneous release, employing in situ UV-Vis spectroscopy, microgravimetric, and electrochemical methods. The stability of ATP subjected to these conditions was also confirmed.

The concepts of dual ion transport in conducting polymer bilayers and electrochemically stimulated ATP release have been combined to construct polymer modified electrodes which make it possible to release ATP as desired and to adjust the ionic concentration of switching media in a well controlled manner. Various outer films were prepared, including poly(*N*-methylpyrrole) : heparin with the possibility of improving of biocompatibility. The cation and anion concentration changes during outer film redox, along with ATP release through the outer film during inner film reduction, were examined.

CHAPTER 2
EXPERIMENTAL

2-1 Electrochemical Techniques

Due to their switchable properties, electroactive polymers are often subjected to a variety of electrochemical methods to investigate their redox reactions. The fundamental characteristic of such experiments is to electrochemically initiate redox reactions of electroactive polymers by applying a selected potential wave form and monitor either the current or the charge produced. A potentiostat is used to control the voltage across the electrodes in order to maintain the potential difference between the working and reference electrodes.

2-1-1 Electrodes and Cells

Most of the electrochemical experiments described in this dissertation were performed with a conventional three electrode configuration under an Ar blanket, as illustrated in Figure 2-1. In this study, electrolyte solutions were purged with Ar prior to starting an experiment in order to remove any dissolved oxygen, which is known to cause irreversible oxidations of neutral polypyrrole rapidly [117]. Ar was allowed to flow above the electrolyte solution to prevent oxygen from re-entering the solution during experiments.

The three electrodes were connected to a potentiostat in which the working electrode potential measured by the reference electrode is fed into a control amplifier to correct for a voltage difference between the actual and the desired value. The current

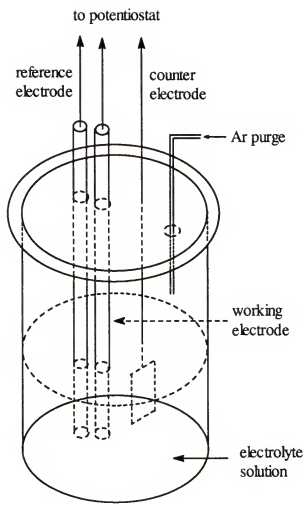

Figure 2-1 Conventional electrochemical cell with three electrodes.

mainly flows between the counter and working electrode to limit the iR induced potential change between the working and reference electrode. An EG&G Princeton Applied Research Model 273 Potentiostat/Galvanostat was used for potential control in all standard electrochemical experiments.

A Pt plate was used exclusively as the counter electrode throughout this study. For experiments using non-aqueous solutions, a Ag/Ag^+ electrode was used as the reference electrode. The Ag/Ag^+ reference electrode consists of a Ag wire immersed in acetonitrile containing 0.1 M tetrabutylammonium perchlorate and 0.01 M silver nitrate. A standard electrode potential of Ag/Ag^+ couple is +0.7996 V vs. SHE. When aqueous electrolyte solutions were used, a Ag/AgCl electrode in a 3 M NaCl aqueous solution, which has a standard electrode potential of 0.223 V vs. SHE, was used as the reference electrode. For in situ spectroscopic measurements equipped with the electrochemical apparatus, Ag wire was used as a quasi-reference electrode to minimize light scattering due to the large size of the Ag/AgCl electrode relative to the cuvette dimensions. Ag wire has 0.08 V higher electrode potential than the Ag/AgCl in a 0.1 M NaCl aq. solution.

Both Au and Pt were used as the working electrodes, on which the polymer films were synthesized and redox switching was studied. The specific working electrodes utilized are further described as follows:

1. **Pt button electrodes**. These electrodes were manufactured by Bioanalytical Systems. A Pt rod is wrapped with electrochemically inert polymer leaving an exposed area of 0.02 cm^2. Most of the voltammetric studies were carried out using this type of electrode. Before the experiment, this electrode was polished with cerium oxide polish, ultrasonicated in water, washed with double distilled water, and wiped clean with a Kimwipes tissue.

2. **Pt plate electrodes**. Plate electrodes were used for the studies in which large concentration changes of a certain ionic species in an electrolyte solution were

required. Before experimentation, these electrodes were cleaned by flame-burning and the rear sides were screened by a paraffin coating.

3. **Au electrodes.** These electrodes were designed for the EQCM study and obtained from Valpey-Fisher. A "key-hole configuration" of gold is evaporated on both sides of a Cr coated quartz crystal wafer surface, as shown in Figure 2-2. An oscillating electric field (0.5 V) is applied perpendicular to the surface. One side of the Au surface is exposed to the solution in order to function as the working electrode. The geometric area of this electrode is 0.71 cm^2. In order to eliminate any impurities on the Au surface, the electrodes were treated with concentrated H_2SO_4, followed by washing with double distilled water and acetone.

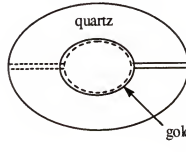

Figure 2-2 Schematic of a Au coated quartz crystal

2-1-2 Film Preparation

The conducting polymers were electrochemically synthesized on the working electrode by using a constant potential electropolymerization at the monomer peak potential determined by cyclic voltammetry (+0.8 V for pyrrole vs. Ag/AgCl). A 0.1 M monomer and supporting electrolyte solution was used unless otherwise mentioned. The potential was held until the charge passed, monitored by a coulometer, reached the desired value.

The redox polymer coated electrodes were prepared by solvent casting. Poly(vinyl ferrocene) was dissolved in dichloromethane (CH_2Cl_2) and a quantitative amount of the solution was cast on to the electrode using a micro syringe. The film thicknesses were controlled by the amount of the solution cast and, in some cases, mass changes were monitored to confirm complete solvent evaporation.

2-1-3 Voltammetric Methods

In order to investigate the redox properties of electroactive polymers, voltammetric methods were employed. In this study, potential step and potential sweep methods were used. In the potential step method, a potential difference is applied between the reference and working electrode and the changes in current or charge were observed. The conducting polymers were electrochemically synthesized by applying the potential at which the monomer is oxidized and stopped when the desired film thickness (measured directly with a profilometer) was obtained, as mentioned in section 2-1-2. The charge passed during electropolymerization was used to estimate film thicknesses. Also, the potential step method was utilized for the study of the redox processes of the electroactive polymer. An initial potential was applied for a sufficient time such that no faradaic processes were occuring. The potential was then stepped to initiate the redox reaction of interest. A second potential step, which is especially useful for the examination of reversible redox processes, was utilized when necessary.

In a potential step experiment with electroactive species present in solution, the faradaic processes proceed so rapidly that the concentration of the reactive species on the electrode approaches zero. In this case, mass transport is controlled by diffusion. Assuming semi-infinite diffusion, the current response is inversely proportional to the square root of time as described by the Cottrell equation [118]:

$$i = nFAC^*D^{0.5}/(\pi^{0.5}t^{0.5}) \qquad (2\text{-}1)$$

where F is Faraday's constant (96,485 C mol^{-1}), n is the number of electrons consumed,

A is the surface area of the electrode (cm^2), C* is the concentration of electroactive species in the bulk of the solution (mol cm^{-3}), and D is the diffusion coefficient ($cm^2\ s^{-1}$). In this model, the diffusion is assumed to be perpendicular to the electrode surface and is valid when the diffusion process is slow and the diffusion layer thickness is much smaller than the electrode dimensions. The integration of Equation 2-1 with respect to time thus gives a charge vs. time relation.

$$Q = nFAC^*D^{0.5}t^{0.5}/\pi^{0.5} \qquad (2\text{-}2)$$

The diffusion coefficient (D) can be obtained by careful analysis of the charge-time relationship.

The application of this concept to polymer modified electrodes to obtain apparent diffusion coefficients, in which electroactive species are bound to the electrode in the form of an electroactive film, has been made. Assuming that the concentration of the electroactive sites is constant across the film at equilibrium; that upon stepping the potential, the equilibrium is reached rapidly at the polymer/electrode interface; and that the slow coupled diffusion of electrons and charge balancing ions leads to semi-infinite linear diffusion conditions within the film, apparent diffusion coefficients can be calculated. In spite of these assumptions, Equation 2-1 is commonly used for the relative comparison of the redox kinetics of polymer modified electrodes.

Another method used to study diffusion processes is to use spectroscopic probe ions as dopants. Miller et al. [107C] derived an absorbance-time relationship from the Cottrell equation using Beer's law:

$$A(t) = A^* - (2D_{app}^{0.5}t^{0.5} / \delta\pi^{0.5})(A^* - A^\infty) \qquad (2\text{-}3)$$

where A^*, A(t), and A^∞ are the initial, time-t, and time-infinity absorbance values, and δ is the film thickness (cm^2). The apparent diffusion coefficient (D_{app}) is then calculated from the slope of a plot of A(t) vs. $t^{0.5}$.

In this dissertation, potential step experiments were combined with the EQCM to investigate both redox processes and ion transport behaviors. D_{app}'s based on UV-Vis absorption intensities were calculated using Equation 2-3.

Potential sweep (cyclic voltammetry, CV) experiments allow for the monitoring of the current change as a function of sweep potential. Instead of stepping the potential to a certain value, a triangular wave potential change is applied to an electrode. The potential is first increased linearly to a maximum and then decreased to the initial potential with a constant preset rate.

The initial and final potentials are selected such that no redox reactions occur. When the potential reaches the oxidation potential of electroactive species in a supporting electrolyte solution, oxidation begins and current starts to flow. As the anodic scan continues, the surface concentration of the reactive species drops and produces a concentration gradient near the electrode. Since the current response is proportional to the slope of the concentration profile of the reactive species, it results in a maximum current response. Subsequently, the slope of the profile continues to decline and the observation is therefore a peak in the current-potential curve. The current at the peak potential (i_p) is given by the Randles-Sevcik equation [118]:

$$i_p = (2.69 \times 10^5) n^{1.5} A D^{0.5} C^* \nu^{0.5} \qquad (2\text{-}4)$$

where ν is the scan rate (V s^{-1}). This equation indicates that increasing the scan rate would reduce the total charge passed during scanning, indicative of a diffusion controlled reaction.

The electroactive polymer coated electrode behaves somewhat differently. Equation 2-4 does not hold and the i_p dependence on the scan rate varies with the experimental conditions, such as electrolytes, indicating that the redox process is not diffusion controlled. When surface concentration (Γ, mol cm^{-2}) of electroactive centers and electroactivity are equated, i.e., no kinetic effect is considered, the peak current is given by the equation below [118].

$$i_p = n^2F^2\Gamma\nu/4RT \qquad (2\text{-}5)$$

The scan rate dependence along with peak potentials and peak separation gives useful information for the study of ion transport.

In this dissertation, cyclic voltammograms of the electroactive polymers were obtained in various electrolyte solutions and characterized by comparing a number of parameters; anodic peak potentials, cathodic peak potentials, peak separations, and their current counterparts. The nature of the surface bound system was also investigated from the scan rate dependence of the peak current.

2-2 Instrumentation

2-2-1 the Electrochemical Quartz Crystal Microbalance

The electrochemical quartz crystal microbalance (EQCM) is a modified version of the quartz crystal microbalance (QCM) operating in contact with solutions, combined with a conventional electrochemical cell. This allows simultaneous monitoring of the mass and current changes occurring at the working electrode during any redox event. The principle of the EQCM was described in Chapter 1.

The schematic diagram of the EQCM system used in this work is shown in Figure 2-3. An AT-cut, Au coated 5 MHz quartz crystal wafer was used as an oscillator, which gave a sensitivity of 18 ng Hz^{-1} cm^2. The potential window was kept below ca. 1.0 V vs. Ag/AgCl due to Au oxidation at high potential. However, it was not a limiting factor in this study since the redox processes of pyrrole and polypyrrole reside within this potential window. Pt is the preferred electrode material due to its excellent electrochemical stability, however, Pt coated quartz crystals are prohibitively expensive at present. The quartz crystal wafer was sealed in the cell via O-rings. The area of the electrode exposed to solutions, determined by the O-ring inner diameter, was 0.71 cm^2.

The circuit diagram of the EQCM employed in this work is shown in Figure 2-4. The EQCM was designed at IBM and constructed in the UT Arlington electronics

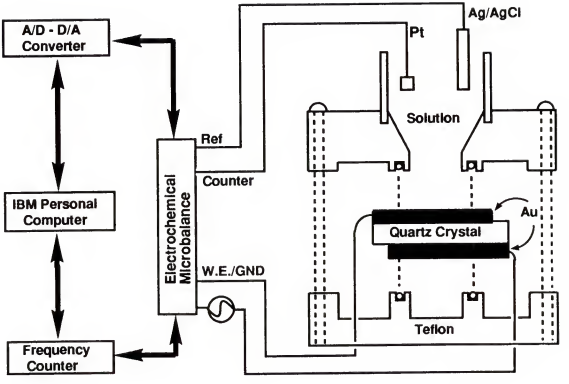

Figure 2-3 Schematic diagram of the EQCM system.

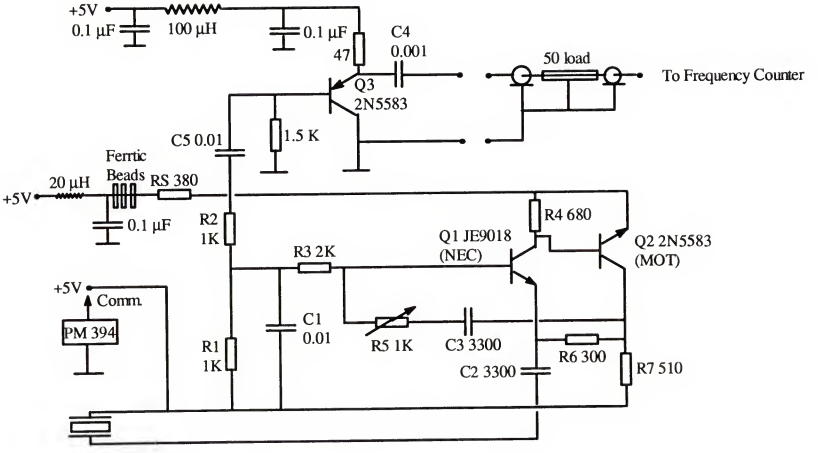

Figure 2-4 The electric circuit diagram of the EQCM employed in the experiments.

shop. It was designed to operate at either 5 MHz or 15 MHz resonance frequencies. In this study, the 5 MHz frequency was exclusively used due to frequent malfunctions at the high resonance frequency. The potentiostat was linked with the QCM to obtain electrochemical as well as frequency responses. The driving potential to the electrochemical cell in the EQCM was converted via a 12 bit digital-to-analog converter and the resulting current response was read via a 16 bit analog-to-digital converter. Both of these converters were contained in a Tecmar Labmaster data acquisition and control board (Scientific Solutions), installed in an IBM AT clone. The driving potential had a voltage range of -2.5 V to +2.5 V, designed to maximize the resolution to which the working electrode potential could be controlled while meeting the required potential range encoutered in electrochemistry. This is important in a potential sweep experiment since a number of small potential steps are approximated to a linear potential sweep. The electrochemical current response was converted to -10 V to +10 V analog responses, corresponding to -10 mA to +10 mA. The resolution of the cell current, determined by the 16 bit analog-to-digital converter, gives a current resolution of 3.1×10^{-7} A.

The resonant frequency changes of the quartz crystal during electrochemical events is measured using a Philips PM6654 frequency counter. The data is sent, via an IBM IEEE-488 General Purpose Interface Bus (GPIB), to a computer. Due to the slow data conversion rate of A/D and D/A, the highest scan rate was about 30 mV s^{-1}.

In the latter phase of this experiment, the EQCM was combined with an IBM compatible 33 MHz 486 computer using a National Instruments AT-MIO-16X multi-function I/O board. This board has 10 µsec, 16-bit sampling A/D and D/A convertors. The data acquisition program was rewritten in C using the National Instrument Lab Windows software package. The new system has attained scan rates as high as 1000 mV s^{-1} in cyclic voltammetric experiments. For frequency voltammetry, in which both current and frequency responses are simultaneously monitored during potential

scanning, the speed is limited to ca. 500 mV sec^{-1}. This is due to the Philips 6654 frequency counter which is interfaced to the new computer by a National Instruments GPIB-PCIIA board. When the PM 6654 is placed in high-speed damp mode, it can only obtain maximum reading rate of 200 sec^{-1}.

2-2-2 In Situ Spectrophotometry

The use of spectroscopic probe ions as moving species makes it possible to directly monitor ionic concentration changes of switching media by spectroscopic techniques. The direct measurement of the spectroscopic intensity changes of probing electrolyte solutions, during redox switching of conducting polymers, was avoided since the concentration changes were so small. Instead, probing ions were first incorporated into conducting polymers, either during synthesis or via exchange process, and their release into spectroscopically inert electrolyte solutions were monitored. Both luminescence and UV-Vis spectroscopy were employed for these studies and potentials were controlled with the EG&G model 273 potentiostat.

For the luminescence study, sodium 2-naphthalenesulfonate (NaNS) was used as a luminescence probe to examine anion incorporation into polypyrrole/poly(styrene sulfonate) (PP/PSS) films during reduction. This luminescence probe technique using NaNS was initially developed by Rajeshwar et al [49]. NS^- release during PP/PSS oxidation was monitored in 0.1 M NaCl solutions utilizing a Perkin-Elmer MPF-44B spectrofluorometer. It is evident that this NS^- release monitor, instead of incorporation, minimizes excimer formation due to the low concentration of NS^-. The NaNS probe was excited at 284 nm and an emission intensity was recorded at 340 nm. The PP/PSS coated Pt electrode was aligned parallel to the excitation light to avoid primary inner filter effect. A Pt plate and Ag wire were used as the counter and quasi reference electrodes respectively. This study will be detailed in Chapter 4.

UV-Vis spectroscopy was employed to investigate electrochemically stimulated adenosine 5'-triphosphate (ATP) release from poly(pyrrole adenosine 5'-triphosphate) (PP-ATP) films, which will be fully described in Chapters 5 and 7. Optical spectra were obtained on a Varian Analytical Instruments Cary 5E UV-Vis-NIR spectrophotometer. The polymer coated Pt electrodes were placed in a cuvette with a Ag wire quasi reference electrode and a Pt plate counter electrode. A 0.5 cm diameter hole was punched in the Pt plate to allow a beam path. The cell design is illustrated in Figure 2-5. The initial electrode potential was held at a value where PP-ATP is in the oxidized state and subsequently scanned or stepped to reduce the film. The UV absorbance change in various electrolyte solutions was monitored at 260 nm.

2-2-3 Others

In some cases, direct measurements of film thicknesses were carried out using a profilometer (Sloan Dektak II). Thicknesses of PP/PSS films, synthesized on Au coated quartz crystals, were obtained by this method. Charges passed during electropolymerization were correlated to film thicknesses to obtain the complete thickness vs. charge relationship.

Scanning electron microscopy (JEOL, JSN-6400) was utilized to investigate PP/PSS film morphology on Au quartz crystal electrodes. PP/PSS films of varied thickness were synthesized and the presence of pinholes in the films were examined.

2-3 Reagents

Pyrrole and N-methylpyrrole (Aldrich) were vacuum distilled and stored in a freezer. Before use, the reagents were further purified by passing through aluminum oxide until colorless. In some cases, pyrrole was vacuum distilled before use and used without further purification.

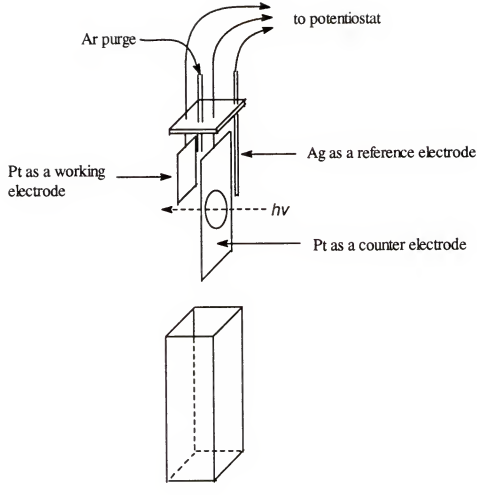

Figure 2-5 Cell design for in situ optical measurements.

The water used in this experiment was double distilled, having a resistance of ~10^6 Ωcm. Organic solvents (CH_2Cl_2 and acetonitrile) were distilled under dehydrating agents (CaH) and immediately used under an Ar blanket to avoid moisture from the air. When hygroscopic electrolytes were used with the organic solvents, the electrolytes were dehydrated by vacuum-drying. The electrolytes were then stored under nitrogen atmosphere until use. Other electrolytes and experimental details will be described fully in the experimental section of each chapter.

CHAPTER 3
LONG-TERM ELECTROCHEMICAL REDOX SWITCHING BEHAVIOR OF POLYPYRROLE (PP)

It is well known that doped polypyrrole (PP) is a relatively stable material in air at open circuit [119]. However, when undoped PP is exposed to oxygen in air, it is easily oxidized. This is also the case for PP in an electrolyte solution containing dissolved O_2. Oxidation of neutral PP is thermodynamically favored since the standard reduction potential of O_2 is more positive than that of PP. The possible reactions are as follows [120].

$$PP + 1/4O_2 + 1/2H_2O \rightleftharpoons PP^+OH^- \qquad \Delta E^0 = 0.134 \text{ V}$$

$$PP + 1/4O_2 + H^+ + A^- \rightleftharpoons 1/2H_2O + PP^+A^- \qquad \Delta E^0 = 0.284 \text{ V}$$

In these examples, no side reactions in the conjugated π-polymer backbone are shown, suggesting that the reversible electroactivity during redox switching could be retained. However, O_2 dissolved in switching media should be removed since it is known that irreversible oxidation of neutral polypyrrole by O_2 can occur rapidly [117].

One of the most important criteria for the applications of PP is the stability under applied potentials. Electrochemical reversibility is followed by irreversible behavior at higher oxidation potentials [45]. The irreversible oxidations consume significantly more charge than the reversible oxidations [121] and lead to a deterioration of the electrical conductivity [46]. The oxidation at which charge storage and conductivity degrade irreversibly is termed "overoxidation". It is generally believed that H_2O and O_2 molecules in the switching media are involved in this reaction. The most commonly referenced overoxidation process of PP is as follows:

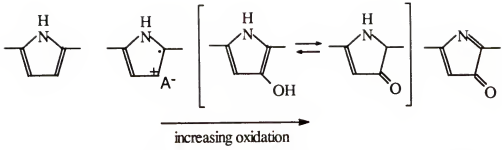

Although overoxidized PP has been reported to have a few interesting properties such as selective ion exclusion [47], overoxidation should be avoided in most cases as it results in reduced electroactivity. Thus, there have been extensive studies on the highest potential which can be reached without fast degradation of the π-conjugation. In the case of PP, it has been reported that fast degradation starts at ca. +0.8 V (vs. SCE) and its rate is proportional to the applied potentials [45B,122]. These stability studies, however, were limited to the investigation at a fixed high potential. No long-term stability changes during redox switches within a normal potential window, in which overoxidation is known to be avoided, has been reported.

Redox switching is accompanied by ion transport to maintain charge neutrality [52-62]. The dominant moving species during the doping/undoping of conducting polymers is primarily determined by polymer-ion-solvent interactions. In general, the ion transport mechanism is complicated [66-79] since neutral species, co-ions and solvent molecules can participate in these processes. This results in complex electrochemical behavior. Therefore, the electrochemical response and the redox switching stability of conducting polymers are affected by the electrolyte and solvent used during electropolymerization and subsequent switching.

The electrochemical behavior of PP, doped by various anions during electropolymerization, has been extensively studied in a variety of electrolyte solutions [57-59]. These studies used cyclic voltammetry as a probe of stability with the assumption that no changes in electroactivity occur over an extended period of time.

The redox potential of PP was found to be dependent on the dopant ions used. In these examples, the same solvent systems were utilized during polymerization and redox switching to minimize the complexity that arises due to solvent exchange.

This chapter describes the long-term electrochemical switching behavior of a number of PP systems. Poly(pyrrole chloride) (PP-Cl), polypyrrole/poly(styrene sulfonate) (PP/PSS), poly(pyrrole *p*-toluene sulfonate) (PP-TOS), and polypyrrole/poly(acrylamido propane sulfonate) (PP/PAMPS) were synthesized and cycled in various electrolyte/solvent media. PP-Cl and PP/PSS films were chosen since they undergo typical anion [28] and cation [58] dominated transport during redox switching. These results were compared to PP-TOS films which are known to possess both cation and anion transport properties [59]. The potential window was limited to the reversible redox processes to avoid overoxidation. The electrolyte/solvent systems used have a large effect on electroactivity and long-term charge capacity which will control their applicability for switching devices.

3-1 Experimental Details

Pyrrole was purified by passage over activated alumina until colorless. Various electrolytes, including sodium chloride, sodium poly(styrene sulfonate) (NaPSS), sodium poly(acrylamido propane sulfonate) (NaPAMPS), lithium perchlorate, tetraethylammonium *p*-toluenesulfonate (TEATOS), hydrochloric acid, tetraethylammonium chloride (TEACl), tetrabutylammonium perchlorate (TBAP), tetrabutylammonium iodide (TBAI), sodium iodide (NaI), and $LiN(SO_2CF_3)_2$ (Du Pont) were used as received. Water was double distilled and acetonitrile (ACN) were dehydrated with P_2O_5. Electrolyte solutions were Ar purged before use.

Electropolymerization and redox switching studies were carried out in a one-compartment cell using an EG&G Model 273 potentiostat and a Pt counter electrode. PP films were deposited on a Pt button electrode (0.02 cm^2) at +0.8 V and +1.1 V in

aq. and organic solutions respectively. All electrode potentials reported in this Chapter are referenced to Ag/AgCl. Polypyrrole films were redox cycled (ca. 20 scans) in order to equilibrate the redox response before carrying out long-term stability experiments unless otherwise mentioned. During redox switching, the electrochemical cell was covered with an Ar blanket. In order to prevent electrolyte concentration fluctuations caused by evaporation of solvent, Ar was passed through a solvent reservoir and then into the cell.

3-2 PP Electrodeposited from Aqueous Media

3-2-1 Comparison of the Long-Term stability of PP

As a control experiment, poly(pyrrole *p*-toluene sulfonate) (PP-TOS), poly(pyrrole chloride) (PP-Cl), and PP/PSS films (ca. 400 nm, 100 mC cm^{-2}) were electrosynthesized in aq. solutions containing the sodium salt of the incorporated anions and redox cycled in 0.1 M $LiClO_4$ (aq.) until equilibrated. Potentials were subsequently stepped between -0.6 V and +0.4 V and held for 20 sec at each potential, monitoring the charge passage (electroactivity) with time. Figure 3-1 demonstrates the retention of electroactivity, the ratio of charge responses relative to a initial charge value ($100Q_t/Q_0$) as shown in the inset, during these steps. While the stability appeared to be similar up to 500 potential switches, the electroactivity of PP-Cl decreased more rapidly than PP/PSS and PP-TOS over longer periods of time. This rapid drop of the elecroactivity of PP-Cl was confirmed in a 0.1 M NaCl (aq.) electrolyte (Figure 3-1d), indicating that this may be an intrinsic property of the anion transport dominated PP-Cl. In this study, PP-TOS showed the highest retention of electroactivity with 90 % after 1100 switches. Both PP-TOS and PP/PSS, though, exhibited monotonous electroactivity decreases with time.

To limit the mobile species to hydronium ions, the stability of redox switching on dopant anions was further investigated using 10 mM HCl (aq.) solutions as the

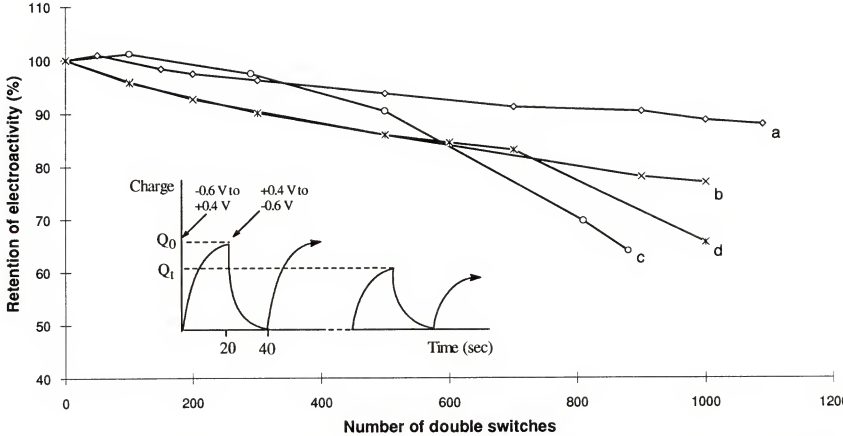

Figure 3-1 The long term stability of (a) PP-TOS, (b) PP/PSS, and (c) PP-Cl films redox switched in 0.1 M $LiClO_4$ (aq.). Curve (d) shows the electroactivity decay of PP-Cl in 0.1 M NaCl (aq.) comparable to (c). Potentials were stepped between -0.6 V and +0.4 V and held for 20 sec at each potential. Inset shows representative charge responses during potential stepping.

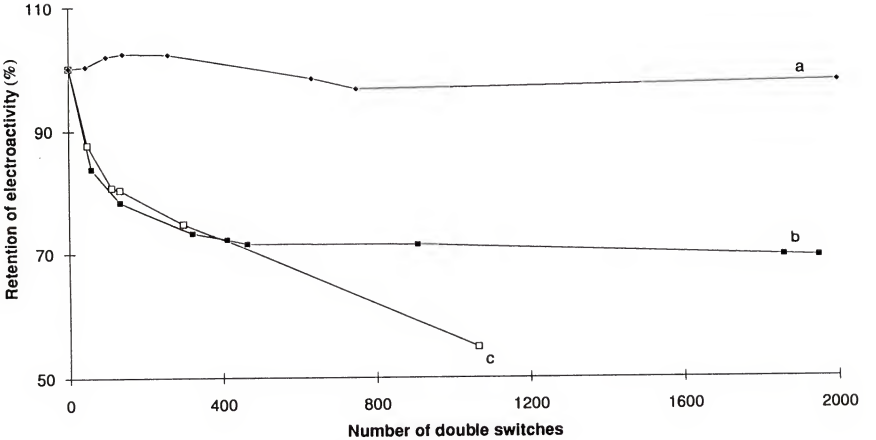

Figure 3-2 Comparison of the switching stability of (a) PP-TOS, (b) PP/PSS, and (c) PP/PAMPS in 10 mM HCl (aq.). The potential was stepped between -0.3 V and +0.4 V, holding for 20 sec at each potential.

switching medium. Figure 3-2 shows the electrochemical stability of PP-TOS, PP/PSS, and PP/PAMPS subjected to the same experimental conditions as above. Again, PP-TOS was more stable than PP/PSS or PP/PAMPS with the difference more distinct. The cyclic voltammogram of PP-TOS exhibited an $E_{1/2}$ of ca. 0.0 V, indicating that TOS^- anions were exchanged with Cl^- anions [123]. If the TOS^- remained in the film, the $E_{1/2}$ would be ca. -0.5 V. On the other hand, both PP/PSS and PP/PAMPS exhibited rapid electroactivity drops during the initial switches. This rapid loss of electroactivity is interesting as we have only observed it for PP/polyelectrolyte composites in acidic solutions where the protons are the dominant mobile ions. Since these experiments were performed in aq. solutions, the results indicate that both the initial dopant anions and the mobile ions can affect the long-term stability of PP.

3-2-2 Ion/Solvent Exchange of PP-Cl

PP-Cl films (ca. 400 nm, 100 mC cm^{-2}) were synthesized and redox switched in various electrolyte/solvent systems. The electroactivity of the PP-Cl films were found to be extremely sensitive to the solvent system as the films are not electroactive in solvents different from those used for electropolymerization. While H_2O synthesized PP-Cl films are electroactive in $LiClO_4$ (aq.) as mentioned above, they are not electroactive in $LiClO_4$/ACN, $LiClO_4$/PC, TBAP/PC, and TEACl/ACN. It is worth noting that the electroactivity of PP-Cl lost in $LiClO_4$/ACN is immediately recovered with a change in switching medium back to $LiClO_4$ (aq.), indicating that no change in the intrinsic properties of PP occurs during exposure to the $LiClO_4$/ACN. Upon reimmersion in $LiClO_4$/ACN, the PP-Cl films become electroinactive again. Since the redox processes of conducting polymers are the coupled behavior of electron transfer between underlying electrodes and coated polymers, and counter ion transport, the electroinactivity of PP-Cl in organic solvent is believed to be due to limited charge balancing ion transport within the polymer matrix. It is likely to occur since as-made

films, equilibrated in water, is incompatible with mobile ions hydrated by organic solvent molecules.

3-2-3 Ion/Solvent Exchange and Long-Term Stability of PP/PSS

The solvent dependence was further investigated with PP/PSS films. PP/PSS films (ca. 400 nm, 100 mC/cm^2) were electrosynthesized in aq. solutions containing 0.1 M NaPSS and redox cycled in various electrolyte/solvent systems until equilibrated. Potentials were subsequently stepped between -0.6 V and +0.4 V and held for 20 sec at each potential, while monitoring the charge passage as a function of time. Figure 3-3 illustrates charge responses during these steps. The similar long-term stabilities in 0.1 M $NaClO_4$ and 0.1 M $LiClO_4$ indicate that the identity of the mobile alkali cations in the same solvent does not affect the electroactivity. PP/PSS, redox switched in $LiClO_4$/ACN (Figure 3.3c), shows a similar stability to PP/PSS in $LiClO_4$ (aq.). This is surprising since PP-Cl film, cycled in the same electrolyte solution, is completely electroinactive. The difference was further investigated by comparing PP/PSS films cycled in TEACl/ACN to PP-Cl films switched in the same electrolyte solutions. Stable current responses were observed with PP/PSS during potential cycling while PP-Cl is electroinactive. Differences in the ion/solvent exchange process between PP/PSS and PP-Cl films appear to result from the different ionic conductivity in the matrix. Since PSS^- is entrapped in the polymer matrix, PP/PSS films possess a higher ionic conductivity than PP-Cl in both reduced and oxidized states [124]. This results in more facile counter ion movement within PP/PSS to balance the charge. Therefore, when PP/PSS films are redox switched in ACN solutions, the energy barrier caused by the solvent incompatibility appears to be compensated by the high ionic conductivity.

While PP/PSS films exhibit relatively stable equilibrated cyclic voltammograms in electrolyte/ACN solutions, they show only slight electroactivity in electrolyte/PC solutions during the first several redox switches, resulting in a rapid loss of

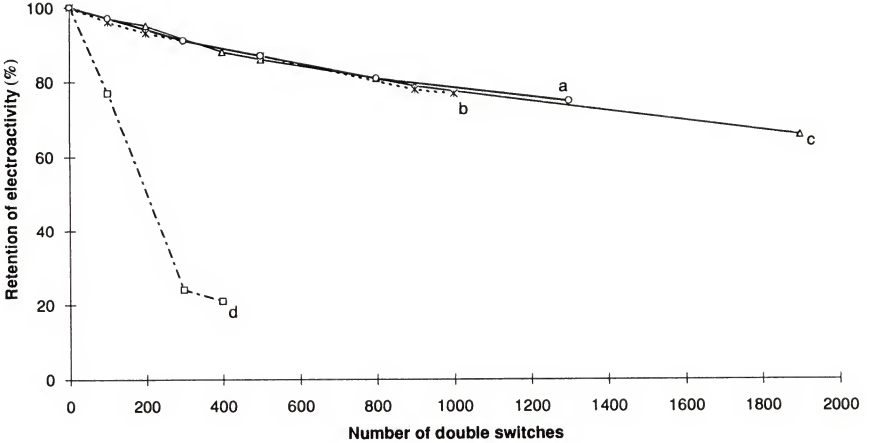

Figure 3-3 The long term stability of PP/PSS redox switched in 0.1 M (a) $NaClO_4$ (aq.), (b) $LiClO_4$ (aq.), (c) $LiClO_4$/ACN, and (d) TEACl/PC solutions. Potentials were stepped between -0.6 V and +0.4 V and held for 20 sec. at each potential.

electroactivity. For example, PP/PSS films, cycled in $LiClO_4$/PC, lose their electroactivity within 10 cycles. The same behaviors is exhibited in TBAI/PC and NaI solutions, indicating that the ion transport is hampered as the solvent system becomes non-polar. In contrast, a PP/PSS film in TEACl/PC is quite stable during redox cycling (ca. 50 scans), but subsequently exhibits a rapid loss of electroactivity during potential stepping as shown in Figure 3-3d. This indicates that the electrolytes, as well as the solvent, can influence the ion exchange and stability in some cases.

3-2-4 Ion/Solvent Exchange and Long-Term Stability of PP-TOS

PP-TOS, the most stable of the systems investigated above in aq. $LiClO_4$ solutions, was also electrosynthesized from a 0.1 M PC solution of TEATOS and 0.1 M pyrrole and its switching response examined in monomer free electrolyte. Its electrochemical response during potential cycling was compared to that of PP-TOS prepared from a 0.1 M aq. solution of NaTOS and 0.1 M pyrrole. The cyclic voltammograms in Figure 3-4 (Left) demonstrate that the electroactivity of PP-TOS (ca. 2 μm, electrodeposited from aqueous NaTOS) increases with the number of scans in NaCl (aq.). A similar electroactivity increase was observed for PP-TOS (ca. 1 μm) in $NaBF_4$ (aq.). On the other hand, a rapid stabilization of the electroactivity of PP-TOS, switched in various electrolyte solutions (aq.), including NaCl (aq.), has been reported [123] with an $E_{1/2}$ = 0.0 V. The cyclic voltammogram of Figure 3-4 (Right) shows the redox peak change of PP-TOS (ca. 400 nm, electrodeposited from TEATOS/PC) in 0.1 M TEACl /PC. While the peaks at ca. 0.0 V (E^{red}) and +0.2 V (E^{ox}) decrease in intensity, the peaks at -0.3 V (E^{red}) and -0.1 V (E^{ox}) grow, maintaining a constant total electroactivity. It is believed that the redox pair at the more positive potentials results from cation transport to balance the charge of TOS^- anions remaining in the film [123]. These TOS^- anions continue to be released out of the film with scanning, which leads to the decrease of the higher potential redox peaks and the growth of the lower potential redox pair. This

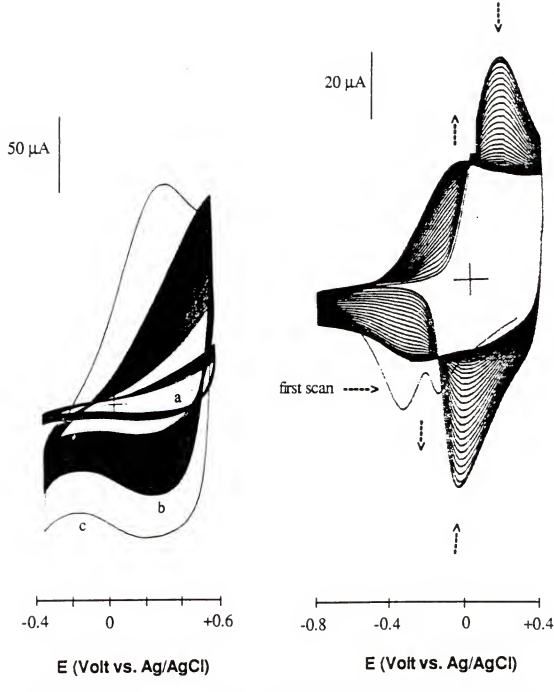

Figure 3-4 Cyclic voltammograms of PP-TOS during scanning at 100 mV s^{-1}. (left) 2 μm thick, synthesized from 0.1 M aq. solution of NaTOS and pyrrole, cycled in a 0.1 M NaCl (aq.). (a) initial 50 scans, (b) 100th to 250th scans, (c) equilibrated CV after 450 scans; (right) 400 nm thick film, synthesized from 0.1 M TEATOS and 0.1 M pyrrole in PC, cycled in 0.1 M TEACl/PC. The CV shows 30 scans.

appears to be a characteristic of the switching medium since the same compensatory behavior was observed when PP-TOS, synthesized from 0.1 M NaTOS (aq.), was cycled in 0.1 M TEACl/PC. It should also be noted that PP-TOS films cycled in $LiClO_4$/ACN show a rapid loss of electroactivity within the initial 10 scans. Compared to the complete electroinactivity of PP/PSS films when cycled in $LiClO_4$/PC, this indicates that complex ion exchange processes occur with PP-TOS films.

The long-term stability of PP-TOS films, electrosynthesized from TEATOS (PC) and TEATOS (aq.) was examined in TEATOS (PC). Although they showed similar cyclic voltammograms, the stabilities to multiple potential switching steps are markedly different as seen in Figure 3-5. Similar to PP/PSS and PP-Cl, PP-TOS films exhibits that the use of different solvents during electrodeposition and redox switching should be avoided to obtain the highest long-term stability.

Figure 3-5 also demonstrates the effect of the switching supporting electrolyte on the long-term stability in PC solutions. In this example, PP-TOS films (400 nm) were synthesized in TEATOS (PC) and redox switched in PC solutions of various supporting electrolytes. Extremely good electroactivity stability of $> 80\%$ was observed after 5000 switches using TEATOS as the switching medium. Interestingly, $LiN(SO_2CF_3)_2$ also showed a relatively high electroactivity stability of 80 % after 2000 switches.

3-3 Conclusions

Ion/solvent exchange processes, and long-term stabilities of PP, are affected by the electrolyte and solvent used for electropolymerization and redox switching. The film composition determines the permeability of dopant ions when different solvents are used between electropolymerization and redox switching.

While PP-Cl (aq.) is electroinactive in organic solvent media, PP/PSS films cycled in ACN electrolyte solutions show a similar electroactivity and long-term stability to those in aqueous electrolyte solutions, indicating that the high ionic conductivity of PP/PSS

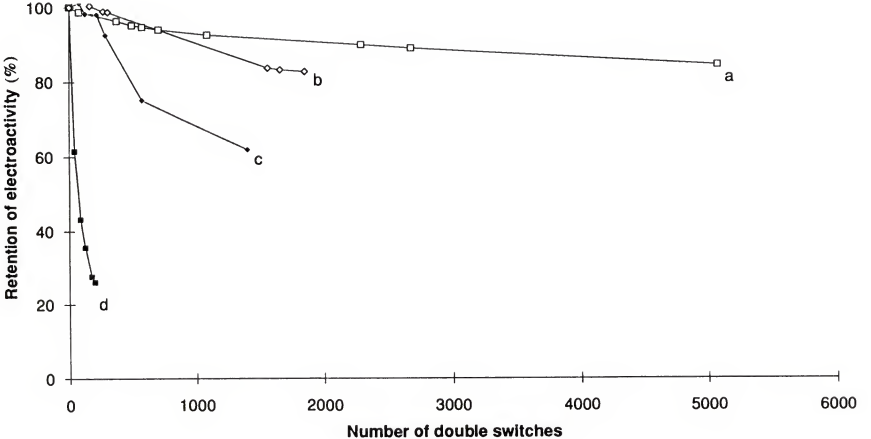

Figure 3-5 Redox switching stability of PP-TOS films with switching conditions as in Figure 3-1. PP-TOS films were synthesized from (a) and (b) PC, (c) aq., and (d) ACN solutions containing 0.1 M TEATOS and 0.1 M pyrrole, and redox switched in (a) 0.1 M TEATOS/PC, (b) 0.1 M $LiN(SO_2CF_3)_2$/PC, (c) 0.1 M TEATOS/PC, and (d) 10 mM $Zn(BF_4)$ and 0.1 M $NaClO_4$/PC.

can compensate for the energy barrier resulting from different solvent systems. In some cases, PP/PSS is electroactive in PC but unstable during the long-term stepping experiments. These facts suggest that the electroactivity of conducting polymers is determined by the solvent polarity differences between polymerization and redox switching as well as the ionic conductivity within the matrix. The electroactivity and long-term stability of PP-TOS films are also dependent on the solvent system. The best long-term stability is obtained when the same solvent system is used in electropolymerization and redox switching.

CHAPTER 4
COMPLEX ION TRANSPORT OF PP/PSS

It is well known that the ion transport during redox switching of conducting polymers is accompanied by co-ions and neutral species (e.g. solvent, salt) movement along with the dominant mobile counter ions. Of these, co-ions transport contributes to the overall charge balance along with counter ions. The extent of co-ion contribution appears to be dependent on the relative mobility of both counter ions and co-ions in the polymer matrix and the electrolyte solution respectively. For example [70], while the charge is maintained mainly by *p*-toluene sulfonate (TOS^-) release during reduction of PP-TOS films in 0.1 M NaCl, this process is also accompanid by Na^+ incorporation into the polymer matrix for the charge balance of TOS^- remaining in the film. Analysis of PP-TOS film reduced in CsCl shows similar cationic content. On the other hand, reduced PP-Cl exhibits less incorporation of cations than does PP-TOS. This indicates that the complex ion transport behavior of electroactive polymers is a strong function of ionic mobilities. Many authors have been studied this subject and their work was detailed in Chapter 1.

Ion transport of PP/PSS, which is known to be cation dominant due to entrapped anionic polyelectrolytes, is also complicated by an anionic contribution at high potentials (potential dependent dual ion transport). It has been reported [77] that the cation dominant transport of PP/PSS at $E < -0.2$ V (vs. SCE) is followed by anion dominant transport at $E > -0.2$ V as evidenced by the EQCM determined mass responses.

In this chapter, the potential dependent dual ion transport behavior of PP/PSS will be described using electrochemical, luminescence probe and microgravimetric methods. The scan rate dependencies of peak currents were compared in NaCl and sodium naphthalene sulfonate (NaNS) solutions. This was carried out to confirm the deviation from the linear i_p-v relationship when large sized-ions are involved in the ion movement. The contribution of anions to charge compensation during redox processes of PP/PSS films was examined with naphthalene sulfonate anions (NS^-) as a luminescence probe. Luminescence intensity changes were monitored as NS^- incorporated PP/PSS films were reduced in NaCl solutions. This process is schematized in Figure 4-1. The top route occurs when the ion transport of PP/PSS is cation specific, while the bottom route indicates a mobile anion. This behavior was further investigated by monitoring EQCM determined mass changes of PP/PSS films during potential stepping and cycling in various electrolyte solutions.

4-1 Experimental Details

Pyrrole was passed over neutral alumina until colorless before use. Electrolytes, including NaCl, NaBr, $NaClO_4$, sodium *p*-toluene sulfonate (NaTOS), and sodium naphthalene sulfonate (NaNS), were used as received. Electrolyte and/or monomer solutions were prepared with double distilled water and were Ar purged before use.

PP/PSS films made on Pt (ca. 800 nm, 0.02 cm^2) were cycled in 0.1 M NaCl and NaNS solutions and cyclic voltammograms were recorded to investigate the effect of anions on current responses. PP/PSS films prepared on Au (ca. 400 nm, 0.71 cm^2) were redox switched in various electrolyte solutions for the study of mass responses resulting from ion movement. For luminescence measurements, films on Pt (ca. 800 nm, 1.5 cm^2) were redox cycled in 10 mM NaNS to equilibrate the electroactivity and subsequently fully oxidized to incorporate NS^-. Luminescence intensity changes during redox switching of the PP/PSS were monitored in 0.1 M NaCl

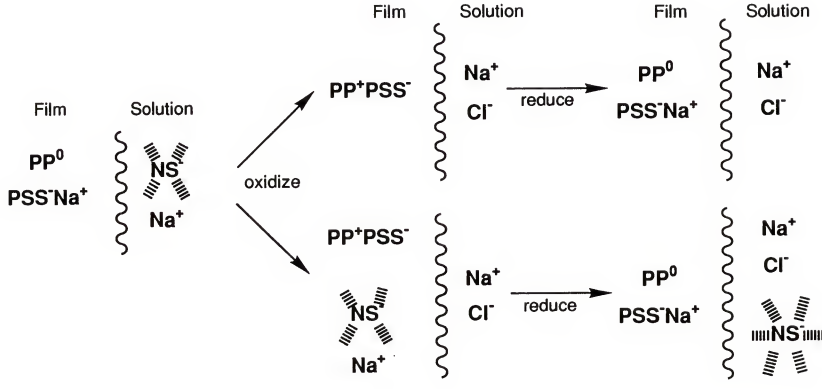

Figure 4-1 Schematic diagram showing a luminescence probe method to elucidate anion involvement in the ion transport of PP/PSS.

solutions. The Ag/AgCl reference and Pt counter electrode were used in most cases. For in situ luminescence measurements, a Ag wire quasi-reference electrode was utilized. Instrumentation for these studies was detailed in Chapter 2.

Typical thicknesses of PP/PSS films were measured with a profilometer (Sloan Dektak II). Correlation between the film thickness obtained and the charge passed during electropolymerization is shown in Figure 4-2 and gives a linear proportionality with the correlation factor of 0.998. The PP/PSS film thicknesses, mentioned throughout this dissertation, are based on these results.

4-2 Dual Ion Transport of PP/PSS

4-2-1 Cyclic Voltammetric Studies

A PP/PSS film prepared on a Pt button electrode was cycled in 0.1 M NaCl and 10 mM NaNS at varied scan rates. Figure 4-3 shows cyclic voltammograms as a function of scan rate between -1.0 V and +0.2 V. The peak separations are greater in NaNS than in NaCl, due to the low concentration of the electrolyte in the 10 mM NaNS solution. A plot of the cathodic peak current vs. scan rate is shown in Figure 4-4, indicating different i_p-v relationships. The linear relation seen when PP/PSS is cycled in NaCl suggests that the redox process follows a surface bound mode. The relation observed in NaNS solutions deviates from linearity and shows a proportionality of i_p to $v^{0.58}$. Although it has been reported [60] that PP/polyelectrolyte films shows a linear i_p-v relationship due to small cation dominant transport, that is not always the case. In this example, the deviation from linearity indicates that NS^- is involved in the redox process. In the case that anion movements occur only in high potential regions, as suggested by Smyrl et al. [77], the i_p-v relation should be linear. Therefore, the non-linearity seen in Figure 4-4 suggests that anions are moving even in the low potential regions ($E < 0.0$ V). It should be noted that the i_p-v relation in NaCl is not influenced by anion transport due to the small size of the anion. The relative contribution of

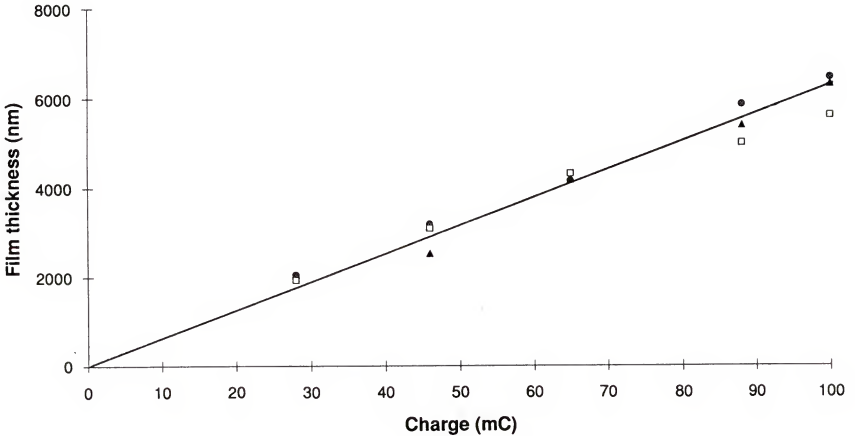

Figure 4-2 PP/PSS film thicknesses (measured by profilometry) vs. polymerization charges.

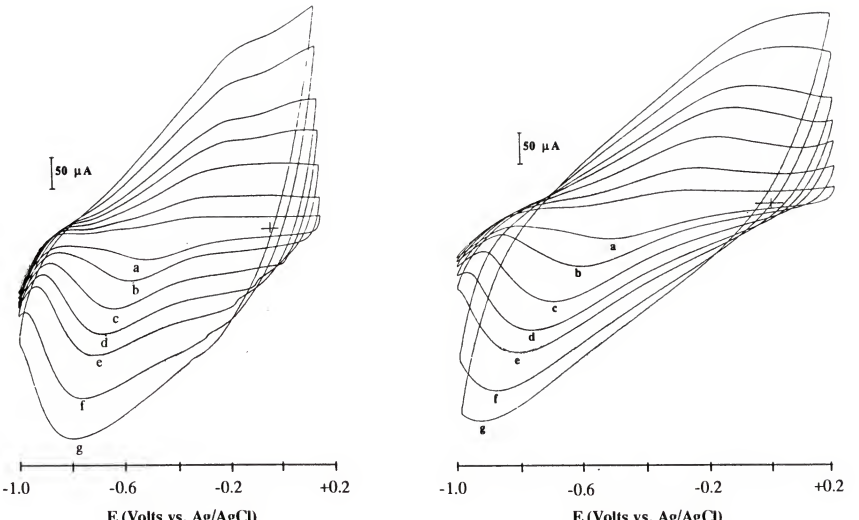

Figure 4-3 Cyclic Voltammograms of PP/PSS in (left) 0.1 M NaCl and (right) 10 mM NaNS solutions. (a) 10 mV s^{-1}, (b) 25 mV s^{-1}, (c) 50 mV s^{-1}, (d) 75 mV s^{-1}, (e) 100 mV s^{-1}, (f) 150 mV s^{-1}, and (g) 200 mV s^{-1}.

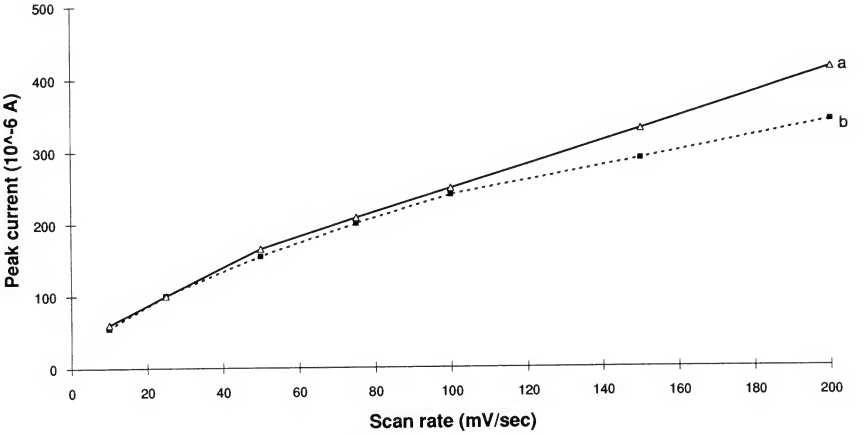

Figure 4-4 Peak currents vs. scan rates of PP/PSS films cycled in (a) 0.1 M NaCl and (b) 10 mM NaNS solutions.

anions and cations appears to change with potential, leading to anion dominant transport at high potentials. This will be addressed further.

4-2-2 Luminescence Probe Methods

To confirm the dual ion transport of PP/PSS more directly, luminescent probe techniques were employed. Luminescent probe methods have proven useful in ion transport studies of conducting polymers [49]. Probe anions (NS^-) are incorporated into a polymer matrix by oxidizing a fully reduced PP/PSS film in a NaNS solution. Upon subsequent reduction of the film, luminescent intensity changes in the switching medium are monitored, to confirm if NS^- anions are involved in the ion transport of PP/PSS.

PP/PSS films were oxidized in 10 mM NaNS solutions in which NS^- serves as an anionic probe. The films were immediately reduced at -0.2 V (vs. Ag/AgCl) in a 10 ml aqueous solution of 0.1 M NaCl. A portion of the NaCl solution was placed in a cuvette and fluorescent intensity changes were monitored with time. Figure 4-5 shows fluorescent intensity increase with reduction time (0.5, 1.0, 1.5, 2.0, 4.0, 5.0, 10.0, 15.0 min.), suggesting that NS^- is released immediately upon switching and continue to slowly leave the film. This result supports the conclusion that both mobile anions and mobile cations play a role in charge balance during PP/PSS redox processes.

Luminescence intensity changes were also monitored in situ during potential scanning. A fully reduced PP/PSS film was oxidized at +0.2 V (vs. Ag wire) in a 0.01 M NaNS solution for 10 minutes to allow the film to attain equilibrium concentrations of both ionic species and solvent. After thorough washing, it was subsequently redox cycled from -0.7 V to +0.2 V (vs. Ag wire) in a 0.1 M aqueous NaCl solution at a scan rate of 10 mV s^{-1}. Concurrent with this cycling, the luminescence intensity of the solution was monitored at 340 nm as shown in Figure 4-6 (curve a) along with the background fluorescence of the solution (curve b) due to

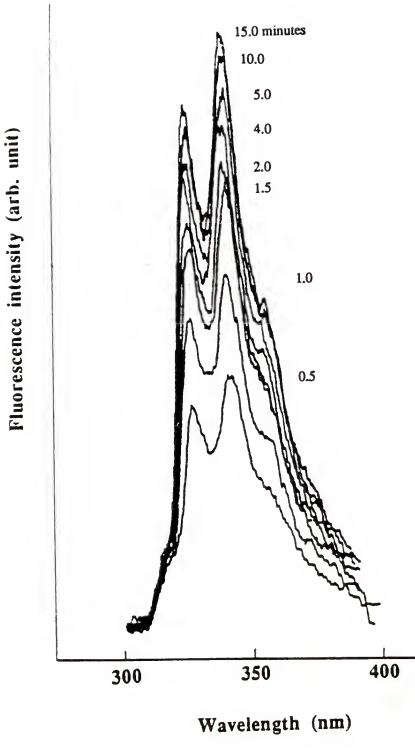

Figure 4-5 Fluorescence intensity increases during reduction of PP/PSS at -0.2 V (vs. Ag/AgCl) in a 10 ml NaCl solution. Measurements were made at 0.5, 1.0, 1.5, 2.0, 4.0, 5.0, 10.0, and 15.0 min. after reduction of PP/PSS which was fully oxidized in a 10 mM NaNS solution.

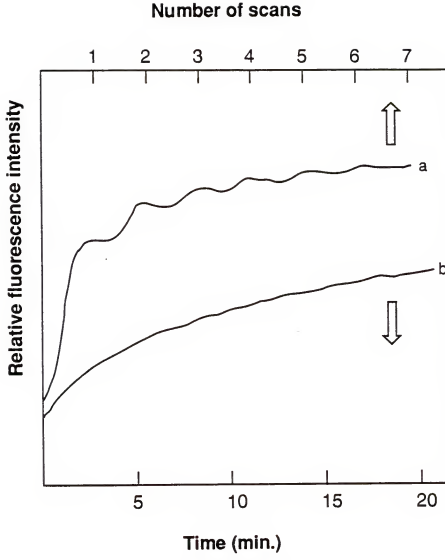

Figure 4-6 (a) Fluorescence intensity changes of 0.1 M NaCl during redox switching of NaNS treated PP/PSS. The film was repeatedly redox cycled at 10 mV s^{-1} between -0.7 V and +0.2 V. (b) Background solution fluorescence due to spontaneous anion exchange of NaNS treated PP/PSS at open circuit.

spontaneous release of NS^- from the film. Spontaneous ion exchange is commonly seen in PP and has been studied quantitatively [80]. The increased overall fluorescent intensity observed during redox cycling indicates that the electrochemical switching has increased the rate of ion exchange with the electrolyte. The time dependent modulation of the fluorescence indicates that the NS^- species are moving in and out of the polymer to some extent during redox switching.

4-2-3 Gravimetric Studies

To examine this in more detail an EQCM study was carried out with a single PP/PSS film. A PP/PSS film was cycled between -1.0 V and +0.2 V (vs. Ag/AgCl) at 25 mV s^{-1} in various aqueous electrolyte solutions including 0.1 M NaCl, NaBr, $NaClO_4$, NaTOS, and 10 mM NaNS (Figure 4-7). While the frequency increases due to Na^+ expulsion are evident in the electrolytes consisting of small anions (Figures 4-7a,b,c) up to -0.2 V, the frequency responses begin to drop at -0.3 V in the electrolytes containing large anions (Figure 4-7d,e). The ratio of anion to cation contribution for the charge balance increases with the increase of the potential as evidenced by the magnitude of the frequency decreases in the high potential regions, indicative of anion dominant transport. It should be noted that the magnitude of the frequency drop is not proportional to the anionic mass with surprisingly large frequency drop observed for the PP/PSS films cycled in NaTOS and NaNS. Since drastically different solvent transport mechanism with the electrolyte is unlikely, the large frequency change is believed to be due to the organic characters of TOS^- and NS^-, which exhibit more facile ionic diffusion through PP matrix.

The effect of varied amounts of NaNS on the ion transport properties of PP/PSS was examined in solutions of constant ionic strength. This is illustrated in Figure 4-8 for solutions having a total electrolyte concentration of 10 mM. As the relative NS^- composition is increased, it can be seen that the anion contribution becomes more and

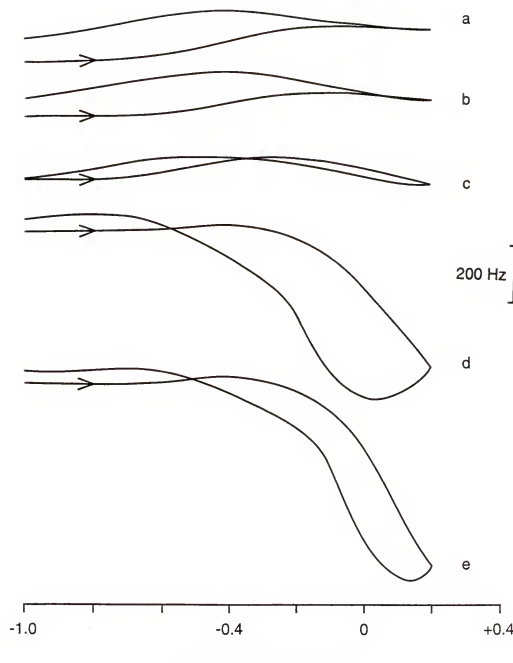

Figure 4-7 Frequency responses of PP/PSS cycled at 25 mV s^{-1} in 0.1 M (a) NaCl, (b) NaBr, (c) $NaClO_4$, (d) NaTOS and 10 mM NaNS aq. solutions.

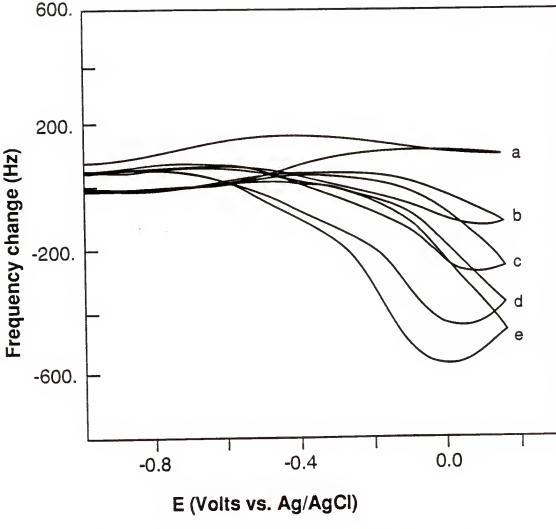

Figure 4-8 Frequency responses of PP/PSS redox cycled at 25 mV s^{-1} in combined NaCl and NaNS electrolytes of constant ionic strength. (a) 10 mM NaCl, (b) 7.5 mM NaCl + 2.5 mM NaNS, (c) 5 mM NaCl + 5 mM NaNS, (d) 2.5 mM NaCl + 7.5 mM NaNS, and (e) 10 mM NaNS.

more dominant indicating that, in spite of their large size, the NS^- anions are quite mobile. This strongly points to the possibility of ion-pair formation and transport in order to retain charge neutrality within a film.

4-3 Conclusions

The ion transport behavior of PP/PSS was investigated using electrochemical, luminescent, and microgravimetric methods. Anion incorporation and release were evident while the ratio of the mobile anions to cations changes with the potential. It was also found that anion transport becomes more dominant when large anionic electrolytes were used.

CHAPTER 5
POLY(PYRROLE ADENOSINE 5'-TRIPHOSPHATE)

There have been several attempts [107] to utilize the ion transport behavior of conducting polymers for ion release devices since Zinger and Miller [107A] reported the controlled release of a neurotransmitter from a polymer coated electrode. Various cationic drugs, such as dopamine and phenothiazine, have been incorporated into cation dominant conducting polymers during reduction and anodically released [107C]. It has also been shown that anionic drugs such as glutamate can be cathodically released in a controlled manner [107A,B]. These systems, however, may exhibit spontaneous drug release, which has hampered development of drug release devices.

Adenosine 5'-triphosphate (ATP) is an important material in biological systems for energy storage and conversion. The hydrolysis of ATP to adenosine 5'-diphosphate (ADP) produces ca. 30 kJ mol^{-1}, which is readily transferred to assist other reactions. Such reactions would be energetically unfavorable in the absence of ATP. An example of this kind of energy transfer is the reaction occurring in the Calvin cycle. The hydrolysis of ATP to ADP provides both the energy and the phosphate group, which phosphoglyceric acid needs for conversion to diphosphoglyceric acid [125].

In this chapter, the electrochemically stimulated release of ATP from poly(pyrrole ATP) (PP-ATP) modified electrodes will be described and this fast ion supply will be compared to relatively slow spontaneous ATP exchange at open circuit. ATP ions are inert towards hydrolytic cleavage during both synthesis and this potential driven release, suggesting that these electrodes may be useful as ATP supply devices. In that

ATP is a multi-ionic species (charge of -3 at pH = 3 to 5 and fully ionized above pH = 7) [125B], and has a relatively high molecular weight (503.18 g mol^{-1} for ATP^{4-}) as shown in Figure 5-1, it is not surprising that PP-ATP is relatively stable to spontaneous ion exchange processes. It has been reported [126] that PP-ATP shows varied electrochemical behaviors in different electrolyte solutions. PP-ATP films cycled in NaCl solutions showed two separate redox processes with increased electroactivity over those cycled in ATP solutions. The observation of these two processes was attributed to sites accessible to only Cl^- ions which are present in the PP matrix. The possibility of ATP release from PP-ATP, however, was not mentioned. More recently, it has been demonstrated [127] that poly(pyrrole chloride) (PP-Cl), prepared by a potential scan driven anion exchange of PP-TOS in a NaCl electrolyte, is electroactive in an ATP solution. The possibility of spontaneous release was not examined and the maximum amount of ATP release appears to be small when taking into account the usual doping level of PP films.

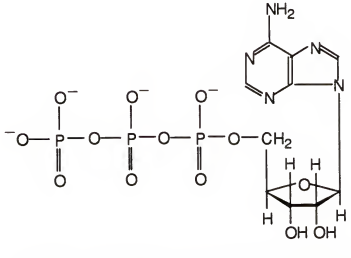

Figure 5-1 Structure of adenosine 5'-triphosphate (ATP)

5-1 Experimental Details

ATP disodium salt (Sigma Chemical), NaCl, CsCl (Aldrich), and $NaClO_4$ (Fisher Scientific) were used without further purification. PP-ATP films with various thicknesses were prepared by potentiostatic polymerization at +0.8 V versus Ag/AgCl, using 0.1 M pyrrole and 20 mM ATP in double distilled and filtered water. Adjustment of pH was not carried out since the polymerization rate is extremely slow at neutral pH and at a pH of ca. 3.4 where the polymerizations were carried out, ATP exists as tri-basic ions. PP-Cl films were also prepared to compare ATP release, using 0.1 M pyrrole and 0.1 M NaCl aqueous solutions. ATP was incorporated into PP-Cl by cycling in 20 mM ATP solutions. The working electrode of the Electrochemical Quartz Crystal Microbalance (EQCM) used for microgravimetric studies was a gold coated quartz crystal, and for spectroscopic studies a Pt plate (1.50 cm^2) was used. The counter electrode was a Pt plate with Ag/AgCl and Ag wire reference electrodes for gravimetric and spectroscopic studies, respectively. Voltammetric studies were carried out on a Pt button electrode with the Ag/AgCl reference and Pt counter electrodes. After electrosynthesis, films were thoroughly rinsed with water and placed in aqueous solutions of various monomer free electrolytes (pH = ca. 5.4).

Capillary zone electrophoresis (CZE) separations [128] of 25 mM NaCl solutions in which PP-ATP films had been reduced at -0.5 V (vs. Ag wire) were carried out to examine the stability of ATP ions subjected to the electropolymerization and electrochemically stimulated release conditions. Separations were performed using fused silica capillaries coated with polyimide (Polymicro Technology). The capillaries (50 μm inner diameter and 350 μm outer diameter) were treated with successive 10 minute rinses of 0.1 M NaOH, H_2O and migration buffer (25 mM sodium phosphate, pH = 7.0). Capillary lengths were 70 cm with an inlet to detector distance of 35 cm. Separations were carried out by applying high voltage (25,000 V) with sample introduction at the high voltage end of the capillary. Hydrodynamic injections

were performed by inserting the inlet of the separation capillary in the sample vial and raising the vial 10 cm for 10 seconds. These conditions result in an injection volume of 2 nl as calculated from the Hagen-Poiseuille equation. Detection was accomplished using a Spectra 100 (Spectra-Physics) variable wavelength detector set at 259 nm. The detector rise time was 1.0 second and was operated at 0.005 absorbance units full scale.

Chronogravimetric, chronocoulometric and UV-Vis absorbance studies were carried out to examine the controlled release of ATP from the PP-ATP films. Mass changes of PP-ATP films in 0.1 M NaCl aqueous solutions at open circuit and -0.5 V (vs. Ag/AgCl), were monitored by the EQCM. Frequency changes of PP-ATP films in various electrolytes were also investigated during potential cycling. ATP concentration changes versus time of 0.1 M $NaClO_4$ and NaCl solutions (aq.) due to ATP release from PP-ATP films were measured in situ using a Cary 5E UV-Vis-NIR spectrophotometer, controlling electrode potentials with an EG&G Model 273 potentiostat/galvanostat. Films prepared on a Pt plate were placed in a cuvette and potentials were applied relative to Ag wire.

5-2 ATP Release from ATP Exchanged PP-Cl films

In order to determine if ATP is mobile in PP-Cl, EQCM measured frequency changes of PP-Cl films were monitored during cycling in 20 mM disodium ATP solutions. PP-Cl films were prepared in 0.1 M pyrrole and 0.1 M NaCl aqueous solutions. Figure 5-2 shows the frequency changes when the electrode is cycled between -0.6 V and +0.2 V (vs. Ag/AgCl). It should be noted that the electroactivity of PP-Cl cycled in ATP solutions is not inhibited when compared to that cycled in NaCl solutions. From Figure 5-2, it is evident that ATP can be reversibly incorporated and released since the frequency decrease during the anodic scans, indicating mass gain, is recovered during the cathodic scans. The frequency difference at -0.6 V can be

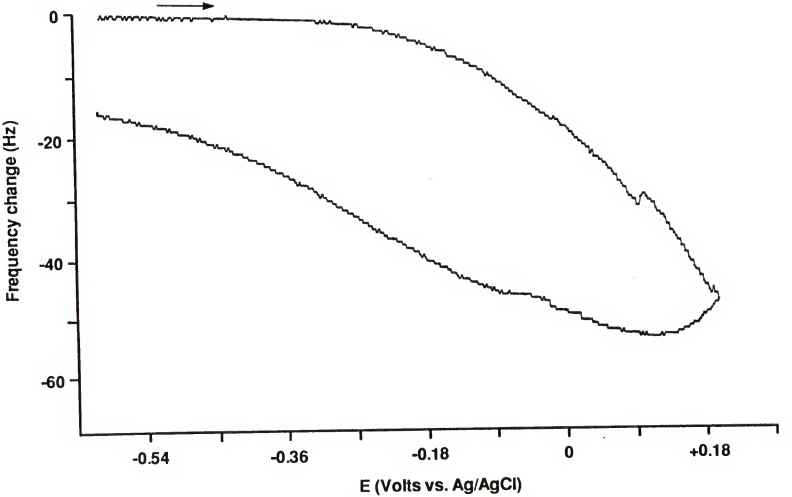

Figure 5-2 Frequency changes of PP-Cl (300 nm), cycled between -0.7 V and +0.2 V in 20 mM ATP solutions

attributed to the difference in the extent of reduction of the film and non-equilibrium concentration of ions and solvent as opposed to permanent ATP entrapment.

This was further verified by monitoring frequency changes during potential stepping. The same film was subjected to repeated potential steps from -0.7 V to +0.2 V and subsequently from +0.2 V to -0.7 V (vs. Ag/AgCl). Figure 5-3 shows the frequency responses during these repeated potential steps. As expected, the first potential step leads to a frequency drop, indicative of ATP incorporation, while the second step increases the frequency as ATP is released. In this instance, the magnitude of the frequency changes for these two processes are the same within experimental error. This suggests that anodically incorporated ATP is cathodically released and does not reside in the polymer matrix. The EQCM results shown above, however, do not preclude possible spontaneous ATP release.

PP-Cl (ca. 300 nm) films, prepared on a Au quartz, were cycled to equilibrate the redox process and held in a 20 mM NaATP solution for 10 min. applying +0.2 V (vs. Ag/AgCl) to incorporate ATP. The films was thoroughly washed with double distilled water and placed in 3 ml of 0.1 M NaCl (aq.). Figure 5-4 compares the UV absorbance changes of NaCl solutions subjected to both electrochemical and spontaneous release of ATP. The spectra were taken after leaving the film at open circuit for 3 hours (Figure 5-4a) and at -0.5 V for 10 min. (Figure 5-4b). The frequency of the microbalance, observed during the electrochemical release at -0.5 V, does not change after 3 min., indicative of complete reduction of the PP film. Interestingly, UV absorbances from these two experiments are quite close, indicating that spontaneous ATP release is fast and complete within 3 hours. These results show that the post-ATP incorporation process is inadequate for ATP release devices.

The fraction of released ATP to the total number of accessible sites was investigated using the post-ATP incorporation of PP-Cl. The number of PP repeating units deposited was obtained from the charge consumed (72 mC) during PP-Cl synthesis and

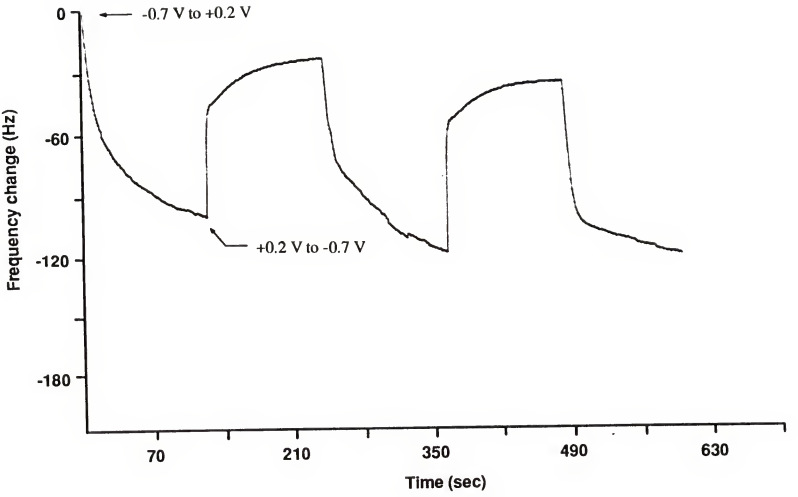

Figure 5-3 Frequency changes of PP-Cl (300 nm), stepped between -0.7 V and +0.2 V in 20 mM ATP solutions

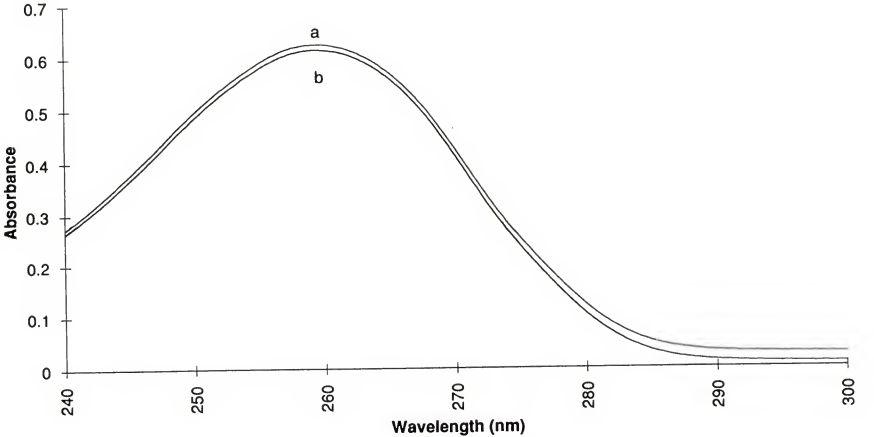

Figure 5-4 UV absorbance increases due to ATP release from ATP incorporated PP-Cl films (300 nm). ATP was incorporated by cycling 10 times and holding the potential at +0.2 V (vs. Ag/AgCl) for 10 min. After thorough washing, films were placed in 0.1 M NaCl solutions. (a) shows spontaneous ATP release after 3 hours and (b) electrochemically induced ATP release at -0.5 V (vs. Ag/AgCl) after 10 min.

the assumption that PP films show a 25 % to 35 % doping level [52]. Assuming a 30 % doping level, 2.26 x 10^{-7} moles of PP repeating units were deposited during electropolymerization. This value was used to calculate the number of moles of ATP which was incorporated during cycling in ATP solutions. Since ATP is present as a tri-anionic dopant in a 20 mM ATP solution of pH = 3.4 (at equilibrium, 4.8 % of ATP^{2-} and 95.2 % of ATP^{3-}), ca. 10 PP repeating units of 30 % doping level are charge balanced by one ATP molecule. Thus, ca. 2.26 x 10^{-8} moles of ATP is required to balance of 2.26 x 10^{-7} moles PP repeat units, when Cl^- is completely exchanged with ATP^{3-}.

The number of moles of ATP released in a 3 ml NaCl solution was calculated using the extinction coefficient of 15.4 x 10^3 M^{-1} cm^{-1} [129] and the maximum absorbance (0.62 from Figure 5-4a) at 260 nm. Quite surprisingly, an order of magnitude higher concentration (1.98 x 10^{-7} moles) than the maximum expected (2.26 x 10^{-8} moles) was obtained. One possible explanation of this is that an excessive amount of ATP sodium salt molecules can be adsorbed through the pores in the polymer matrix and on the polymer film surface. These molecules are released during subsequent reduction, likely due to morphology changes during redox switches.

5-3 Electrochemical Preparation of PP-ATP films

Since an ion exchange process for ATP incorporation is not appropriate for the construction of ATP release devices due to fast spontaneous release, ATP release directly from PP-ATP films was studied. PP-ATP films were electrochemically prepared in 0.1 M pyrrole and 20 mM disodium ATP (pH = 3.4) aqueous solutions. Using the EQCM, both frequency and charge changes during electropolymerization at various pH's were monitored as shown in Figure 5-5.

Qian and Pei [40C,D] reported that the polymerization of pyrrole in a buffer solution is greatly affected by medium pH. They found that PP films produced at pH <

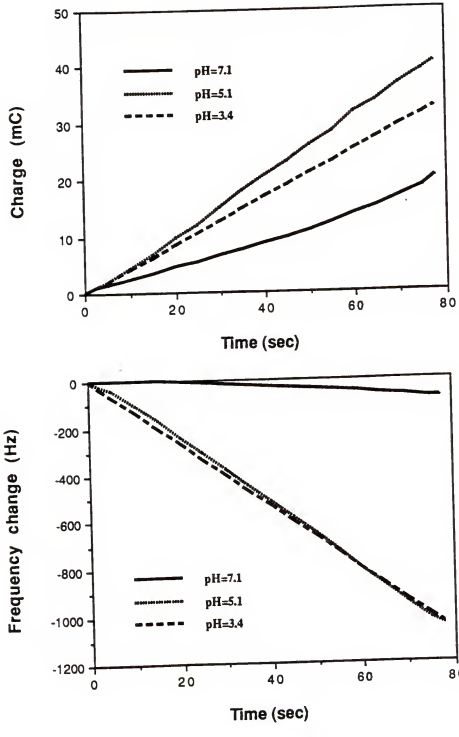

Figure 5-5 Charge (top) and frequency (bottom) changes at various pH's during PP-ATP electrosynthesis.

3.5 gives uniform and highly conducting films, while films are non-uniform, or not produced, at pH > 4. The pH limit, at which polymerization becomes sluggish, depended on buffer species, supporting electrolytes, and working electrode substrates. They compared anodic current responses during polymerization by adding a H^+ scavenger into the polymerization media and proposed that the protonation of pyrrole before monomer oxidation is a rate determining step. Polymerization at high pH for a long time (30 min.) produced an electroinactive ultrathin layer, which prevents film formation. Their conclusions appear to hold in a buffered system and correspond to the results shown in Figure 5-5. Since disodium ATP also plays a role of buffer, maintaining bulk and electrode surface pH the same, it is not surprising that the polymerization charge at pH = 7.1 increases most slowly. This is more evident when frequency changes are compared. The frequency decrease at pH = 7.1 is negligible relative to those at low pH, indicating that virtually no film is formed at neutral pH solution. This appears to be due to mixed effects of fast H^+ removal, preventing protonation of pyrrole, and causing electroinactive film formation, as explained above. The difference between pH = 5.1 and 3.4 can be seen by the distinct differece in the charge vs. the number of polymer repeating units relationship shown in Figure 5-6. The number of polymer repeat units was calculated from the frequency changes in Figure 5-5 (bottom) using the Sauerbrey equation [87]. In Figure 5-6, the number of electrons (n) consumed per polymer repeat unit during electropolymerization can be determined from the slope. When compared to a reported n = 2.2 - 2.4 for the pyrrole polymerization [29,31], a higher n-value indicates that more electrons are needed to produce the same mass of polymer deposition. It was determined that more electrons are consumed as the pH becomes higher, supporting the fact that ultrathin layer formation affects film deposition in this study. Therefore, further polymerizations were performed without pH correction.

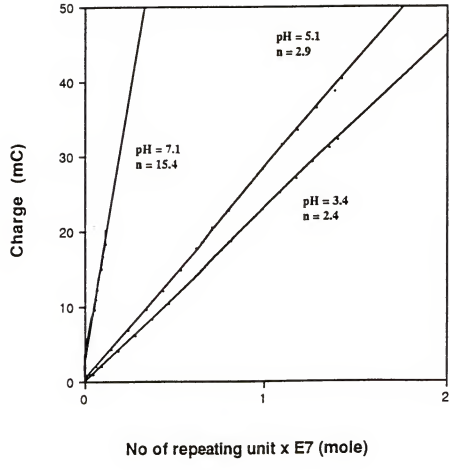

Figure 5-6 Charge vs. number of polymer repeat units during PP-ATP electropolymerization at various pH's.

5-4 Voltammetric Studies

Cyclic voltammetry of PP-ATP in various electrolytes was first studied by Boyle et al. [126]. They found that cyclic voltammograms of PP-ATP films, cycled in NaCl solutions, results in two separate redox pairs. The low potential redox process ($E_{1/2}$ = -0.33 vs. SCE) was proposed to be due to cation dominant transport and the high potential redox process ($E_{1/2}$ = -0.07 V vs. SCE) as anion dominant transport, which results in partial ATP release. However, no further experimental evidence was given for ion movement.

PP-ATP films were prepared on a Pt button electrode and potential cycled in various electrolytes. Figure 5-7 (left) shows cyclic voltammograms in 0.1 M NaCl, poly(styrene sulfonic acid) sodium salt (NaPSS), and poly(vinylpyridine hydrochloride) (PVPy·HCl) at 100 mV s^{-1}. When cycled in NaCl, two separate reduction peaks are observed, indicating that ATP is partially released and PP-ATP possesses potential dependent dual ion transport. PSS^- anionic polyelectrolytes and $PVPyH^+$ cationic polyelectrolytes in the switching medium do not penetrate into the film so that they cannot function as charge balancing ions because of their size. This allowed us to identify which ion transport mechanism was responsible for each redox pair. In a NaPSS solution, the high potential reduction peak is completely suppressed while the low potential redox peaks remain constant. The opposite behavior is observed in a $PVPyH^+$ solution, suggesting that the high and low potential redox processes are accompanied by anion and cation transport respectively.

The scan rate dependence of two redox peaks are shown in Figure 5-7 (right) in 0.1 M NaCl. It can be seen that the reduction peak currents for both processes are directly proportional to the scan rate. This indicates that the total electroactivity of the film is preserved and the redox reaction behaves as a surface bound mode as described in Chapter 1.

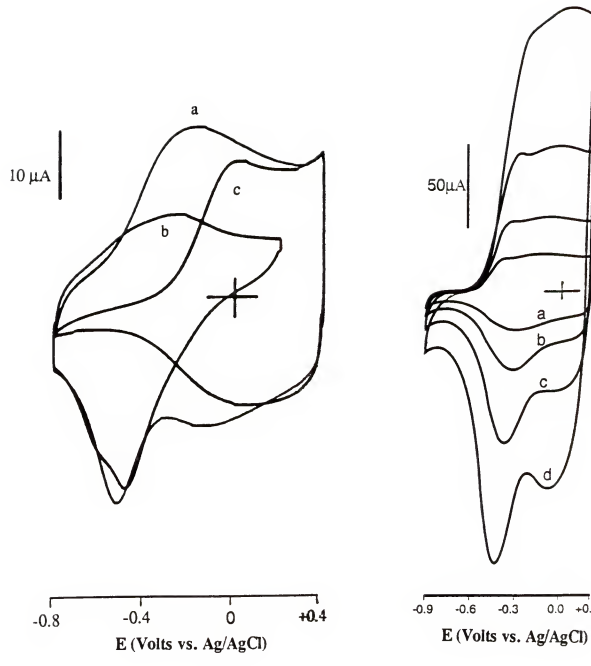

5-7 Cyclic voltammograms (left) of PP-ATP (450 nm on a Pt button) in 0.1 M (a) NaCl, (b) NaPSS, and (c) PVPy-HCl aq. solutions. v = 100 mV s^{-1} Cyclic voltammograms (right) of PP-ATP (800 nm on a Pt button) in 0.1 M NaCl at (a) 50 mV s^{-1}, (b) 100 mV s^{-1}, (c) 200 mV s^{-1}, and (d) 400 mV s^{-1}.

In order to further confirm the dual ion transport, which results from ATP release, the EQCM was utilized in various electrolytes. Figure 5-8 and 5-9 illustrates equilibrated frequency responses of PP-ATP films (ca. 200 nm and 500 nm) during potential cycling in 0.1 M CsCl, NaCl, and $NaClO_4$ aqueous solutions. Since anions are dominant mobile species at the high potentials, the frequency will decreases during anodic scans due to anion incorporation. Although this effect can be seen in $NaClO_4$, it is not obvious in CsCl and NaCl. This is partly attributable to continuous cation expulsion at high potentials, which balances frequency decreases by Cl^- to some extent. This can be verified by the fact that the frequency decrease in NaCl at E > -0.1 V is slightly greater than that in CsCl.

5-5 Electrochemically Stimulated ATP Release from PP-ATP

5-5-1 Spontaneous vs. Electrochemical ATP Release

Since the voltammetric results do not preclude the possibility of spontaneous ATP release, which can also show anion dominant transport at high potentials, ATP release was spectroscopically investigated. A PP-ATP film (ca. 500 nm) on a Pt flag electrode, prepared as described above, was placed in a 0.1 M $NaClO_4$ aqueous solution of 3 cm^{-3} at open circuit for 21 hours. Another film, prepared under the same conditions was cycled 9 times between -1.0 V and 0.0 V (vs. Ag wire) at 10 mV s^{-1} in the same solution. UV-Vis absorbance spectra for both solutions are shown in Figure 5-10 with a peak at 260 nm, indicative of ATP release. While the PP-ATP film is relatively stable to spontaneous ion exchange processes at open circuit, appreciable amounts of ATP were released during potential cycling over a much shorter time period. In fact, most of the ATP is released during the first scan with continued small increased increments in ATP concentration up to 9 scans (ca. 92 % of the accessible ATP). Further scanning shows no noticeable absorbance increase suggesting all of the accessible ATP is released from the film. In many cases, the mobile ionic species in electroactive

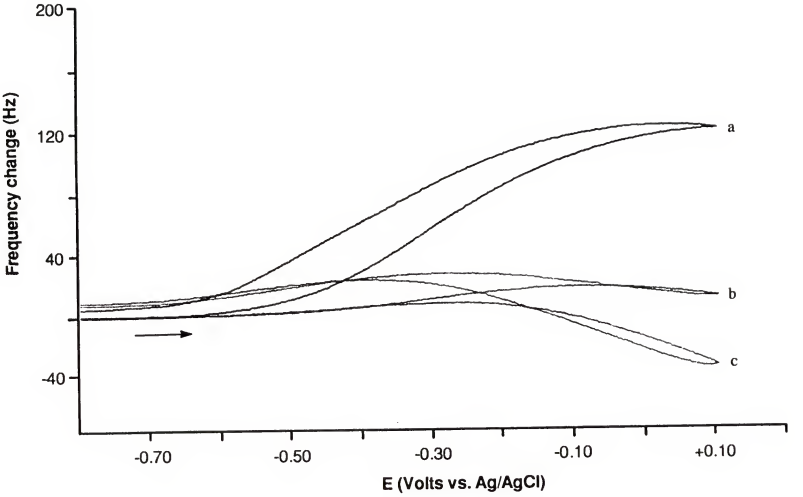

Figure 5-8 Frequency changes of PP-ATP (200 nm), cycled in 0.1 M (a) CsCl, (b) NaCl, and (c) $NaClO_4$ at 25 mV s^{-1}.

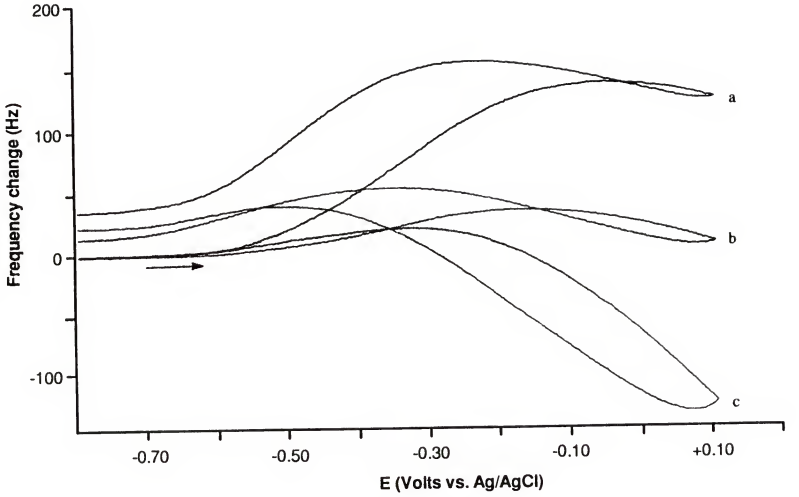

Figure 5-9 Frequency changes of PP-ATP (500 nm), cycled in 0.1 M (a) CsCl, (b) NaCl, and (c) $NaClO_4$ at 25 mV s^{-1}.

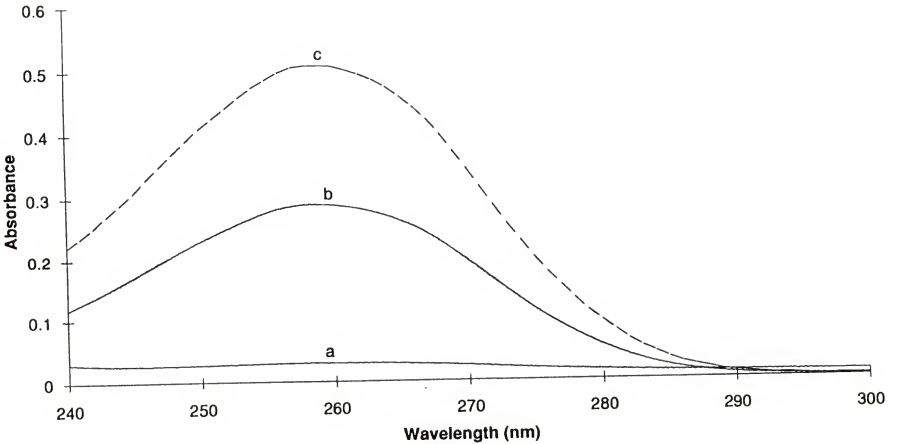

Figure 5-10 Comparison of electrochemically stimulated and spontaneous ATP release showing (a) no ATP release for 21 hours at open circuit, (b) concentration standard of 2×10^{-5} M ATP, and (c) *ca.* 70 % release of total ATP after 9 potential scans.

polymers during redox switching can also be spontaneously exchanged with bathing electrolyte. The fact that a negligible amount of ATP is released at open circuit indicates that, in the charged state of the polymer, the ATP is strongly electrostatically bound. The small amount of spontaneous ATP release without electrochemical switching is likely due to weakly bound ATP at the film surface.

5-5-2 Potential Dependent ATP Release

In order to determine the potential dependence of the ATP release, the UV absorbance of ATP was monitored at the wavelength of maximum absorption (260 nm), as the potential was stepped from 0.0 V (vs. Ag wire) where the PP is in its oxidized state, to varied negative potentials in 0.1 M $NaClO_4$. Fast electrochemically stimulated ATP release is evident from an immediate absorbance increase by stepping to -0.5 V (vs. Ag wire) where the PP is fully reduced as shown in Figure 5-11. With potential steps to -0.4 V or less, only small absorbance increases are observed as the ATP tends to remain entrapped in the film. Comparison of ATP release rates between step potential and potential cycling methods indicates that ATP is released much faster using the potential cycling method, suggesting that the equilibrium state is reached more quickly with cycling. These results suggest that the amounts of released ATP and its rate are tunable with carefully controlled potential applications to the electroactive polymer.

5-5-3 Electrolyte Effects on ATP Release

A PP-ATP film was placed in 0.1 M NaCl and $NaClO_4$ solutions and UV absorbance changes of the electrolyte during potential cycling were monitored at the wavelength of 260 nm (Figure 5-12). The film was initially in the oxidized state at 0.0 V (vs. Ag wire) and subsequently subject to cycling between 0.0 V and -1.0 V. The absorbance increase is not noticeable, until the potential reaches -0.5 V, which is

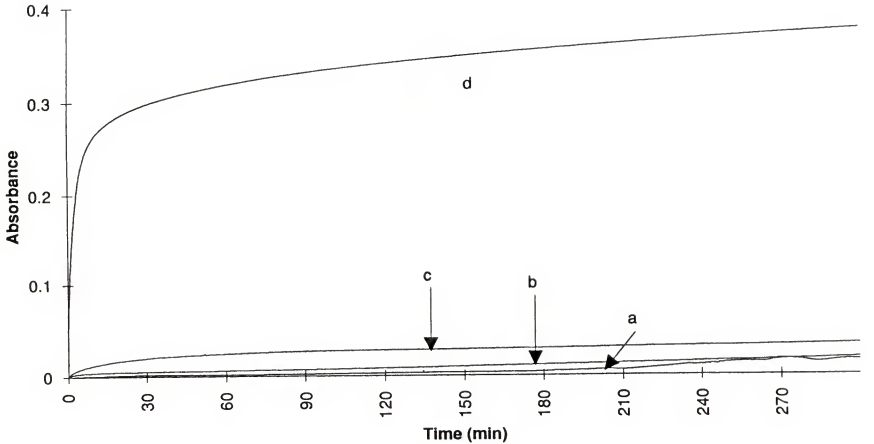

Figure 5-11 UV absorbance changes at 260 nm with various step potential applications in 0.1 M $NaClO_4$: (a) open circuit; from 0.0 V to (b) -0.2 V, (c) -0.4 V, and (d) -0.5 V (vs. Ag wire).

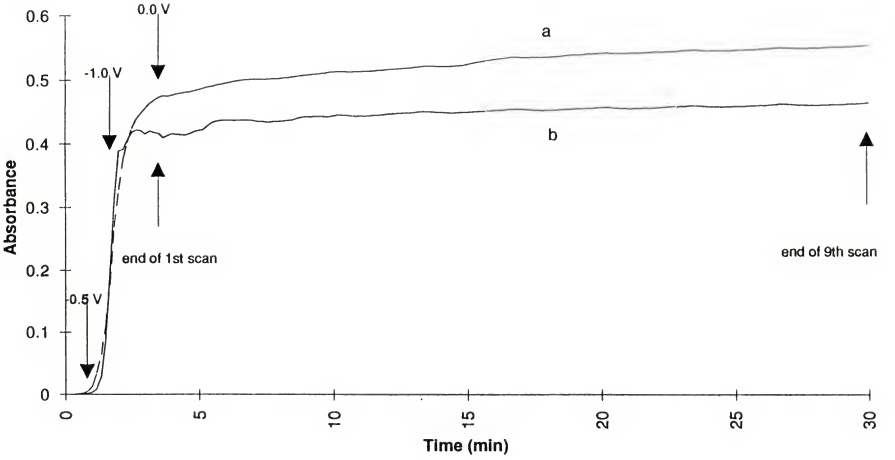

Figure 5-12 UV absorbance changes at 260 nm during potential cycling between -1.0 V and 0.0 V (vs. Ag wire) in 0.1 M (a) NaCl and (b) $NaClO_4$ at 10 mV s^{-1}.

consistent with the results shown in Figure 5-11. After passing the critical potential (-0.5 V), the absorbance increases rapidly, indicative of electrochemically stimulated ATP release. The absorbance increase to ca. 0.45 AU (> 80 % relative to the maximum absorbance after 9 scans) is observed during the first potential scan in both electrolytes. Further scans show only slight absorbance increases and reaches the maximum absorbance after ca. 9 scans.

Figure 5-12 also indicates that the amount of electrochemically releasable ATP is independent of electrolytes used since the similar maximum absorbances are observed in both NaCl and $NaClO_4$. This suggests that this ATP release system, applied to different electrolyte conditions such as buffered electrolyte solutions, will show similar behaviors.

The electrolyte effect on ATP release was further investigated using the EQCM. A PP-ATP film (ca. 500 nm) on a Au quartz crystal electrode was cycled between -0.9 V and +0.1 V (vs. Ag/AgCl) in a 0.1 M $NaClO_4$ solution at 25 mV s^{-1}. Another film, equilibrated by cycling in 0.1 M NaCl was subjected to electrolyte solution change to 0.1 M $NaClO_4$. Frequency changes of two instances were compared in Figure 5-13. It shows that the frequency decrease at E > -0.3 V, resulting from ATP release, is slightly greater when PP-ATP is pre-equilibrated in NaCl prior to cycling in $NaClO_4$. In spite of this small electrolyte dependence, the result of Figure 5-13 is consistant with the UV absorbance measurements shown in Figure 5-12 in that the identity of electrolytes does not drastically change the ATP release.

5-5-4 Stability of ATP during Electrochemical Release

Possible hydrolytic cleavage of ATP ions subjected to incorporation during electropolymerization and electrochemically stimulated release was examined by capillary zone electrophoresis (CZE). The CZE sample solution was prepared by reducing a PP-ATP film in 25 mM NaCl at -0.5 V (vs. Ag wire) for 1 hour. All CZE

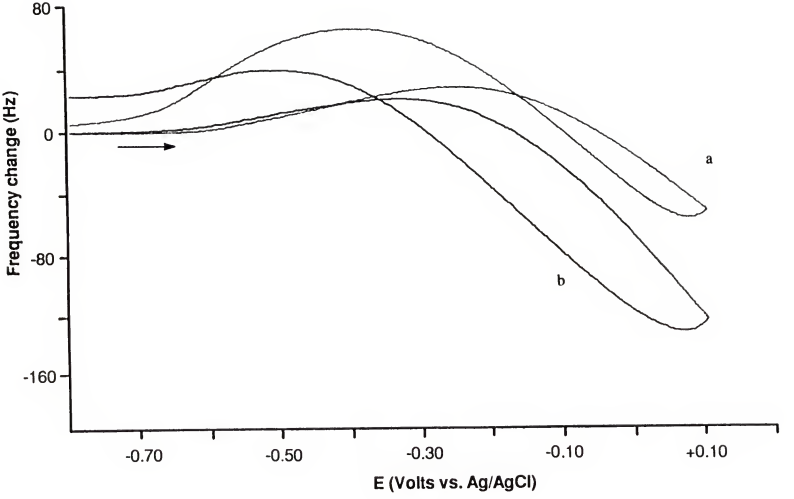

Figure 5-13 Frequency changes of PP-ATP (500 nm), cycled in 0.1 M $NaClO_4$ at 25 mV s^{-1}: (a) as made film and (b) after cycling in 0.1 M NaCl until equilibration.

separation results were obtained within 8 hours after preparing the solution. Retention times of this electrolyte was compared with those for a solution consisting of adenosine 5'-monophosphate (AMP), adenosine 5'-diphosphate (ADP) and ATP (ca. 2 mM each) as shown in Figure 5-14. It can be seen that the PP-ATP release solution contains only ATP, indicative of ATP stability during these electrochemical experiments. It should be noted that the small peak at 170 seconds also appears with a blank NaCl solution and its area does not vary with the injection volume of the ATP solution.

5-5-5 EQCM Studies during ATP Release

EQCM determined mass changes during ATP release were also investigated to support the spectroscopic results. PP-ATP films with the same thicknesses as used for spectroscopic studies were prepared on a Au coated quartz crystal. Frequency changes in 0.1 M NaCl were compared at open circuit (spontaneous exchange) and during step reduction of the polymer at -0.5 V (vs. Ag/AgCl) (Figure 5-15). The relatively stable frequency response (no net mass change) of the PP-ATP at open circuit is consistent with the spectroscopic result shown in Figure 5-10 and 5-11 as there is no evidence of ion exchange. Upon reduction at -0.5 V, a sharp frequency drop (mass gain) followed by a rather smooth frequency increase (mass loss) is observed. Examination of the charge passed during this reduction shows that ca. 11 mC out of 16.8 mC is passed during the initial frequency drop. From these results, it can be inferred that most of the reduced sites of PP-ATP films are initially ($t < 40$ sec) charge-balanced by the dominantly mobile Na^+ ions during the initial stage of reduction due to their faster diffusion rate. ATP sodium salts are subsequently ($t > 40$ sec) released during the later stage. It should be noted that the EQCM measures the net mass flux and these results do not preclude significant initial ATP release at short times.

The effectiveness of a PP-ATP film as an ATP release device can be confirmed by examining the ratio of electrochemically released ATP to initially incorporated ATP

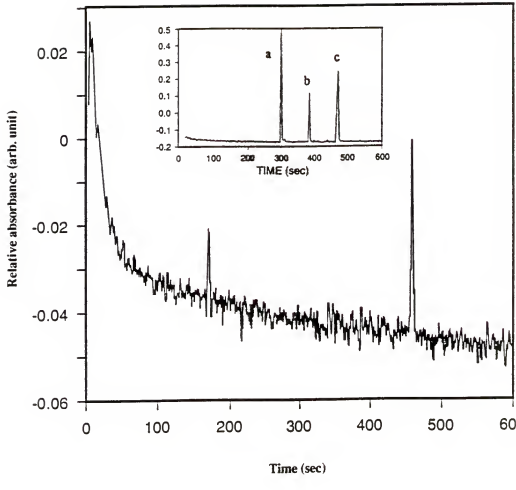

5-14 Capillary zone electrophoresis of a 25 mM NaCl solution in which the PP-ATP film was reduced at -0.5 V (vs. Ag wire) for 1 hour. Inset shows separation of (a) AMP, (b) ADP, and (c) ATP under identical conditions.

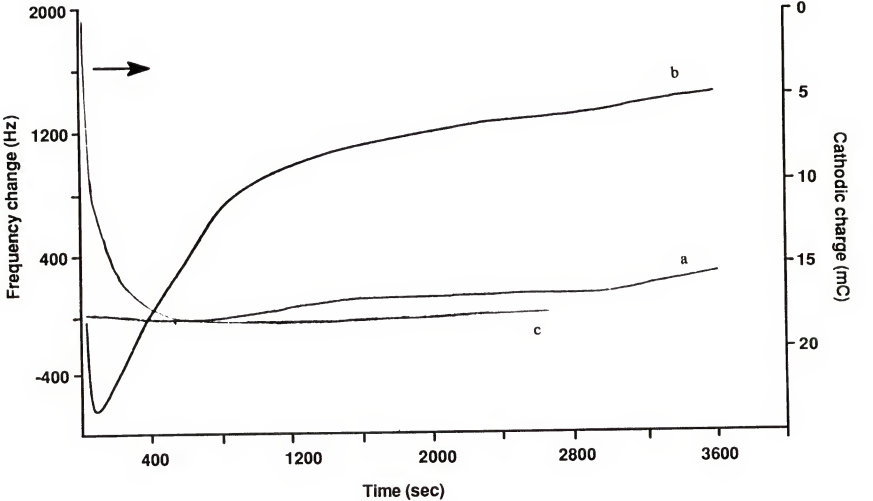

5-15 Frequency responses of PP-ATP films (500 nm) in 0.1 M NaCl at (a) open circuit and (b) step potential from 0.0 V to -0.5 V (vs. Ag/AgCl) along with (c) cathodic charge change.

during electropolymerization. The doping level of the PP-ATP film was obtained from the chronocoulometric results of Figure 5-15c. A cathodic charge of 17 mC during polymer reduction, correlated with 142 mC passed during electropolymerization, indicates that +0.27 charges per PP repeat unit are counter-balanced by 0.09 mole of ATP tri-anions. This doping level is consistent with PP doped by many systems. This value was subsequently utilized to obtain the total PP repeat unit and ATP composition in the PP-ATP film used for UV-Vis measurements. PP-ATP film (ca. 500 nm), electropolymerized on a Pt flag (1.50 cm^2), are composed of 1.4 x 10^{-6} moles of PP repeat units and 1.2 x 10^{-7} moles of ATP. The number of moles of ATP released after 9 redox potential scan was calculated from the maximum absorbance (5.01, Figure 5-15c, ε = 15.4 x 10^3 dm^3 mol^{-1} cm^{-1} [129]). It can be seen that 9.7 x 10^{-8} moles of ATP (ca. 79 %) were released. The fact that such a substantial amount of ATP is released in a relatively short period of time, suggests that PP-ATP films can be utilized as promising ATP supply devices.

5-6 Conclusions

It was found that PP-ATP films release ATP when the films reach a certain critical reduction potential. Spontaneous ATP release does not occur over a long period of time, as investigated over ca. one day. This is distinguished from various conducting polymer based drug release system reported so far, in which spontaneous release was substantial. It was also revealed that ATP is inert during electropolymerization and electrochemically stimulated ATP release.

These results indicate that it is possible to develop finely controllable ATP supply devices. The rate and the amounts of ATP release could be controlled by the electrode potential and the number of redox switches.

CHAPTER 6
DUAL ION TRANSPORT IN ELECTROACTIVE POLYMER BILAYERS

A polymer bilayer represents a polymer modified electrode consisting of two physically segregated layers of electroactive materials with different redox potentials. It has been shown that the bilayer, which consists of a high redox potential inner film and a low redox potential outer film, possesses interesting properties when subjected to electrochemical switching, including charge trapping for energy storage [130]. In these instances, the outer film is electrically separated from the electrode by the reduced (insulating) inner film. Therefore, the outer film remains in the oxidized state, irrespective of the redox states of the inner films, mimicking rectified (unidirectional) current flow.

The first bilayer work, showing rectification behavior, was reported in 1981 by Abruna et al. [130A] who utilized various polypyridinium complexes with Ru to investigate charge trapping in outer films. They subsequently extended the rectification concept to other electroactive polymers [130B-G] such as poly(vinyl ferrocene) and polypyridinium complexes of Os and Fe.

Their pioneering work immediately stimulated further research for the construction of bilayers in which trapped charges are stable for a long period of time. Various heterojunctions between a redox polymer and a conducting polymer [131], two conducting polymers [132], polypyrrole derivatives with different pendant redox sites [133], and polypyrrole with CuSCN as organic and inorganic semiconductors [134]

have been studied. Using polythiophene (PT) outer layers and polypyrrole (PP) inner layers, Shirakawa et al. proposed that p-n junction rectifiers can be constructed when outer films are dense [135]. In this study, anion dominant PP was fully reduced at a potential where PT was simultaneously n-doped. The resulting bilayer contained anions remaining in PP and charge balancing cations in PT, mimicking p-n heterojunctions. However, the electrochemical response of conducting polymer bilayers, constructed with the inner film having a lower oxidation potential than the outer film, have only been probed to a limited extent [132B]. None of these studies addressed the ion transport behavior of bilayers.

Using the bilayer concept, many interesting properties other than rectification behavior can be obtained. For example, surface properties of polymer modified electrodes can be controlled by a bilayer construction. It has been reported that the application of an outer polymer layer enables the use of soluble ion exchange polymers as the inner layer for electrode surface modification [136]. The use of biopolymers as the outer layer to improve biocompatibility is another interesting example of this concept and will be described in Chapter 7. In addition, electroactive polymer bilayer electrodes, which are composed of low redox potential inner films and high redox potential outer films, will be promising for the purpose of multiple ion control devices. In this instance, the identity of the mobile ions (cations or anions) will be controlled by polymer-ion interactions of individual layers. A change in redox state of the inner film will lead to emission or incorporation of ionic species within a certain potential window. Ion transport of the outer layer can occur over a different potential window, leading to different ion transport behaviors at well separated potentials (dual ion transport).

Dual ion transport through bilayer construction should be distinguished from the complex ion transport of PP/PSS, described in Chapter 4. In PP/PSS, low potential ($E \leq -0.2$ V vs. Ag/AgCl) cation dominated transport [58,59] is altered to anion

dominated in the high potential ($E \geq 0.0$ V vs. Ag/AgCl) portion of the scan [74,77]. In this instance, there appears to be appreciable mixed ion transport (possibly along with ion-pairs and solvent) over a wide range of potential, and adjustment of the cation/anion ratio at a specific potential is unlikely.

In this chapter, the electrode potential controlled dual ion transport properties of a conducting polymer bilayer will first be described. The bilayer consists of sequentially electropolymerized PP/PSS inner film and poly(*N*-methylpyrrole chloride) (PNMP-Cl) outer film. PP/PSS has a 0.5 V lower redox potential than PNMP and cation dominated transport at potentials $\leq$ -0.2 V vs. Ag/AgCl in contrast to the anion dominated transport of PNMP-Cl observed during switching at potentials $\geq$ +0.2 V vs. Ag/AgCl. The electroactivity and dominant mobile ionic species of the bilayer components (i.e., cation and anion dominant transport properties of PP/PSS and PNMP respectively) are preserved in the bilayer configuration. A transition between cation and anion dominant transport with a clear switch was observed. However, due to the possibility of diffusion of the second monomer into the inner film prior to its electropolymerization, the nature of the bilayer interface is difficult to ascertain [132A,137] and the dual ion transport process was complex.

The dual ion transport study was thus subsequently extended to bilayers, composed of PP/PSS inner films and poly(vinyl ferrocene) (PVFc) outer films. Cation dominant PP/PSS has a 0.6 V lower redox potential than PVFc which is anion dominant during switching at potentials > +0.45 V vs. Ag/AgCl [94,96]. The bilayers were prepared by casting PVFc solutions onto electropolymerized PP/PSS films. As the PVFc used is of high molecular weight (50,000 g mol^{-1}), diffusion of the PVFc into the PP/PSS is inhibited and, thus, the interface was expected to be more distinct.

In order to ascertain that the film has an electrochemically distinct bilayer structure, methyl viologen dichloride ($MV^{2+}Cl_2$) was utilized as an electrochemical probe. PP/PSS films $\geq$ 550 nm in thickness gave complete coverage of the metal electrode. At

410 nm thickness, coverage was greater than 99 % as observed by scanning electron microscopy with small pinholes visible. The possibility of electrical contact between the PVFc outer film and underlying metal electrode was examined and the distinct interface between the inner and outer layer was elucidated.

The ion transport properties of PP/PSS : PVFc bilayers were studied using electrochemical and microgravimetric methods in various electrolyte solutions. The bilayers have discrete ion transport processes at well separated potentials indicative of independent redox reactions for each component. The amounts of each mobile ionic species can be controlled by changing the thickness of inner and/or outer films. The bilayer possesses a potential window of decreased net mass response in between the redox potentials of PP/PSS and PVFc. PP/PSS exhibits a substantial net mass change between -0.1 V and +0.6 V vs. Ag/AgCl, as evidenced by a 120 Hz frequency drop of a 410 nm PP/PSS cycled in 0.1 M $NaClO_4$ (aq.), which can be attributed to anion dominant transport. The net mass change of the bilayer in this potential window is almost negligible in $CsClO_4$ ($\Delta f \cong 10$ Hz) electrolyte and relatively small changes in $NaClO_4$ ($\Delta f \cong 40$ Hz) electrolyte, suggesting that a more balanced counter directional movement of cations and anions occurs as the outer film prohibits excessive anion transport to the inner film.

This bilayer system is unique compared to the PP/PSS : PNMP-Cl bilayer mentioned above in several aspects. Casting of polymer solutions as outer films eliminates molecular interpenetration of polymer chains into the inner film matrix yielding a more distinct interface between the layers as schematized in Figure 6-1. This system undergoes individual ion transport at more highly separated electrode potentials. The absolute amounts of each ion can be controlled by adjusting the film thicknesses. This is not always the case with sequential electropolymerization methods due to possible inner film degradation through overoxidation during electrodeposition of the outer film.

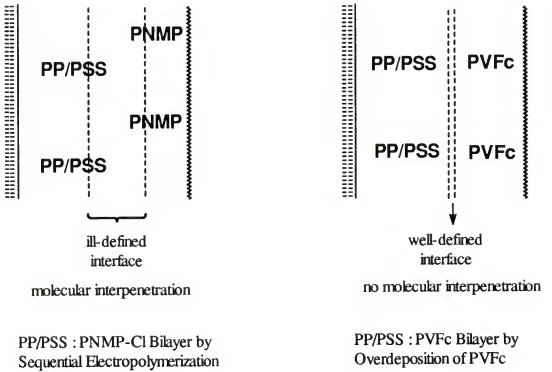

Figure 6-1 Schematic diagram showing polymer-polymer interface in bilayers.

6-1 Experimental Details

Pyrrole was purified by passage over activated alumina until colorless. *N*-methylpyrrole (Aldrich) was vacuum distilled and used immediately. Poly(vinylferrocene) and electrolytes (purity > 99 %) were used as received. Electrolyte and/or monomer solutions were prepared with double distilled water and were Ar purged before use.

All cyclic voltammograms were obtained using an EG&G Princeton Applied Research Model 273 Potentiostat/Galvanostat. Ag/AgCl and platinum were used as reference and counter electrodes, respectively. All further potentials are reported relative to this reference electrode. A Pt button (0.02 cm^2) and Au electrode (0.71 cm^2) were used as working electrodes for electrochemical studies. The Electrochemical Quartz Crystal Microbalance (EQCM) was used to measure mass changes associated with the redox process of the electroactive polymer under investigation by monitoring the change in the resonant frequency of an oscillating quartz crystal.

A PP/PSS : PNMP-Cl bilayer film was prepared in aqueous solutions by first electropolymerizing 0.1 M pyrrole in 0.1 M NaPSS at +0.8 V and immediately electropolymerizing 0.1 M *N*-methylpyrrole in 0.1 M NaCl on top of it at +0.9 V. The electropolymerization of the *N*-methylpyrrole was carried out as quickly as possible to avoid diffusion of the monomer into the bulk of the PP/PSS. Typical film thicknesses for these depositions were between 150 - 300 nm.

In PP/PSS : PVFc bilayers, PP/PSS inner films were prepared in the same way as above. After thorough washing with H_2O and CH_2Cl_2, these films were placed in CH_2Cl_2 for 20 minutes and air dried. Aliquots of CH_2Cl_2 solutions of 2 mM PVFc were cast on the dried PP/PSS films. Complete solvent evaporation was confirmed by monitoring the mass change with the EQCM at open circuit. It was found that the PVFc concentration of the CH_2Cl_2 solution is critical in preparing homogeneously cast films.

The extent of the PP/PSS film coverage on a Au electrode was investigated by the electrochemical probe technique [47B] along with scanning electron microscopy (JEOL, JSN-6400). PP/PSS films of various thicknesses were fully reduced in 2 cm^{-3} of 0.1 M $NaClO_4$ aqueous solutions applying -1.0 V for 10 min. The potential was subsequently stepped to -0.5 V and 2 cm^{-3} of 0.1 M $NaClO_4$ and 30 mM methyl viologen (MV^{2+}) aqueous solutions were added, yielding a 15 mM MV^{2+} electrochemical probe solution. The potential was scanned between -0.5 V and -1.0 V and the current response of the high potential redox couple [138] of methyl viologen ($MV^{2+} = MV^{+}$) was monitored with film thickness.

The inner film thicknesses, determined using a combination of profilometry and coulometry methods, were 280, 410, 610 or 790 nm thick, yielding a surface coverage of 4.0×10^{-7}, 6.0×10^{-7}, 9.0×10^{-7} or 1.2×10^{-6} mols cm^{-2} of polypyrrole repeat units. The PVFc outer films contained 2.8×10^{-8} (21 nm), 5.6×10^{-8} (42 nm), 8.4×10^{-8} (64 nm), 1.4×10^{-7} (105 nm), 2.8×10^{-7} (210 nm) or 4.2×10^{-7} (315 nm) mols cm^{-2} of VFc units, based on the amount and concentration of PVFc solutions used. The surface coverage of the PP/PSS inner film was calculated from a density [58] of 1.27 g cm^{-3} and the thickness of the PVFc outer film was determined from a density of 1.18 g cm^{-3} as measured by flotation.

6-2 PP/PSS : PNMP-Cl

6-2-1 Coelectroactivity of Bilayers

Cyclic voltammetric measurements were carried out with a bilayer on a Pt button working electrode. The film was scanned between -0.8 V to +0.6 V in 0.1 M $NaClO_4$ aqueous solutions until the current response was stable. Figure 6-2 shows the scan rate dependence of the cyclic voltammograms. The PP/PSS inner film is electroactive with an $E_{1/2}$ = -0.2 V in the presence of the PNMP outer film. The oxidation and reduction of the PNMP can be seen with peaks at an $E_{1/2}$ = +0.4 V. The linear dependence of

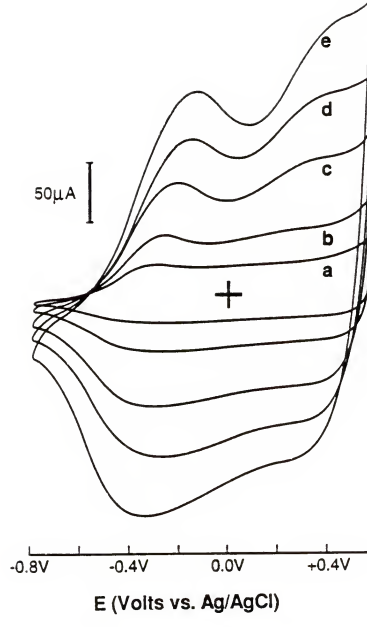

Figure 6-2 Cyclic voltammograms of a PP/PSS : PNMP-Cl bilayer cycled in a 0.1 M $NaClO_4$ aqueous solution at (a) 25 mV s^{-1}, (b) 50 mV s^{-1}, (c) 100 mV s^{-1}, (d) 150 mV s^{-1}, (e) 200 mV s^{-1}.

the current responses with scan rate is due to the surface bound nature of the electroactive sites of both polymers. While these experiments demonstrate the coelectroactivity of the bilayer, they yield no information on ion transport and subsequent microgravimetric analyses were carried out.

6-2-2 Dual Ion Transport of PP/PSS : PNMP-Cl

The direction of dominant ion flux (either into or out of the film) during oxidative doping of PP/PSS, PNMP-Cl and a bilayer was investigated utilizing the EQCM. A PP/PSS (ca. 300 nm), a PNMP-Cl (ca. 150 nm) and a bilayer film (ca. 300 nm PP/PSS and 150 nm PNMP-Cl) were electrosynthesized on Au working electrode, using the conditions outlined above, and equilibrated by several potential scans between -1.0 V to +0.5 V until their frequency and current responses remained constant. Figure 6-3 shows frequency changes during scanning after equilibration in various electrolyte solutions. Frequency responses increase up to -0.2 V due to Na^+ release during oxidation of PP/PSS. Above -0.2 V, PP/PSS : PNMP in a NaPSS electrolyte solution gives no substantial frequency change, indicating that PSS^- is too bulky to diffuse into the polymer matrix. On the other hand, the frequency decrease is evident in small anionic electrolyte solutions as anions move into the film above -0.2 V. It should be noted that this frequency decrease results from both anion dominant transport of PP/PSS at high potentials and PNMP oxidation. The greater frequency decrease in NaF than in NaCl may be due to the different mobilities of anions through the PNMP-Cl.

The dual ion transport of PP/PSS : PNMP-Cl was also investigated during subsequent oxidation of individual layers in 0.1 M $NaClO_4$ (aq.). Frequency changes during oxidation were monitored after applying a step potential from -1.0 V to -0.2 V. After equilibration at this potential for 20 min., the potential was subsequently stepped to +0.5 V. Using this two step process, the first step oxidized the PP/PSS while the

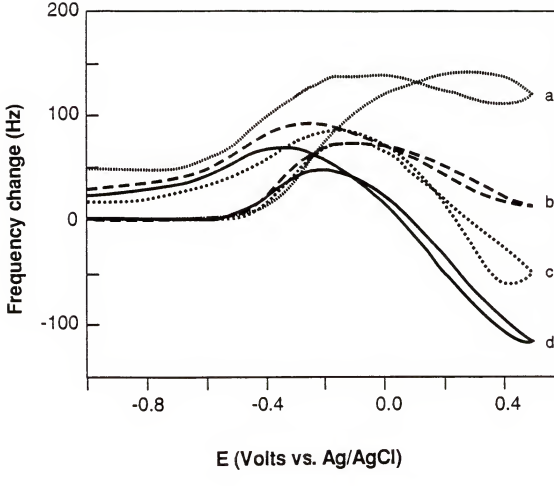

Figure 6-3 Frequency responses during potential scanning of PP/PSS : PNMP-Cl at 25 mV s^{-1} in 0.1 M (a) NaPSS, (b) NaCl, (c) NaF, and (d) $NaClO_4$.

PNMP remained reduced. The second step subsequently oxidized the PNMP. The frequency results shown in Figure 6-4 illustrate the dual ion transport properties of the bilayer. The PP/PSS film, both alone and as the inner film of the bilayer, shows cation dominated transport at -0.2 V as the frequency increases (mass loss due to emission of Na^+). The cation release rate of the bilayer during the initial stage of oxidation is a little slower due to the presence of the PNMP outer layer, but equilibrates at the same frequency difference as the PP/PSS film alone. This indicates that the electroactivity of the PP/PSS inner film does not decrease. With a step to -0.2 V the PNMP is not oxidized and no mass transport (zero frequency change) is observed.

Subsequent stepping of the potential to +0.5 V was then used to oxidize the PNMP. In all cases a frequency loss (mass gain due to inclusion of ClO_4^-) is observed. The smallest response was observed for PP/PSS and this potential dependent reversal of the dominant ion flux was described in Chapter 4. Compared to the PP/PSS film, the frequency response of the PNMP and the bilayer films are large due to the anion incorporation into the PNMP to neutralize the positive charge. The magnitudes of these frequency responses are similar indicating that the bulk of the ion transport is occurring in the PNMP outer layer of the bilayer. Most of the anion incorporation occurs immediately after application of the potential, which demonstrates relatively fast oxidation of the PNMP outer film. On the other hand, anion penetration through the PNMP outer film towards the PP/PSS inner film in the bilayer is hampered leading to a tail in the frequency drop.

6-3 PP/PSS : PVFc

6-3-1 Distinct Interface of Bilayers

In order to ascertain the bilayer's distinct structure, a combination of SEM and electrochemical studies were employed. PP/PSS film thicknesses greater than 680 nm gave complete coverage of the electrode as observed by SEM. Slightly thinner films,

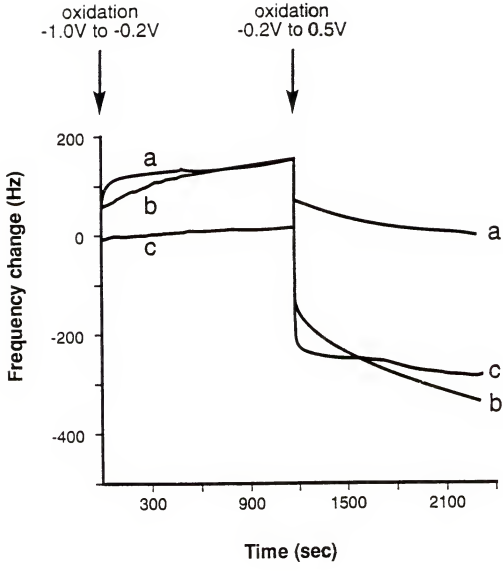

Figure 6-4 Frequency responses during potential stepping of (a) PP/PSS (*ca.* 300 nm), (b) PP/PSS : PNMP-Cl (*ca.* 300 nm : 150 nm), and (c) PNMP-Cl (*ca.* 150 nm) in 0.1 M $NaClO_4$.

approximately 410 nm thick, exhibited a low density of pinholes, with coverage > 99 %.

The electrochemical redox pair $MV^{2+} \rightleftharpoons MV^{+}$ was examined at fully reduced PP/PSS films of various thicknesses to study this coverage further [47B]. PP/PSS films were electrochemically prepared on Au and reduced by holding the potential at -1.0 V in 0.1 M $NaClO_4$ (aq.) for 10 min. The potential of the film was adjusted to -0.5 V and the solution made 15 mM in MV^{2+}. The potential was immediately scanned between -0.5 V and -1.0 V monitoring the current responses of the $MV^{2+} \rightleftharpoons MV^{+}$ redox couple. Representative cyclic voltammograms are shown in Figure 6-5. The shapes of the CV's are not well-defined since the redox process occurs on a poorly conducting PP/PSS.

The peak currents of the MV probe decreases as the PP/PSS film thickness increases as illustrated for the cathodic peak in Figure 6-6. This indicates that the PP/PSS film coverage is incomplete with thickness below ca. 410 nm. Coverage becomes complete between 410 and 550 nm of PP/PSS. These results indicate that there is minimal contact of PVFc to the underlying metal electrode. As the PVFc used is of high molecular weight, diffusion of the PVFc into the PP/PSS is inhibited and, thus, the electrodes constructed are bilayers.

6-3-2 Cyclic Voltammetric Studies

Cyclic voltammetric (CV) measurements were carried out on (a) PP/PSS, (b) PVFc and (c) a PP/PSS : PVFc bilayer cycled at 25 mV sec^{-1} on a Au working electrode as shown in Figure 6-7. The single components were cycled over their respective redox processes and the bilayer was cycled between -0.8 V to +0.6 V in 0.1 M $NaClO_4$ (aq.) until the current response reached a steady state for each case. These CV's indicate that the electroactivity of the inner film is not substantially altered in the bilayer system and that the redox process of PP/PSS is not hampered by the presence of the reduced

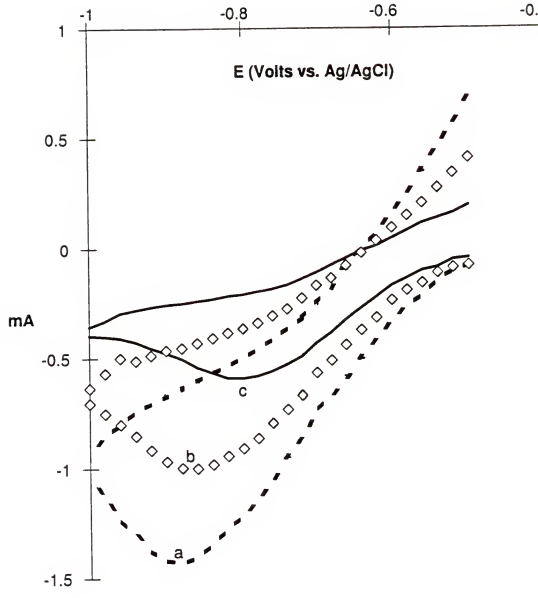

Figure 6-5 Electrochemical responses of a MV^{2+} probe at fully reduced PP/PSS films of (a) 280 nm, (b) 345 nm, and (c) 550 nm thicknesses, cycled from -0.5 V to -1.0 V in 15 mM MV and 0.1 M $NaClO_4$ solutions.

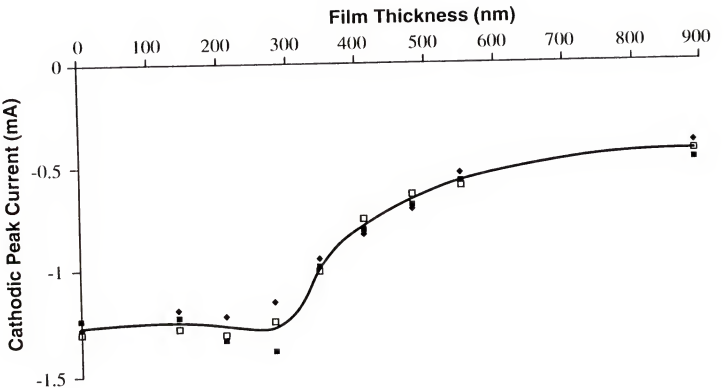

Figure 6-6 Effect of PP/PSS film thickness on the cathodic peak current of $MV^{2+} = MV^{+}$.

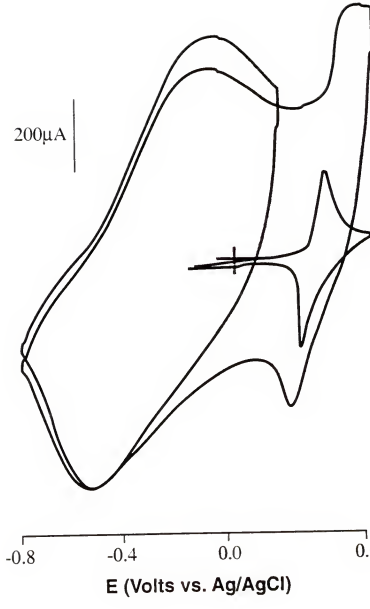

Figure 6-7 Cyclic voltammograms of (a) PP/PSS (6.0×10^{-7} mols cm^{-2} of polymer repeat units, 410 nm), (b) PVFc (1.4×10^{-7} mols cm^{-2} of VFc units, 105 nm) and (c) a bilayer of PP/PSS (6.0×10^{-7} mols cm^{-2}, 410 nm) and PVFc (1.4×10^{-7} mols cm^{-2}, 105 nm), on Au electrodes (0.71 cm^2) in 0.1 M $NaClO_4$ aqueous solutions at 25 mV sec^{-1}.

outer film. The cathodic current response of the PVFc outer film is similar to PVFc when it is directly coated on the metallic electrode.

Although it has been reported that the cyclic voltammogram of a PVFc film in a NaCl solution is complicated due to delamination [94], this does not appear to occur with the bilayers as the electroactivity remains for a high number (> 100) of scans. This is illustrated by comparison of the CV response of PP/PSS and a PP/PSS : PVFc bilayer between -0.9 V and +0.6 V as shown in Figures 6-8a and 6-8b respectively. In these experiments 4.0 x 10^{-7} mols cm^{-2} of polypyrrole repeat units and 1.4 x 10^{-7} mols cm^{-2} of VFc units were utilized. There is an approximately 30 % loss of electroactivity after 50 scans determined by the decrease in the current of each peak. While this reduction in electroactivity is evident, the bilayer stability is sufficient for a useful study of its ion transport behavior. It should be noted that PP/PSS, which is subject to overoxidation at high potentials, exhibits a similar electroactivity stability as the bilayer.

6-3-3 Modification of Anion Incorporation in PP/PSS

Since the CV measured electroactivity of the bilayer gives no information on ion transport, microgravimetric analyses were carried out utilizing the EQCM. A bilayer of PP/PSS (4.0 x 10^{-7} mols cm^{-2}) and PVFc (8.4 x 10^{-8} mols cm^{-2}) was equilibrated by several potential scans in 0.1 M NaCl (aq.) between -1.0 V and +0.6 V until its frequency and current responses remained constant. The reproducible frequency responses of (a) the bilayer and (b) the PVFc film on the Au electrode are shown in Figure 6-9. The frequency increases attributable to Na^+ release from the PP/PSS inner film are evident at potentials lower than -0.1 V in Figure 6-9a. This is followed by a potential window of no net mass transport (zero frequency change) up to +0.45 V. This behavior is worth noting because it is known that the ion transport properties of PP/PSS is anion dominated over this high potential region [74,77], as compared in the

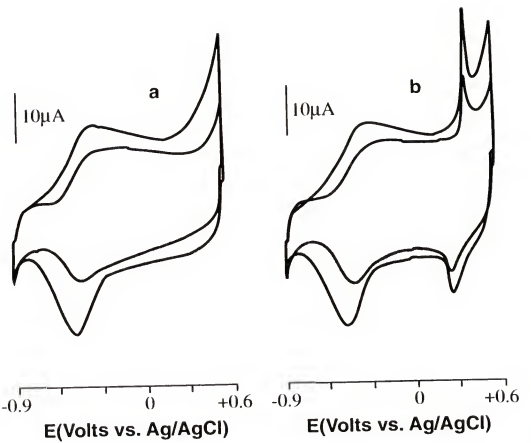

Figure 6-8 Cyclic voltammograms of (a) PP/PSS (4.0×10^{-7} mols cm^{-2} of polymer repeat units, 280 nm) and (b) a bilayer of PP/PSS (4.0×10^{-7} mols cm^{-2}, 280 nm) and PVFc (1.4×10^{-7} mols cm^{-2},105 nm) on Pt button electrodes (0.02 cm^2) in 0.1 M NaCl aqueous solutions at 25 mV sec^{-1}. The electroactivity was compared between the initial scan and 50'th scan.

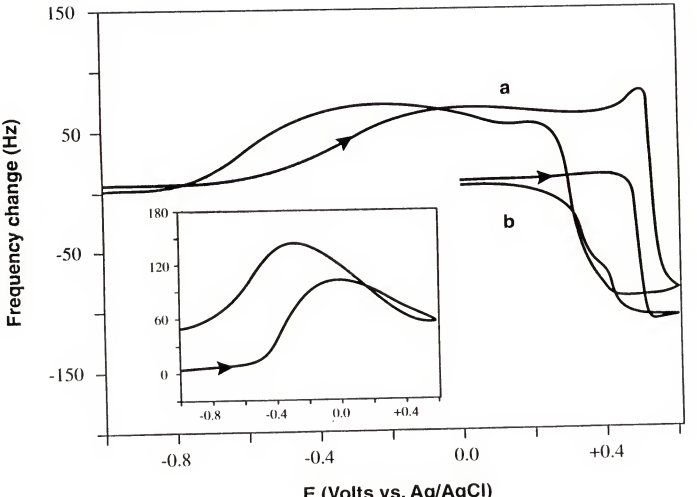

Figure 6-9 EQCM frequency responses of (a) a bilayer (4.0×10^{-7} mols cm^{-2} of PP/PSS, 280 nm and 8.4×10^{-8} mols cm^{-2} of PVFc, 64 nm) (b) PVFc (8.4×10^{-8} mols cm^{-2} of PVFc) and PP/PSS (inset, 4.0×10^{-7} mols cm^{-2} of PP/PSS) cycled in 0.1 M NaCl aqueous solutions at 25 mV sec^{-1}.

inset to Figure 6-9. This region of no net mass change is intriguing, yet does not indicate that ion and/or solvent transport is completely inhibited. It is likely that the amount of anion compensation occurring in the high potential PP/PSS region is significantly lower in the bilayer relative to a PP/PSS film alone. This will be addressed further.

The small frequency increase (20 Hz) between +0.45 V and +0.5 V is likely due to charge balancing by excess PSS anionic sites at the PP/PSS surface interacting with nearby PVFc sites. We have previously shown these PSS^- sites to be reactive to complexation with polycations [139]. In these bilayers, free NaPSS units at the interface release cations to counter-balance the oxidized PVFc units. This is confirmed by the facts that a PVFc film alone does not show this small frequency increase (Figure 6-9b), and that bilayers with varied amounts of PVFc exhibit identically small frequency increases independent of film thicknesses. This frequency increase is immediately followed by a sharp frequency decrease at +0.5 V indicating fast Cl^- movement into the PVFc film.

In order to elucidate the details of the ion transport in the no net mass flux region, PP/PSS : PVFc bilayers were examined in different electrolytes. Results utilizing 0.1 M $NaClO_4$ and $CsClO_4$ are shown in Figure 6-10. These results demonstrate that the frequency response of the bilayer (PP/PSS : PVFc = 410 nm : 105 nm) between -0.2 V and +0.45 V is quite different from PP/PSS (410 nm) alone (compare Figure 6-10a and 6-10b). It is evident that the magnitude of the frequency change (120 Hz) observed for PP/PSS in the high potential region is reduced by constructing the bilayer. The 40 Hz decrease in frequency between -0.1 V and +0.4 V present in $NaClO_4$ is even smaller (Δf = 10 Hz) when cycling in 0.1 M $CsClO_4$ (aq.) as shown in Figure 6-10c. These frequency changes are consistent with the fact that both anions and cations are moving in opposite directions between the redox processes for each polymer. The measured frequency response, which is the sum of the positive and negative mass flux,

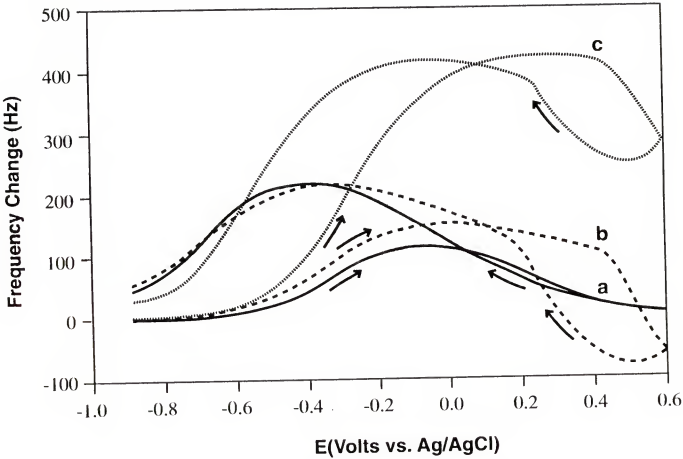

Figure 6-10 EQCM frequency responses of (a) PP/PSS, and a bilayer (PP/PSS : PVFc = 410 nm : 105 nm) cycled in (b) 0.1 M $NaClO_4$ and (c) 0.1 M $CsClO_4$ at 25 mV sec^{-1}.

can be balanced to zero net change by judicious choice of electrolyte and bilayer film thicknesses. These microgravimetric results indicate that it is possible to prepare polymer modified electrodes possessing dual ion transport properties at discrete potentials which also exhibit a suppressed mass flux over a wide range of potential between the two redox processes.

6-3-4 Control of the Cation to Anion Ratio

The relative cation/anion transport ratio, and the absolute amount of each ion transported during redox of the separate bilayer components, can be controlled by adjusting film thicknesses. Bilayer films with the same inner film thickness (610 nm = 9.0×10^{-7} mols cm^{-2} of polypyrrole repeat units) and varied outer film thicknesses were constructed by casting different amounts of PVFc solutions. In this study, PVFc film coverages of 2.8×10^{-8} (21 nm), 5.6×10^{-8} (42 nm), 8.4×10^{-8} (64 nm), 1.4×10^{-7} (105 nm), 2.8×10^{-7} (210 nm), and 4.2×10^{-7} (315 nm) mols cm^{-2} were employed. Frequency changes during potential scanning were monitored in 0.1 M $CsClO_4$ between -0.9 V and +0.6 V as shown in Figure 6-11. The frequency increases between -0.4 V and -0.1 V, due to PP/PSS controlled cation dominant transport, are identical. On the other hand, the frequency decreases between +0.45 V and +0.6 V, due to PVFc controlled anion dominant transport, scale with the amount of PVFc.

Frequency changes during oxidation of these bilayers were also monitored with a double potential step experiment by applying a step potential from -0.9 V to 0.0 V in 0.1 M $CsClO_4$ (aq.) and, after equilibration at this potential for 20 sec, subsequently stepping the potential to +0.6 V. Using this two-step process, the first step oxidizes the PP/PSS while the PVFc remains neutral and subsequently the second step oxidizes the PVFc as shown in Figure 6-12. In the first step, the magnitude and rate of the frequency response are independent of PVFc film thicknesses, demonstrating that the outer layer does not affect the ion transport properties of the inner layer. The

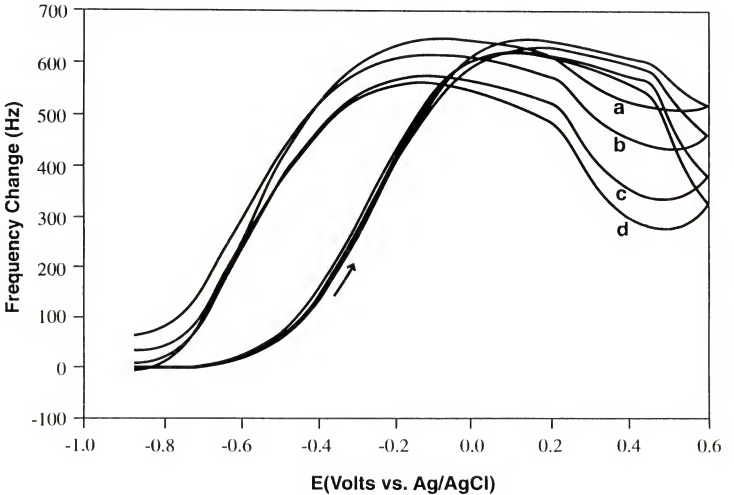

Figure 6-11 Comparison of EQCM frequency responses of bilayers with varied amounts of PVFc (a) 610 nm PP/PSS and 42 nm PVFc, (b) 610 nm PP/PSS and 105 nm PVFc, (c) 610 nm PP/PSS and 210 nm PVFc, and (d) 610 nm PP/PSS and 315 nm PVFc during cycling in 0.1 M $CsClO_4$ at 25 mV sec^{-1}.

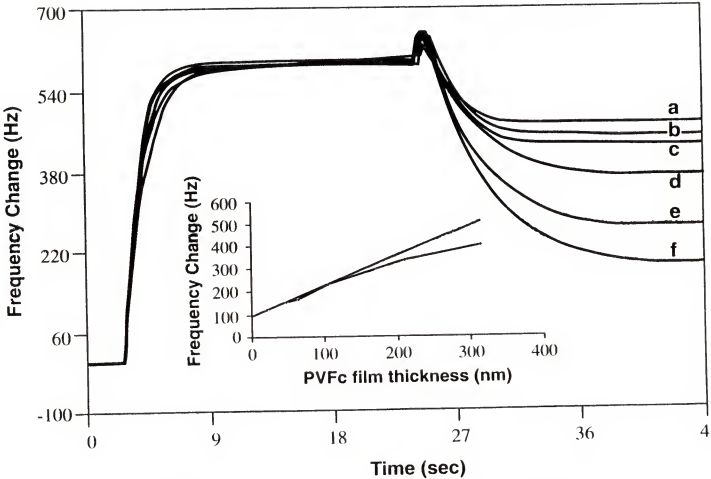

Figure 6-12 Comparison of EQCM frequency responses of bilayers consisting of 610 nm PP/PSS with varied amounts of PVFc; (a) 610 nm PP/PSS and 21 nm PVFc, (b) 610 nm PP/PSS and 42 nm PVFc, (c) 610 nm PP/PSS and 64 nm PVFc, (d) 610 nm PP/PSS and 105 nm PVFc, (e) 610 nm PP/PSS and 210 nm PVFc, and (f) 610 nm PP/PSS and 315 nm PVFc upon the application of step potentials from -0.9 V to 0.0 V and to +0.6 V in 0.1 M $CsClO_4$ aqueous solutions. Inset shows Δf during second potential step as a function of PVFc outer layer thickness.

frequency results from the second step show that the magnitude of ClO_4^- ion movement is proportional to the number of moles of VFc units as shown in the inset of Figure 6-12. The frequency decrease is proportional to the PVFc film thickness in the bilayers of relatively thin PVFc. The increase of the PVFc film thicknesses leads to slightly smaller frequency changes than expected, indicating that incomplete oxidation of PVFc occurs within the experimental time scale. The 90 - 95 Hz drop in frequency with no PVFc outer film is due to the anion dominant transport of PP/PSS along with solvent incorporation at high potentials. This excess mass increase becomes more distinguishable with an increase in the PP/PSS inner layer thicknesses in the bilayer configuration.

The relative cation/anion transport ratios of bilayers containing different inner film thickness and constant outer film thickness, were also investigated. PP/PSS film coverages of 6.0 x 10^{-7}, 9.0 x 10^{-7} and 1.2 x 10^{-6} mols cm^{-2} (410, 610, 790 nm respectively) were used, maintaining PVFc outer film coverage at 1.4 x 10^{-7} mols cm^{-2} (105 nm). Frequency responses of the fully reduced bilayers during double potential step oxidation in 0.1 M $CsClO_4$ from -0.9 V to 0.0 V, and subsequently from 0.0 V to +0.6 V, are shown in Figure 6-13. The frequency increase during the first potential step is approximately proportional to the inner film thickness. The increase of the inner film thicknesses from 410 nm to 610 and 790 nm results in frequency increases of 187 and 367 Hz respectively. The frequency decrease resulting from the PVFc outer film oxidation does not appear to be correlated with the VFc content. The frequency drop during oxidation of the PVFc of the bilayer consisting of the 790 nm thick PP/PSS inner film (Figure 6-13c) is larger than expected, when compared to the frequency changes of the bilayers consisting of the 280 nm and 550 nm thick PP/PSS inner films (Figures 6-13a and 6-13b). This greater frequency response is likely due to the difference in the extent of anion incorporation associated with continued doping of PP/PSS as detailed earlier. This demonstrates that the cation/anion ratio in the

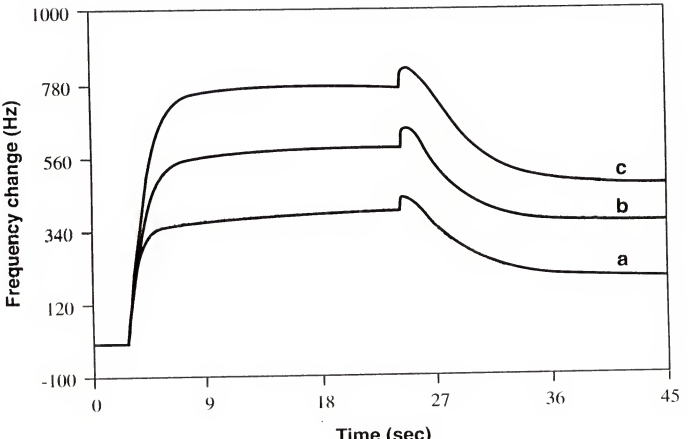

Figure 6-13 Comparison of EQCM frequency responses of bilayers consisting of (a) 410 nm PP/PSS and 105 nm PVFc, (b) 610 nm PP/PSS and 105 nm PVFc, and (c) 790 nm PP/PSS and 105 nm PVFc upon the application of step potentials from -0.9 V to 0.0 V and subsequently from 0.0 V to +0.6 V in 0.1 M $CsClO_4$ aqueous solutions.

potential window between redox processes of each polymer is affected by the inner film thickness as well as the outer film thickness.

6-4 Conclusions

By constructing a bilayer (or possibly multilayers) of electroactive and ion transporting polymers, where the redox states of the polymers are sufficiently separated in potential, a single electrode can be made to absorb and emit specific ions over controllable potential ranges. This dual ion transport was investigated through PP/PSS : PNMP-Cl and PP/PSS : PVFc bilayers and is outlined in Figure 6-14.

PP/PSS : PNMP-Cl bilayers have separate redox switching potentials and electrode potential dependent dual ion transport behavior, exhibiting cation dominated transport at low potentials and anion dominated transport at high potentials. The bilayers also exhibit an inhibited net mass flux potential window between two redox processes.

PP/PSS : PVFc bilayers, consisting of varied inner and outer film thicknesses, show independent ion transport behavior at well separated redox potentials. A suppressed anion flux region between the redox process of the respective PP/PSS and PVFc component is present. This region can be balanced to zero net change by judicious choice of electrolyte and bilayer film thicknesses. The relative anion to cation ratio can be controlled by altering the thicknesses of each polymer film. These results indicate that it is possible to construct dual ion transport devices which may be used for the controlled release of ions from electroactive membranes along with regulation of ionic concentrations in electrolyte solutions.

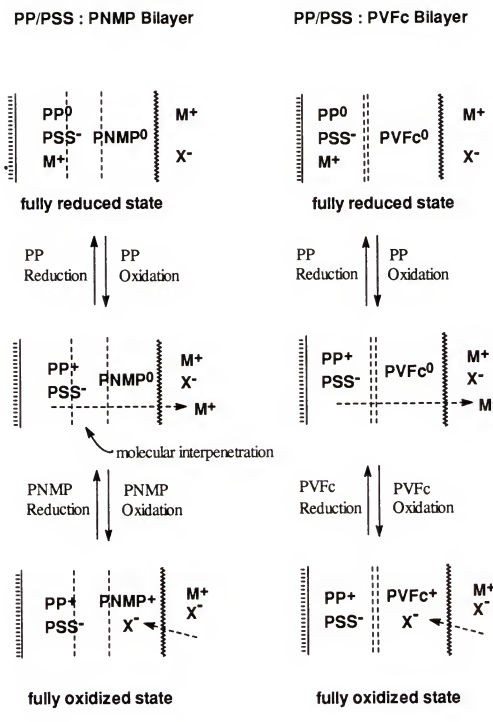

Figure 6-14 Schematic diagram of dual ion transport of bilayers.

CHAPTER 7
PP-ATP : PNMP BILAYERS

The electrochemically stimulated release of ATP from PP-ATP films was previously discussed in Chapter 5. While ATP was not spontaneously exchanged with small anions in bathing solutions over a long period of time, an appreciable amount (ca. 80 %) of the ATP was released within a few minutes during the reduction of PP. ATP ions were inert towards hydrolytic cleavage during both synthesis and potential driven release, suggesting that PP-ATP electrodes may be useful as ATP supply devices. To the best of our knowledge, this use of PP-ATP as an ATP release device is the first conducting polymer based biomolecule release system in which spontaneous release can be ignored.

Polymer modified electrodes, exhibiting cation and anion dominant behavior at separate potentials (potential dependent dual ion transport), were described in Chapter 6. The ion transport behavior of bilayers, which consist of relatively low redox potential conducting polymer inner films (e.g. PP/PSS) and relatively high redox potential electroactive polymer outer films (e.g. PNMP-Cl, PVFc), were studied when they are subjected to consecutive redox switches of each component. Ion transport of inner films was not hampered by the presence of outer films and the amount of each ionic species, either incorporated or released, was proportional to the individual film thickness (i.e. the number of electroactive site). The construction of bilayers is the most efficient method to prepare a polymer modified electrode possessing dual ion transport properties. For example, in the case of block copolymers, in which

intrinsically cation dominant and anion dominant electroactive polymers constitute chain segments, self doping may complicate ion transport behavior.

In this chapter, the ion transport properties of electrochemically synthesized bilayers which consist of PP-ATP inner films and PNMP outer films with various dopant anions will be described. PNMP-Cl, PNMP/PSS and PNMP/heparin (PNMP/HPN) were used as outer films. PNMP/HPN was utilized as HPN may ultimately yield biocompatible surface. The EQCM was first employed to simultaneously monitor charge and mass changes in bilayers during redox switching of an individual layer. UV spectroscopy was utilized to compare the amount and rate of ATP release upon varying the thickness of each layer.

7-1 Experimental Details

Pyrrole and *N*-methylpyrrole (Aldrich) were passed over activated alumina until colorless before use. ATP disodium salt, heparin (HPN) sodium salt (Sigma Chemical), poly(styrene sulfonate) sodium salt and NaCl (Aldrich) were used as received. All electrolytes used were analytical grade whose purities exceeded 98 %.

PP-ATP inner films of varied thicknesses (150 nm, 300 nm, 750 nm) were potentiostatically prepared by polymerizing 0.1 M pyrrole in 20 mM ATP aq. solutions at +0.8 V (vs. Ag/AgCl). The polymerizations were carried out at a pH of ca. 3.4 where ATP exists as tri-basic ions. pH adjustment was not carried out since the polymerization rate is slow at a neutral pH. PNMP-Cl outer films of various thicknesses (150 nm, 300 nm, 450 nm, 750 nm) were potentiostatically synthesized on top of the PP-ATP from 0.1 M NaCl and pyrrole aq. solutions at +0.8 V (vs. Ag/AgCl). PNMP/PSS and PNMP/HPN outer films were prepared in a similar manner, using 0.1 M *N*-methylpyrrole/0.1 M PSS sodium salt and 0.1 M *N*-methylpyrrole/10 mM HPN sodium salt aq. solutions respectively. The preparation of PNMP outer films was carried out as quickly as possible to avoid diffusion of the monomer into the bulk

of the PP-ATP inner film. Typical exposure times of PP-ATP to the NMP polymerization medium were between 20 - 30 seconds. The film thicknesses were calculated from the amount of charge passed during electropolymerization, using 240 mC cm^{-2} explained in Chapter 1.

For voltammetric, spectroscopic and ion selective electrode (ISE) studies, a Pt button (0.02 cm^2), Pt plate (0.75 cm^2) and Pt plate (6.25 cm^2) were used as working electrodes respectively. The counter electrode was a Pt plate with a Ag/AgCl reference electrode for gravimetric and voltammetric studies. Ag wire was used as the quasi-reference electrode for spectroscopic measurements. After electrosynthesis, bilayer films were thoroughly rinsed with water and placed in 0.1 M NaCl monomer free aq. solutions (pH = 5.4) unless otherwise mentioned.

Chronocoulometric and microgravimetric studies were carried out to reveal charge and mass changes during subsequent reduction of each layer. Bilayers were placed in 0.1 M NaCl aq. solutions and fully oxidized by applying +0.6 V (vs. Ag/AgCl) for 1 min. The potentials were then stepped to 0.0 V to reduce outer films while maintaining inner films oxidized. After holding the potential for 10 min. at 0.0 V, the inner films were fully reduced at -0.6 V to release ATP.

ATP concentration changes of 0.1 M NaCl aq. solutions (3.5 cm^3), due to ATP release from bilayers, were measured with time in situ using a Cary 5E UV-Vis-NIR spectrophotometer, controlling electrode potentials with an EG&G Model 273 potentiostat/galvanostat.

7-2 Electrochemical and Microgravimetric Studies

7-2-1 Cation Dominant PNMP/HPN

Heparin (HPN) is a sulfated polysaccharide which is generated by certain types of cells that are abundant in the lining of arterial blood vessels [125]. It has a repeating unit of six sugar residues, each consisting of an alternating sequence of sulfate

derivatives glucosamine and gluconic acid as shown below. Heparin is a powerful inhibitor of blood clotting. This polyelectrolyte was used as a dopant during electropolymerization of *N*-methylpyrrole.

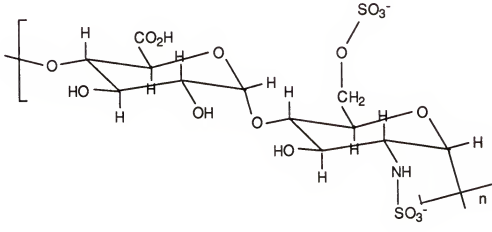

In order to confirm the fact that PNMP/HPN possesses cation dominant transport properties, mass changes of a PNMP/HPN film (300 nm) during redox cycles were monitored along with current responses in 0.1 M NaCl electrolyte. Figure 7-1 shows the expected frequency increase (mass loss) during positive potential scans, indicative of cation release. The cyclic voltammogram of PNMP/HPN shows an $E_{1/2}$ of +0.1 V (hereafter, potentials are relative to Ag/AgCl) which is significantly lower than that of PNMP with small mobile dopant anions. The shift of the $E_{1/2}$ results from a difference in the ion transport mechanism. In Chapter 3, it was shown that PP-TOS films cycled in 0.1 M NaCl (aq.) exhibited two redox peaks. The lower potential redox process, which slowly disappears with the number of scans as TOS^- anions are released, is attributed to cation dominant transport. Similarly, cation dominant PNMP/PSS shows a low $E_{1/2}$ (ca. +0.1 V), while anion dominant PNMP-Cl has a relatively high $E_{1/2}$ (ca. +0.5 V). This effect of ion transport on the $E_{1/2}$ of polypyrrole has been previously

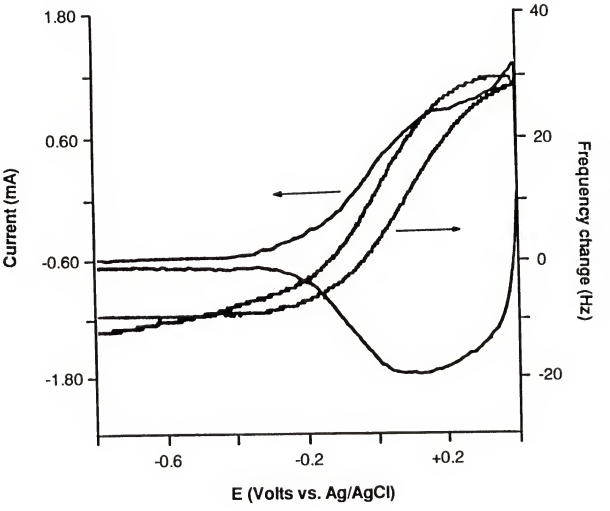

Figure 7-1 Frequency and current responses of PNMP/HPN (300 nm on Au) in a 0.1 M NaCl aq. solution at 25 mV s^{-1}.

reported [72], confirming PP to have two redox processes consistent with a lower potential cation dominant and a higher potential anion dominant region.

7-2-2 CV and EQCM Studies of Bilayers

Bilayers, consisting of PP-ATP inner films and PNMP outer films with various charge balancing anions, were electrochemically constructed. Their electrochemical responses were examined and compared with cyclic voltammograms of single component films in 0.1 M NaCl aq. solutions. PNMP outer films were prepared by applying +0.8 V immediately after immersing the PP-ATP films in 0.1 M *N*-methylpyrrole aq. solutions to prevent monomer diffusion into inner films, as mentioned previously.

The equilibrated cyclic voltammogram of PP-ATP : PNMP-Cl shows separate redox behaviors, indicating that the redox process of each film is not altered in the bilayers as demonstrated in Figure 7-2 (left). Similar co-electroactivity of PP/PSS : PNMP-Cl was described in Chapter 6. The difference in the electrochemical responses between bilayer and single layer films can be seen during the reduction of PP-ATP. As mentioned earlier, PP-ATP single layer films show two reduction peaks due to different ion transport mechanisms, while the PP-ATP in bilayers only shows one reduction peak at -0.5 V. This is likely due to the inhibited anion transport through the reduced outer film. The electrochemical responses of PP-ATP : PNMP/PSS and PP-ATP : PNMP/HPN, shown in Figure 7-2 (middle) and 7-2 (right) respectively, are similar to PP-ATP : PNMP-Cl except for the lower $E_{1/2}$ of the PNMP outer films synthesized with the polyelectrolytes.

Mass and charge changes of these bilayers during potential steps were monitored in 0.1 M NaCl aq. solutions using the EQCM. Bilayers were initially conditioned by full oxidation at +0.6 V for 1 min to equilibrate the ionic composition through the film. The films were subsequently subjected to a potential step to 0.0 V and held for 10 min.

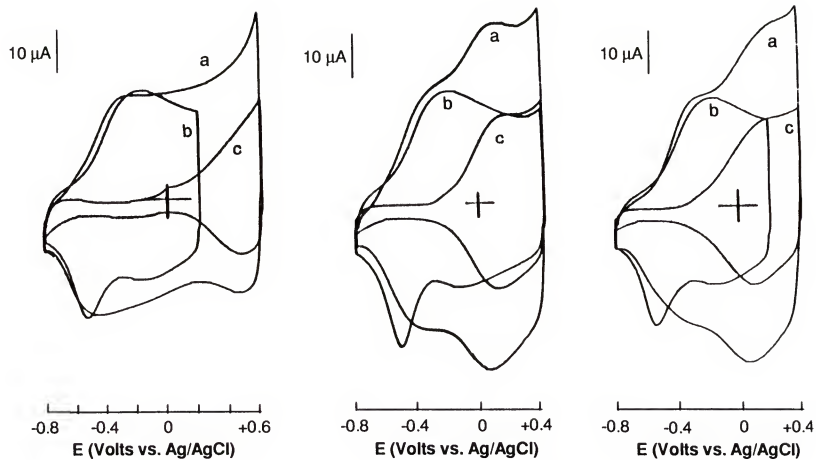

Figure 7-2 Cyclic voltammograms of (left) [(a) PP-ATP : PNMP-Cl, (b) PP-ATP, (c) PNMP-Cl], (middle) [(a) PP-ATP : PNMP/HPN, (b) PP-ATP, (c) PNMP/HPN], and (right) [(a) PP-ATP : PNMP/PSS, (b) PP-ATP, (c) PNMP/PSS] cycled in 0.1 M NaCl aq. solutions at $v = 100$ mV s^{-1}. Each film thickness is 300 nm.

This was followed by a second potential step to -0.6 V. Using this two step process, the first step reduced PNMP outer films while PP-ATP remained oxidized. The second step subsequently reduced the PP-ATP inner films. The frequency results of 300 nm : 150 nm bilayers, shown in Figure 7-3 (top), illustrate frequency increases (mass loss) for PP-ATP : PNMP-Cl and frequency decreases (mass gain) for PP-ATP : PNMP/PSS and PP-ATP : PNMP/HPN during the first potential step. This is expected since Cl^- is released from the outer layer of PP-ATP : PNMP-Cl while Na^+ is incorporated into the outer layer of PP-ATP : PNMP/PSS and PP-ATP : PNMP/HPN during the first potential step. The frequency results of 300 nm : 300 nm bilayers during the first potential step, shown in Figure 7-3 (bottom), show slightly greater frequency responses, indicating that the amounts of moving species are a function of the film thicknesses.

The frequency responses due to ion transport from the PP-ATP inner films during the second potential step are complicated due to the presence of outer films. As noted earlier in Chapter 5, the EQCM monitored reduction of PP-ATP single films show a sharp initial frequency drop, followed by a smooth frequency increase. This was explained by the fact that most of the reduced sites of PP-ATP films are rapidly charge balanced by the dominantly mobile Na^+ ions during the initial stage of reduction as a result of their faster diffusion rate. Similar frequency drops are observed during the initial stages of reduction of PP-ATP : PNMP/PSS and PP-ATP : PNMP/HPN, while PP-ATP : PNMP-Cl shows continuous frequency decreases. Unlike PP-ATP single films, smooth frequency decreases are observed after the sharp frequency drops for PP-ATP : PNMP/PSS and PP-ATP : PNMP/HPN of 300 nm : 150 nm thicknesses, followed by rather steep frequency increases (Figure 7-3 (top)b,c). PP-ATP : PNMP/PSS and PP-ATP : PNMP/HPN with thicker outer films (Figure 7-3 (bottom)b,c) show continuous frequency decreases within the experimental time scale. It should be noted that these frequency responses were monitored immediately after

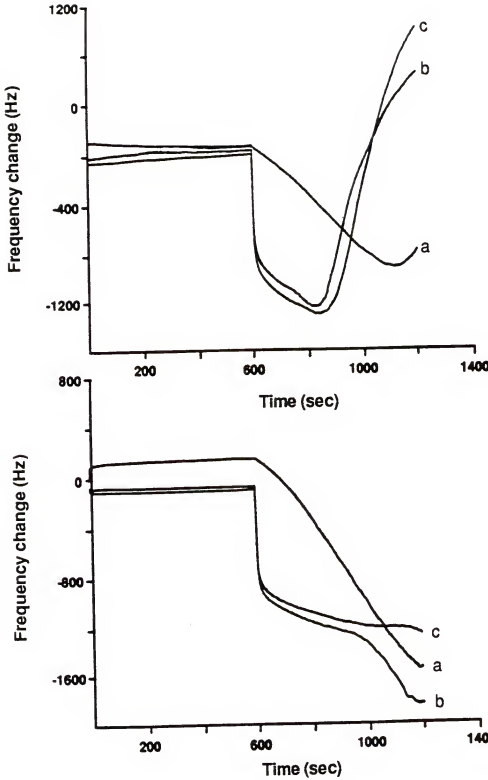

Figure 7-3 Frequency changes of (a) PP-ATP : PNMP-Cl, (b) PP-ATP : PNMP/HPN and (c) PP-ATP : PNMP/PSS for (top) 300 nm : 150 nm and (bottom) 300 nm : 300 nm. Potentials were stepped from +0.6 V to 0.0 V and subsequently to -0.6 V in 0.1 M NaCl aq. solutions.

film preparation before equilibration. This suggests that the results do not preclude significant initial ATP release during frequency decreases since the EQCM measures the net mass flux.

The difference in initial frequency responses during reduction of the inner films between PP-ATP : PNMP-Cl and PP-ATP : PNMP/polyelectrolyte is due to different ionic conductivity of the outer films. Reduced PNMP/polyelectrolyte has higher ionic conductivity than reduced PNMP-Cl [123]. This affects the mobility of the moving species (Na^+, ATP^{3-}, solvent, etc.) through the outer film since the corresponding charge response of PP-ATP : PNMP-Cl indicates slow reduction of the inner film, as shown in Figure 7-4. This suggests that the instantaneous incorporation of Na^+ is inhibited by the reduced PNMP film of low ionic conductivity. Slower ion transport through PNMP-Cl is also observed during the reduction of the outer films at the first potential step.

In addition, Figure 7-4 demonstrates that the charge changes during the first potential step are related to the film thicknesses as ca. 3.8 mC and ca. 5.0 mC are passed for 150 nm and 300 nm PNMP outer films respectively. The lack of direct proportionality may be due to insufficient reduction of the thicker 300 nm PNMP films within the experimental time scale. This implies that it is possible to alter the amount of moving ions for the control of ionic concentrations of switching media by changing film thicknesses.

7-3 In Situ Spectroscopic Studies

ATP release into supporting electrolyte from bilayers was spectroscopically monitored at the maximum absorbance of ATP (260 nm) during reduction of PP-ATP inner films. PP-ATP : PNMP-Cl bilayers with varied thicknesses of inner and outer films were prepared on a Pt plate. After thorough washing with distilled water, the bilayer films were placed in a cell containing 3.5 cm^3 aq. solutions of 0.1 M NaCl. A

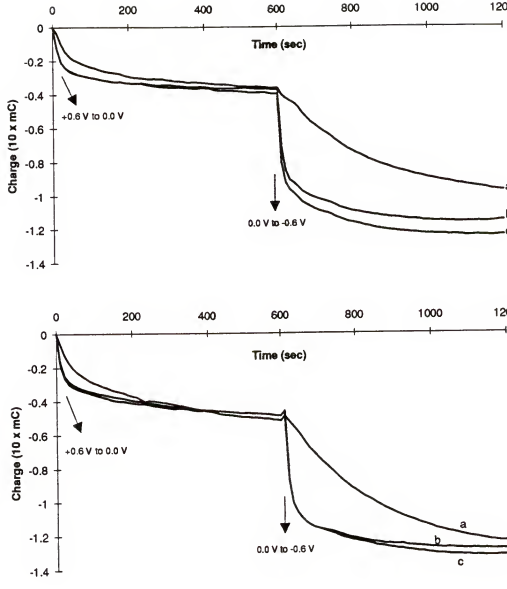

Figure 7-4 Charge changes of (a) PP-ATP : PNMP-Cl, (b) PP-ATP : PNMP/HPN and (c) PP-ATP : PNMP/PSS for (top) 300 nm : 150 nm and (bottom) 300 nm : 300 nm. Potentials were stepped from +0.6 V to 0.0 V and subsequently to -0.6 V (vs. Ag/AgCl) in 0.1 M NaCl aq. solutions.

Ag wire (+0.08 V vs. Ag/AgCl) and a Pt plate were used as the reference and counter electrode respectively. Further potentials in this chapter are relative to this reference electrode.

After electrosynthesis, the bilayers were conditioned for oxidation at +0.6 V for 1 min. The potentials were then stepped to 0.0 V to reduce the outer films while measuring the UV absorbance of the electrolyte at 260 nm as a function of time. UV absorbance changes during this process are negligible, as shown in Figures 7-5 and 7-6, indicating that the ATP remains entrapped in the film during the reduction of the outer films and concurrent Cl^- release. The potential dependence of ATP release from PP-ATP single films was described in Chapter 5 and only small absorbance increases were observed with potential steps down to -0.4 V. Application of the dual ion transport concept to PP-ATP : PNMP-Cl bilayers allows incorporation of reactive anions (cations for PP-ATP : PNMP/PSS and PP-ATP : PNMP/HPN) into the outer films by repeated redox switching at high potential. These ions can subsequently be released during the first potential step along with ATP release at low potential.

Potentials were stepped to -0.6 V to stimulate ATP release by reducing the inner films. Figure 7-5 illustrates UV absorbance changes in electrolyte containg bilayers with different outer film thicknesses. It is evident that ATP is released most rapidly when no outer film is present and the absorbance quickly reaches a maximum value of 0.13 within ca. 3 min. (Figure 7-5a). This value was used to calculate the fraction of released ATP from PP-ATP. Assuming a 0.27 doping level (see Chapter 5), PP-ATP inner films (0.75 cm^2) are composed of 4.2 x 10^{-7} mol of polymer repeat units and 3.8 x 10^{-8} mol of ATP. By using the extinction coefficient of 15.4 x 10^3 dm^3 mol^{-1} cm^{-1} [129], it was determined that 2.95 x 10^{-8} mol of ATP were released. This leads to the conclusion that the ratio of ATP released to initially incorporated ATP during electropolymerization is ca. 80 %. The ratio of released ATP from PP-ATP : PNMP-Cl at a certain time is inversely related to the outer film thickness. For example, the

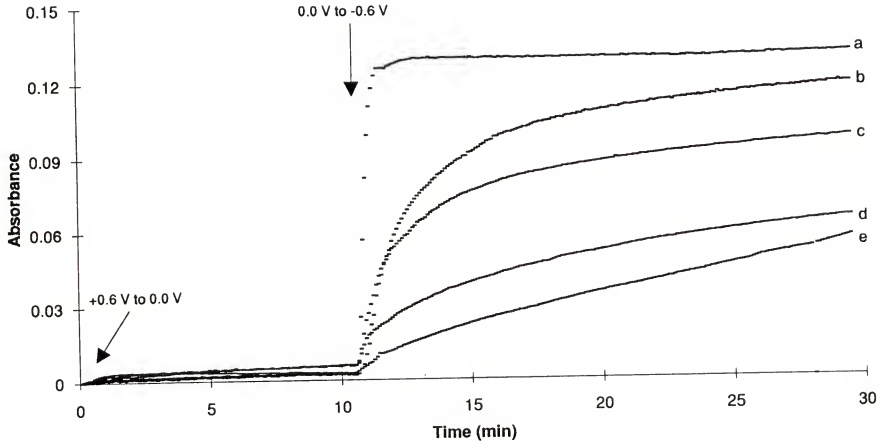

Figure 7-5 UV absorbance changes of electrolyte, measured at 260 nm for PP-ATP : PNMP-Cl bilayers with varied outer film thicknesses. PP-ATP (300 nm) : PNMP-Cl [(a) no film, (b) 150 nm, (c) 300 nm, (d) 450 nm, (e) 750 nm] bilayers in 0.1 M NaCl were subjected to potential (vs. Ag wire) steps.

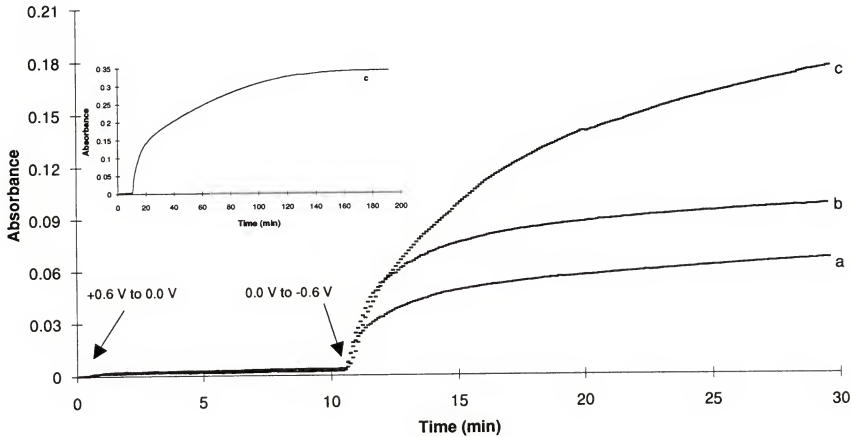

Figure 7-6 UV absorbance changes measured at 260 nm. PP-ATP [(a) 150 nm, (b) 300 nm, (c) 750 nm] : PNMP-Cl (300 nm) bilayers in 0.1 M NaCl were subjected to potential (vs. Ag wire) steps. Inset shows the maximum ATP release from a PP-ATP : PNMP-Cl (750 nm : 300 nm) bilayer.

values calculated after 10 min. at -0.6 V in Figure 7-5, are 63 %, 51 %, 30 % and 22 % for bilayers consisting of 150 nm, 300 nm, 450 nm and 750 nm thick PNMP-Cl outer films, respectively. The UV absorbances due to ATP release from bilayers continue to increase with time, suggesting that the maximum value (80 %) may ultimately be reached over an extended period of time.

UV absorbance changes in electrolytes induced by switching bilayers, consisting of varied thicknesses of PP-ATP inner films and 300 nm PNMP-Cl outer films, were monitored while reducing the inner films at -0.6 V (Figure 7-6). Initial ATP release rates are similar since outer film thicknesses are identical. After the initial surge of ATP, the increase of the UV absorbance is proportional to the PP-ATP inner film thickness. PP-ATP : PNMP-Cl of 750 nm : 300 nm gives a continuous but relatively rapid increase of the UV absorbance, which is ultimately leveled off (Figure 7-6, inset). This result is useful as the amounts of ATP released in a given time can be controlled by increasing PP-ATP film thicknesses.

PP-ATP : PNMP/HPN were electrochemically synthesized to combine biocompatibility with ATP release. The cation dominant transport of PNMP/HPN was described above. Bilayers with different outer film thicknesses were subjected to the same potential steps as PP-ATP : PNMP-Cl and UV absorbance changes of the electrolyte were measured with time, as shown in Figure 7-7. While a negligible UV absorbance increase is again seen during the outer film reduction, rapid ATP release is observed upon reduction of the inner films. The amounts of ATP released at a certain point is related to the outer film thickness as in PP-ATP : PNMP-Cl. The initial UV absorbance increases in electrolytes containing bilayers with 150 nm and 300 nm outer film thicknesses (Figure 7-7b and 7-7c) especially rapid and followed by rather smooth increases when compared to Figure 7-5b and 7-5c. This can be related to fast ion transport through the PP/HPN films which have higher ionic conductivity than reduced PNMP-Cl.

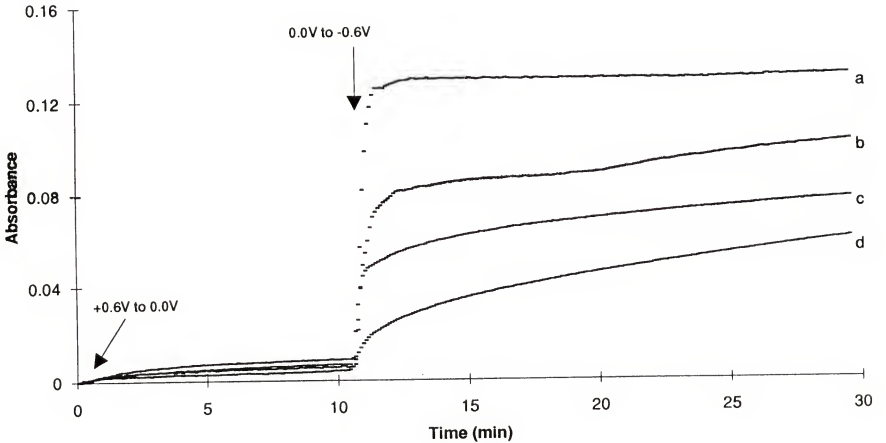

Figure 7-7 UV absorbance changes measured at 260 nm. PP-ATP (300 nm) : PNMP/HPN [(a) no film, (b) 150 nm, (c) 300 nm, (d) 750 nm] bilayers in 0.1 M NaCl were subjected to potential (vs. Ag wire) steps.

UV absorbance changes in the electrolyte indeced by PP-ATP : PNMP/PSS during potential steps, are shown in Figure 7-8. Again little ATP release is observed during the outer film reduction as expected. The second potential step stimulates ATP release whose rates are slower than PP-ATP single films. As seen with PP-ATP : PNMP/HPN, initial ATP release rates with outer film thicknesses are independent of the outer film thickness. The total amount of ATP released is independent of PNMP/PSS thicknesses with ca. 60 % released after 20 min reduction. This is surprising since it indicates that teh identity of entrapped polyelectrolyes can differently affect the ion mobility.

Apparent diffusion coefficients (D_{app}) were calculated from the initial slope of a plot of A(t) vs. $t^{1/2}$. Assuming semi-infinite linear diffusion and using Beer's law, integration of the current response gives:

$$A(t) = A_i - (2D_{app}{}^{1/2}\, t^{1/2}\, \delta^{-1}\, \pi^{-1/2})(A_i - A_f) \qquad (7\text{-}1)$$

where A_i, A(t) and A_f are the initial , time-t and time-infinity absorbance values and δ is the film thickness [107C]. The initial short time ATP release region was used for determination of D_{app} and the maximum absorbance value (0.13) at long times was used as A_f. Table 7-1 shows that the presence of outer layers retards the rate of ATP release in all examples and the extens of D_{app} decreases are related to the composition of the outer film. While ATP diffusion through PNMP-Cl becomes slower with the film thickness as expected, the increase of PNMP/PSS thicknesses does not appear to significantly affect ATP diffusion. Although the D_{app} of PP-ATP : PNMP/HPN decreases with the increase of the outer film thickness, it is appear to be small relative to PP-ATP :PNMP-Cl. These D_{app} values (except PP-ATP : PNMP-Cl = 300 nm : 750 nm) are similar to those reported for a single polymer layer [49,58,60,62], indicating that the ATP release through reduced PNMP outer films is significantly retarded at the initial stage. It should be noted that the values are only useful for the

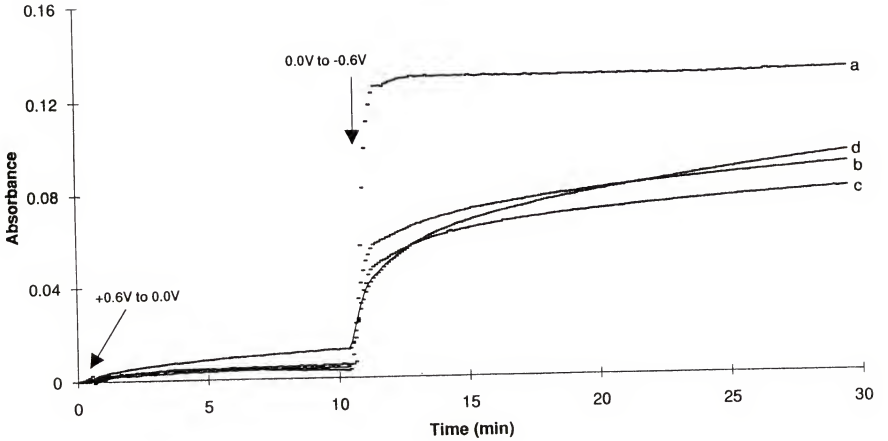

Figure 7-8 UV absorbance changes measured at 260 nm. PP-ATP (300 nm) : PNMP/PSS [(a) no film, (b) 150 nm, (c) 300 nm, (d) 750 nm] bilayers in 0.1 M NaCl were subjected to potential (vs. Ag wire) steps.

Table 7-1 Comparison of apparent diffusion coefficients for PP-ATP based bilayers (PP-ATP = 300 nm).

film	outer film thickness (nm)	$10^{10} D_{app}$ ($cm^2\ s^{-1}$)
PP-ATP	300	4.75
PP-ATP : PNMP-Cl	150	2.29
	300	1.63
	750	5.44×10^{-3}
PP-ATP : PNMP/PSS	150	1.26
	300	2.52
	750	3.01
PP-ATP : PNMP/HPN	150	1.68
	300	0.247
	750	0.375

relative comparison since outer film which remains reduced during ATP release can affect the diffusion process.

7-4 Conclusions

Bilayers consisting of PP-ATP inner films and PNMP outer films were constructed. For outer films, PNMP-Cl was used as an anion transport layer, and PNMP/HPN and PNMP/PSS were examined for cation transport during redox switching at high potentials. Spectroscopic results show that ATP is not released during the low potential outer film redox processes. Electrochemically stimulated ATP release was turned on when PP-ATP inner films were reduced. The amounts of released ATP were proportional to the PP-ATP inner film thicknesses and the rates were related to outer film thicknesses and compositions.

These dual ion transport concepts through bilayer construction is outlined in Figure 7-9. By constructing a bilayer of PP-ATP (or possibly other anionic biomolecules or drugs which can be electrochemically released) and PNMP-Cl (or possibly other reactive anions), a single polymer modified electrode can serve as an anion absorption and emission device of small anionic electrolytes along with ATP release. PP-ATP : PNMP/polyelectrolyte bilayers can release or absorb small cations (or possibly cationic biomolecules or drugs) during high potential redox switching along with ATP released at low potentials.

PP-ATP : PNMP-Cl

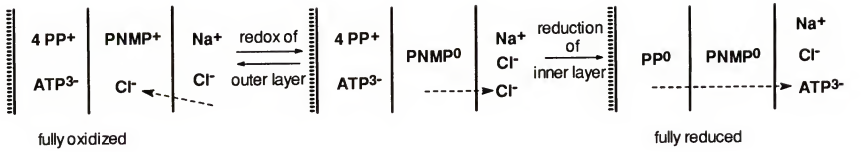

PP-ATP : PNMP/PE

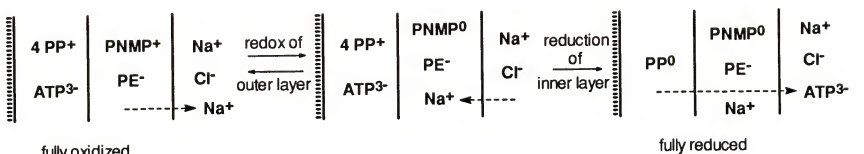

Figure 7-9 Schematic diagram showing the control of ion flux and electrochemically stimulated ATP release.

REFERENCES

1. Ito, T.; Shirakawa, H.; Ikeda, S. *J. Polym. Sci., Polym. Chem.* **1974**, *12*, 11.

2. Chiang, C. K.; Park, Y. W.; Heeger, A. J.; Shirakawa, H.; Louis, E. J.; MacDiarmid, A. G. *Phys. Rev. Lett.* **1977**, *39*, 1098.

3. (A) Akagi, K.; Sakamaki, K.; Shirakawa, H. *Synth. Met.* **1993**, *55*, 779.
   (B) Reibel, D.; Nuffer, R.; Mathis, C. *Synth. Met.* **1993**, *55*, 791.

4. Bredas, J. L.; Chance, R. R.; Silbey, R. *Phys. Rev. B* **1982**, *26*, 5843.

5. (A) Niziurski-Mann, R. E.; Scordilis-Kelly, C.; Liu, T.-L.; Cava, M. P.; Carlin, R. T. *J. Am. Chem. Soc.* **1993**, *115*, 887.
   (B) Abdou, M. S. A.; Xie, Z. W.; Leung, A. M.; Holdcroft, S. *Synth. Met.* **1992**, *52*, 159.

6. (A) Diaz, A. F.; Kanazawa, K. K.; Gardini, G. P. *J. Chem. Soc., Chem. Commun.* **1979**, 635.
   (B) Kanazawa, K. K.; Diaz, A. F.; Geiss, R. H.; Gill, W. D.; Kwak, J. F.; Logan, J. A.; Rabolt, J. F.; Street, G. B. *J. Chem. Soc., Chem. Commun.* **1979**, 854.

7. Dall'Ollio, A.; Dascola, Y.; Gardini, G. P. *C. R. Acad. Sci.* **1969**, *267*, 4336.

8. Diaz, A. F. *Chem. Scr.* **1981**, *17*, 142.

9. Tourillon, G.; Garnier, F. *J. Electroanal. Chem.* **1982**, *135*, 173.

10. Wellinghoff, S. T.; Kedrowski, T.; Lenekhe, S.; Tshida, T. *J. Phys. Paris Colloq.* **1983**, *677*, C3.

11. Waltman, R. J.; Bargon, J.; Diaz, A. *J. Phys. Chem.* **1984**, *88*, 4343.

12. Bargon, J.; Mohamand, S.; Waltman, R. J. *IBM J. Res. Develop.* **1983**, *27*, 330.

13. (A) Ivory, P. M.; Miller, G. G.; Sowa, J. M.; Shacklette, L. W.; Chance, R. R.; Baughman, R. H. *J. Chem. Phys.* **1979**, *71*, 1506.
   (B) Delamar, M.; Lacaze, P. C.; Dumousseau, J. Y.; Dubois, J. E. *Electrochim. Acta* **1982**, *27*, 330.

14. Rault-Berthelot, J.; Simonet, J. *J. Electroanal. Chem.* **1985**, *182*, 187.

15. (A) Diaz, A. F.; Logan, J. A. *J. Electroanal. Chem.* **1980**, *111*, 111.
(B) MacDiarmid, A. G.; Chiang, J. C.; Halpern, M.; Huang, H. S.; Mu, S. L.; Somasiri, N. L. D.; Wu, W.; Yaniger, S. I. *Mol. Cryst. Liq. Cryst.* **1985**, *121*, 173.
(C) Genies, E. M.; Tsintavis, C.; Syed, A. A. *Mol. Cryst. Liq. Cryst.* **1985**, *121*, 181.

16. (A) Potts, H. A.; Smith, G. F. *J. Chem. Soc.* **1957**, 4018.
(B) Chiang, Y.; Whipple, E. B. *J. Am. Chem. Soc.* **1963**, *85*, 2763.

17. Gau, S. C.; Milliken, J.; Pron, A.; MacDiarmid, A. C.; Heeger, A. J. *J. Chem. Soc., Chem. Commun.* **1979**, 662.

18. Gardini, G. P. *Adv. Heterocyclic Chem.* **1973**, *15*, 67.

19. (A) Street, G. B.; Clarke, T. C.; Krounbi, M.; Kanazawa, K.; Lee, V.; Pfluger, P.; Scott, J. C.; Weiser, G. *Mol. Cryst. Liq. Cryst.* **1982**, *83*, 1285.
(B) Shimidzu, T.; Ohtani, A.; Iyoda, T.; Honda, K. *J. Chem. Soc., Chem. Commun.* **1986**, 1414.

20. Salmon, M.; Kanazawa, K. K.; Diaz, A. F.; Krounbi, M. *J. Polym. Sci.* **1982**, *20*, 187.

21. Warren, L. F.; Walker, J. A.; Anderson, D. P.; Rhodes, C. G.; Buckley, L. J. *J. Electrochem. Soc.* **1989**, *136*, 2286.

22. Chandler, G. K.; Pletcher, D. *Special Reports Electrochemistry, Royal Society Chemistry, London,* **1985**, *10*, 117.

23. (A) Christensen, P. A.; Hamnett, A. *Electrochim. Acta* **1991**, *36*, 1263.
(B) Lang, P.; Chao, F.; Costa, M.; Garnier, F. *Polymer* **1987**, *28*, 668.

24. (A) Raymond, D. E.; Harrison, D. J. *J. Electroanal. Chem.* **1993**, *361*, 65.
(B) Raymond, D. E.; Harrison, D. J. *J. Electroanal. Chem.* **1990**, *296*, 269.
(C) Tanaka, K.; Shichiri, T.; Wang, S.; Yamabe, T. *Synth. Met.* **1988**, *24*, 203.

25. John, R.; Wallace, G. G. *J. Electroanal. Chem.* **1991**, *306*, 157.

26. Fermin, D. J.; Scharifker, B. R. *J. Electroanal. Chem.* **1993**, *357*, 273.

27. Bruckenstein, S.; Sharkey, J. W. *J. Electroanal. Chem.* **1988**, *241*, 211.

28. Bose, C. S. C.; Basak, S.; Rajeshwar, K. *J. Phys. Chem.* **1992**, *96*, 9899.

29. (A) Wegner, G. *Agnew. Chem. Int. Ed. Engl.* **1981**, *20*, 361.
(B) Baker, C.; Reynolds, J. R. *J. Electroanal. Chem.* **1988**, *251*, 307.

30. (A) Scharifker, B. R.; Garcia-Pastoriza, E.; Marino, W. *J. Electroanal. Chem.* **1991**, *300*, 85.
(B) Lowen, S. V.; Van Dyke, J. D. *J. Polym. Sci. Polym. Chem.* **1990**, *28*, 451.

31. Qiu, Y.-J.; Reynolds, J. R. *J. Polym. Sci., Polym. Chem.* **1992**, *30*, 1315.

32. (A) Otero, T. F.; Tejada, R.; Elola, A. S. *Polymer* **1987**, *28*, 651.
(B) Fletcher, S.; Halliday, C. S.; Gates, D.; Westcott, M.; Lwin, T.; Nelson, G. *J. Electroanal. Chem.* **1983**, *159*, 267.

33. Inoue, T.; Yamase, T. *Bull. Chem. Soc. Jpn.* **1983**, *56*, 985.

34. Genies, E. M.; Bidan, G.; Diaz, A. F. *J. Electroanal. Chem. Interfacial Electrochem.* **1983**, *149*, 101.

35. (A) Waltman, R. J.; Bargon, J. *Tetrahedron* **1984**, *40*, 3963.
(B) Tanaka, K.; Shichiri, T.; Toriumi, M.; Yamabe, T. *Synth. Met.* **1989**, *30*, 271.

36. (A) Eberson, L. *Acta Chem. Scand.* **1980**, *B34*, 747.
(B) Otero, T. F.; Rodriguez, J. *Synth. Met.* **1992**, *51*, 307.

37. (A) Cheng, K. M.; Bloor, D.; Stevens, G. C. *Polymer* **1988**, *29*, 1709.
(B) Janssen, W.; Beck, F. *Polymer* **1989**, *30*, 353.
(C) Schimeisen, M.; Beck, F. *J. Appl. Electrochem.* **1989**, *19*, 401.

38. (A) Noufi, R.; Frank, A. J.; Nozik, A. J. *J. Am. Chem. Soc.* **1981**, *103*, 1849.
(B) Bull, R. A.; Fan, F. R.; Bard, A. J. *J. Electrchem. Soc.* **1983**, *130*, 1636.

39. (A) Wernet, W.; Monkenbusch, M.; Wegner, G. *Mol. Cryst. Liq. Cryst.* **1985**, *118*, 193.
(B) Wegner G.; Ruhe, R. *Faraday Disscuss. Chem. Soc.* **1989**, *88*, 333.
(C) Kiani, M. S.; Mitchell, G. R. *Synth. Met.* **1992**, *48*, 203
(D) Omastova, M.; Kosina, S.; Skakalova, V.; Jancula, D. *Synth. Met.* **1993**, *53*, 227.
(E) Wynne, K. J.; Street, G. B. *Macromolecules* **1985**, *18*, 2361.
(F) Belanger, D.; Laperriere, G.; Gravel, L. *J. Electrochemical. Soc.* **1990**, *137*, 365.
(G) Ye, F.; Noftle, R. E.; DesMarteau, D. D. *Synth. Met.* **1993**, *60*, 141.

40. (A) Zinger, B.; Shaier, P.; Zemel, A. *Synth. Met.* **1991**, *40*, 283.
(B) Couves, L. D.; Porter, S. J. *Synth. Met.* **1989**, *28*, C761.
(C) Qian, P.; Pei, Q.; Huang, Z. *Makromol. Chem.* **1991**, *192*, 1263.
(D) Pei, Q.; Qian, R. *J. Electroanal. Chem.* **1992**, *322*, 153.

41. Qian, R.; Li, Y.; Yan, B.; Zhang, H. *Synth. Met.* **1989**, *28*, C51.

42. (A) Buckly, L. J.; Roylance, D. K.; Wnek, G. E.; *J. Polym. Sci. B.* **1987**, *25*, 2179.
(B) Kuwabata, S.; Okamoto, K.; Yoneyyama, H. *J. Polym. Sci. Faraday Trans.* **1988**, *84*, 2317.

43. (A) Bates, N.; Cross, M.; Lines, R.; Walton, D. *J. Chem. Soc., Chem. Commun.* **1985**, 871.
(B) Shimidzu, T.; Ohtani, A.; Iyoda, T.; Honda, K. *J. Chem. Soc. Chem. Commun.* **1986**, 1415.
(C) Noftle, R. E.; Pletcher, D. *J. Electroanal. Chem.* **1987**, *227*, 229.
(D) Gieselman, M. B.; Reynolds, J. R. *Macromolecules* **1990**, *23*, 3118.
(E) Fan, F. F.; Bard, A. J. *J. Electrochem. Soc.* **1987**, *133*, 301.
(F) Chiu, H.-T.; Lin, J.-S.; Huang, C.-M. *J. Appl. Electrochem.* **1992**, *22*, 358.

44. (A) Glatzhofer, D. T.; Ulanski, J.; Wegner, G. *Polymer* **1987**, *28*, 449.
(B) Miller, L. L.; Zhou, Q. X. *Macromolecules* **1987**, *20*, 1594.
(C) Warren, L. F.; Anderson, D. P. *J. Electrochem. Soc.* **1987**, *134*, 101.

45. (A) Rosseinsky, D. R.; Morse, N. J.; Slade, R. C. T.; Hix, G. B.; Mortimer, R. J.; Walton, D. J. *Electrochim. Acta* **1991**, *36*, 733.
(B) Schlenoff, J. B.; Xu, H. *J. Electrochem. Soc.* **1992**, *139*, 2397.

46. (A) Asavapiriyanont, S.; Chandler, G. K.; Gunawardena, G. A.; Pletcher, D. *J. Electroanal. Chem.* **1984**, *177*, 229.
(B) Haimerl, A.; Merz, A. *J. Electroanal. Chem.* **1987**, *220*, 55.

47. (A) Freund, M.; Brajter-Toth, A. *Anal. Chem.* **1989**, *61*, 1048.
(B) Witkowski, A. Brajter-Toth, A. *Anal. Chem.* **1992**, *64*, 635.

48. West, K.; Jacobsen, T.; Zachau-Christiansen, B.; Careem, M. A.; Skaarup, S. *Synth. Met.* **1993**, *55*, 1412.

49 Krishna, V.; Ho, Y.-H.; Basak, S.; Rajeshwar, K. *J. Am. Chem. Soc.* **1991**, *113*, 3325.

50 Zhao, H.; Price, W. E.; Wallace, G. G. *Polymer* **1993**, *34*, 16.

51 Sabatani, E.; Redonio, A.; Rishpon, J.; Rudge, A.; Rubinstein, I.; Gottesfeld, S. *J. Chem. Soc. Faraday Trans.* **1993**, *89*, 287.

52. (A) Evans, G. P. in *Electrochemical Science and Technology of Polymers,* Vol 1, Gerisher and C. W. Tobias, Eds., VCH, Weinheim **1990**.
(B) Skotheim, T. A. Ed., *Handbook of Conducting Polymer*, Mercel Dekker, Inc. New York **1986**.

53. Onoda, M.; Nakayama, H.; Morita, S.; Yoshino, K. *Synth. Met.* **1993**, *55*, 1343.

54. Hunter, T. B.; Tyler, P. S.; Smyrl, W. H.; White, H. S. *J. Electrochem. Soc.* **1987**, *134*, 2198.

55. Onikubo, T.; Lin, R.-J.; Kaneko, M. *J. Electroanal. Chem.* **1993**, *361*, 143.

56. Qiu, Y.-J.; Reynolds, J. R. *Polym. Eng. Sci.* **1991**, *31*, 417.

57. Okano, M.; Fujishima, A.; Honda, K. *J. Electroanal. Chem.* **1985**, *185*, 393.

58. Baker, C. K.; Qiu, Y.-J.; Reynolds, J. R. *J. Phys. Chem.* **1991**, *95*, 4446.

59. Naoi, K.; Lien, M.; Smyrl, W. *J. Electrochem. Soc.* **1991**, *138*, 440.

60. Shimidzu, T.; Ohtani, A.; Iyoda, T.; Honda, K. *J. Electroanal. Chem.* **1987**, *224*, 123.

61. Laviron, E. *J. Electroanal. Chem.* **1972**, *39*, 1.

62. Genies, E. M.; Bidan, G,; Diaz, A. F. *J. Electroanal. Chem.* **1983**, *149*, 101.

63. Curtin, L. S.; Komplin, G. C.; Pietro, W. *J. Phys. Chem.* **1988**, *92*, 12.

64. Tsai, E. W.; Pajkossy, T.; Rajeshwar, K.; Reynolds, J. R. *J. Phys. Chem.* **1988**, *62*, 3560.

65. Schlenoff, J. B.; Chien, J. C. W. *J. Am. Chem. Soc.* **1987**, *109*, 6269.

66. Kaufmann, J. H.; Kanazawa, K. K.; Street, G. B. *Phys. Rev. Lett.* **1984**, *53*, 2461.

67. Genies, E. M.; Pernaut, J. M. *Synth. Met.* **1984**, *10*, 117.

68. Inoue, M. B.; Nebesny, K. W.; Fernando, Q.; Castillo-Ortega, MA. M.; Inoue, M. *Synth. Met.* **1990**, *38*, 205.

69. (A) Miller, L. L.; Zinger, B.; Zhou, Q.-X. *J. Am. Chem. Soc.* **1987**, *109*, 2267.

(B) Lian, G.; Dong, S. *J. Electroanal. Chem.* **1989**, *260*, 127.
(C) Dong, S.; Lian, G. *J. Electroanal. Chem.* **1990**, *291*, 23.
(D) Breen, W.; Cassidy, J. F.; Lyons, M. E. G. *J. Electroanal. Chem.* **1991**, *297*, 445.

70. Zhou, Q.-Z.; Kolaskie, C. J.; Miller, L. L. *J. Electroanal. Chem.* **1987**, *223*, 283.

71. Lee, I. C. *J. Electroanal. Chem.* **1992**, *340*, 333.

72. John, R.; Wallace, G. G. *J. Electroanal. Chem.* **1993**, *354*, 145.

73. Shinohara, H.; Kojima, J.; Aizawa, M. *J. Electroanal. Chem.* **1989**, *266*, 297.

74. Reynolds, J. R.; Pyo, M.; Qiu, Y.-J. *Synth. Met.* **1993**, *55*, 1388.

75. (A) Hillman, A. R.; Swann, M. J.; Bruckenstein, S. *J. Electroanal. Chem.* **1990**, *291*, 147.
(B) Bruckenstein, S.; Wilde, C. P.; Shay, M.; Hillman, A. R. *J. Phys. Chem.* **1990**, *94*, 787.
(C) Hillman, A. R.; Loveday, D. C.; Swann, M. J.; Bruckenstein, S.; Wilde, C. P. *J. Chem. Soc. Faraday Trans.* **1991**, *87*, 2047.

76. Lasky, S.; Buttry, D. A. *J. Am. Chem. Soc.* **1988**, *110*, 6258.

77. Lien, M.; Smyrl, W. H. *J. Electroanal. Chem.* **1991**, *309*, 333.

78. Zhong, C.; Doblhofer, K. *Electrochim. Acta.* **1990**, *35*, 1971.

79. Chesher, D. A.; Christensen, P. A.; Hamnett, A. *J. Chem. Soc. Fraraday Trans.* **1993**, *89*, 303.

80. Tsai, E. W.; Pajkossy, T.; Rajeshwar, K.; Reynolds, J. R. *J. Phys. Chem.* **1988**, *92*, 3560.

81. (A) Novak, P.; Kotz, R.; Hass, O. *J. Electrochem. Soc.* **1993**, *140*, 37.
(B) Barbero, C.; Miras, M. C.; Hass, O.; Kotz, R. *J. Electrochem. Soc.* **1991**, *138*, 669.
(C) Barbero, C.; Miras, M. C.; Kotz, R. *Electrochim. Acta* **1992**, *37*, 429.
(D) Barbero, C.; Miras, M. C.; Hass, O.; Kotz, R. *J. Electroanal. Chem.* **1991**, *310*, 437.

82. (A) Benje, M.; Hofmann, U.; Pitterman, U.; Weil, K. G. *Ber. Bunsenges. Phys. Chem.* **1988**, *92*, 1257.
(B) Bruckenstein, S.; Swathirajan, S. *Electrochim. Acta* **1985**, *30*, 851.

(C) Schumacher, R.; Muller, A.; Stockel, W. *J. Electroanal. Chem.* **1987**, *219*, 311.

83. Ward, M. D. *J. Electroanal. Chem.* **1989**, *273*, 79.

84. (A) Deakin, M.; Li, T.; Melroy, O. *J. Electroanal. Chem.* **1988**, *243*, 343.
(B) Cheek, G. T.; O'Grady, W. E. *J. Electroanal. Chem.* **1990**, *277*, 341.

85. Curie, P.; Curie, J. *C. R. Acad. Sci.* **1880**, *91*, 294.

86. Buttry, D. A.; Ward, M. D. *Chem. Rev.* **1992**, *92*, 1355.

87. Sauerbrey, G. Z. *Phys.* **1959**, *155*, 206.

88. Ullevig, D. M.; Evans, J. M.; Albrecht, M. G. *Anal. Chem.* **1982**, *54*, 2341.

89. Lasky, S. J.; Buttry, D. A. *ACS Symo. Ser.* **1989**, *403*, 237.

90. (A) Schumacher, R.; Gordon, J.; Melroy, O. *J. Electroanal. Chem.* **1987**, *216*, 127.
(B) Muller, A.; Wicker, M.; Schumacher, R.; Schindler, R. N. *Ber. Bunsenges. Phys. Chem.* **1988**, *92*, 1395.

91. (A) Bruckenstein, S.; Wilde, C. P.; Shay, M.; Hillman, A. R. Loveday, D. C. *J. Electroanal. Chem.* **1989**, *258*, 457.
(B) Hillman, A. R.; Loveday, D. C.; Bruckenstein, S.; Wilde, C. P. *J. Chem. Soc. Faraday Trans.* **1990**, *86*, 437.
(C) Ward, M. D. *J. Electrochem. Soc.* **1988**, *135*, 2747.

92. (A) Hillman, A. R.; Swann, M. J.; Bruckenstein, S. *J. Phys. Chem.* **1991**, *95*, 3271.
(B) Bruckenstein, S.; Wilde, C. P.; Hillman, A. R. *J. Phys. Chem.* **1990**, *94*, 6458.
(C) Bruckenstein, S.; Wilde, C. P.; Hillman, A. R. *J. Phys. Chem.* **1993**, *97*, 6853.

93. (A) Feldman, B. J.; Melroy, O. R. *J. Electroanal. Chem.* **1987**, *234*, 213.
(B) Aoki, K.; Miyamoto, T.; Ohsawa, Y. *Bull. Chem. Soc. Jpn.* **1989**, *234*, 213.

94. Varineau, P. T.; Buttry, D. A. *J. Phys. Chem.* **1987**, *91*, 1292.

95. Hillman, A. R.; Loveday, D. C.; Bruckenstein, S. *Langmuir* **1991**, *7*, 191.

96. Ward, M. D. *J. Phys. Chem.* **1988**, *92*, 2049.

97. Hillman, A. R.; Bruckenstein, S. *J. Chem. Soc. Faraday Trans.* **1993**, *89*, 339.

98. (A) Rishpon, J.; Redondo, A.; Derouin, C.; Gottesfeld, S. *J. Electroanal. Chem.* **1990**, *294*, 73.
(B) Rubinstein, I.; Rishpon, J.; Sabatini, E.; Redondo, A.; Gottesfeld, S. *J. Am. Chem. Soc.* **1990**, *112*, 6135.

99. Servagent, S.; Vieil, E. *J. Electroanal. Chem.* **1990**, *280*, 227.

100. Baker, C. K.; Reynolds, J. R. *Synth. Met.* **1989**, *28*, C21.

101. Doblhofer, K. *J. Electroanal. Chem.* **1992**, *331*, 1015.

102. Feldberg, S. W. *J. Am. Chem. Soc.* **1984**, *106*, 4671.

103. Pickup, P. G.; Osteryoung, R. A. *J. Electroanal. Chem.* **1985**, *195*, 271.

104. (A) Saveant, J. M. *J. Electroanal. Chem.* **1986**, *201*, 211.
(B) Saveant, J. M. *J. Electroanal. Chem.* **1987**, *238*, 1.
(C) Saveant, J. M. *J. Phys. Chem.* **1988**, *92*, 1011.
(D) Saveant, J. M. *J. Phys. Chem.* **1988**, *92*, 4526.
(E) Andrieux, C. P.; Saveant, J. M. *J. Phys. Chem.* **1988**, *92*, 6761.
(F) Saveant, J. M. *J. Electroanal. Chem.* **1988**, *242*, 1.
(G) Saveant, J. M. *J. Electroanal. Chem.* **1991**, *302*, 91.

105. Yeu, T.; Nguyen, T. V.; White, R. E. *Electrochem. Sci. Tech.* **1988**, *135*, 1971.

106. (A) Kaneto, K.; Maxfield, M.; Nairns, D. P.; MacDiarmid, A. G. *J. Chem. Soc. Faraday Trans.* **1982**, *78*, 3417.
(B) Kaner, R. B.; MacDiarmid, A. G. *J. Chem. Soc. Faraday Trans.* **1984**, *80*, 2019.
(C) Shacklette, L. W.; Elsenbaumer, R. L.; Chance, R. R.; Sowa, J. M.; Ivory, D. M.; Miller, G. G.; Baughman, R. H. *J. Chem. Soc. Chem. Commun.* **1982**, *361*.
(D) Kaneto, K.; Yoshno, K.; *Kino Zairyo* **1984**, *4*, 8.
(E) Novak, P.; Vielstich, W. *J. Electrochem. Soc.* **1990**, *137*, 1681.
(F) MacDiarmid, A. G.; Mu, S.-L.; Somasiri, N. L. D.; Wu, W. *Mol. Cryst. Liq. Cryst.* **1985**, *121*, 187.
(G) Echigo, Y.; Asami, K.; Takahashi, H.; Inoue, K. *Synth. Met.* **1993**, *55-57*, 3611.
(H) Genies, E.; Hany, P.; Santier, Ch. *Synth. Met.* **1989**, *28*, C647.
(I) Mammone, R. J.; Binder, M. *J. Electrochem. Soc.* **1988**, *135*, 1057.

107. (A) Zinger, B.; Miller, L. L. *J. Am. Chem. Soc.* **1984**, *106*, 6861.
(B) Blankespoor, R.; Miller, L. L. *J. Chem. Soc., Chem. Commun.* **1985**, 90.
(C) Zhou, Q.-X.; Miller, L. L.; Valentine, J. R. *J. Electroanal. Chem.* **1989**, *261*, 147.

(D) Hepel, M.; Fijalek, Z.; Dentrone, L. *Polymer Preprints* **1992**, *33*, 106.

108.(A) Slater, J. M.; Paynter, J.; Watt, E. J. *Analyst* **1993**, *118*, 379.
(B) Pearce, T. C.; Gardner, J. W.; Friel, S.; Bartlett, P. N.; Blair, N. *Analyst*, **1993**, *118*, 371.
(C) Nishizawa, M.; Matsue, T.; Uchida, I. *Anal. Chem.* **1992**, *64*, 2642.
(D) Shinohara, H.; Khan, G. F.; Ikariyama, Y.; Aizawa, M. *J. Electroanal. Chem.* **1991**, *304*, 75.
(E) Genies, E. M.; Marchesiello, M. *Synth. Met.* **1993**, *57*, 3677.
(F) Shaolin, M.; Huaiguo, X.; Bidong, Q. *J. Electroanal. Chem.* **1991**, *304*, 7.
(G) Hoa, D. T.; Suresh Kumar, T. N.; Punekar, N. S.; Srinivasa, R. S.; Lal, R.; Contractor, A. Q. *Anal. Chem.* **1992**, *64*, 2645.

109 Kondo, K.; Suwa, M.; Ozaki, A.; Takemoto, K. *J. Electroanal. Chem.* **1992**, *333*, 143.

110 Thackeray, J. W.; White, H. S.; Wrighton, M. S. *J. Phys. Chem.* **1985**, *89*, 5133.

111.Li, S.; Macosko, C. W.; White, H. S. *Science* **1993**, *259*, 957.

112.(A) Burroughes, J. H.; Bradley, D. D. C.; Brown, A. R.; Marks, R. N.; Mackay, K.; Friend, R. H.; Burns, P. L.; Holmes, A. B. *Nature*, **1990**, *347*, 539.
(B) Burn, P. L.; Holmes, A. B.; Kraft, A.; Bradley, D. D. C.; Brown, A. R.; Friend, R. H.; Gymer, R. W. *Nature* **1992**, *356*, 47.
(C) Gustafsson, G.; Cao, Y.; Treacy, G. M.; Klavetter, F.; Colaneri, N.; Heeger, A. J. *Nature* **1992**, *357*, 477.

113.(A) Bloor, D. *Nature* **1991**, *349*, 738.
(B) White, H. S.; Kittlesen, G. P.; Wrighton, M. S. *J. Am. Chem. Soc.* **1984**, *106*, 5375.
(C) Kittlesen, G. P.; White, H. S.; Wrighton, M. S. *J. Am. Chem. Soc.* **1984**, *106*, 7389.

114.(A) Otero, T. F.; Angulo, E.; Rodriguez, J.; Santamaria, C. *J. Electroanal. Chem.* **1992**, *341*, 369.
(B) Pei, Q.; Inganas, O. *J. Phys. Chem.* **1992**, *96*, 10507.
(C) Otero, T. F.; Rodriguez, Z.; Angulo, E.; Santamaria, C. *Synth. Met.* **1993**, *57*, 3713.

115.(A) Jozefowicz, M.; Yu, L. T.; Perichon, J.; Buvet, R. *J. Polym. Sci.* **1969**, *C22*, 1187.
(B) MacDiarmid, A. G.; Chiang, J.-C.; Huang, W. S.; Humphrey, B. D.; Somasiri, N. L. D. *Mol. Cryst. Liq. Cryst.* **1985**, *125*, 309.
(C) Ochmanska, J.; Pickup, P. G. *J. Electroanal. Chem.* **1991**, *297*, 211.

116. Tatsuma, T.; Watanabe, T.; Watanabe, T. *J. Electroanal. Chem.* **1993**, *356*, 245.

117. (A) Diaz, A. F.; Castillo, J. I.; Logan, J. A.; Lee, W.-Y.; *J. Electroanal. Chem.* **1981**, *129*, 115.
(B) Street, G. B.; Clarke, T. C.; Krounbi, M.; Kanazawa, K.; Lee, V.; Pfluger, P.; Scott, J. C.; Weiser, G. *Mol. Cryst. Liq. Cryst.* **1982**, *83*, 1285.

118. Abruna, H. D. *Coord. Chem. Rev.* **1988**, *86*, 135.

119. Patil, A. O.; Heeger, A. J.; Wudl, F. *Chem. Rev.* **1985**, *88*, 183.

120. Li, Y.; Qian, R. *Synth. Met.* **1993**, *53*, 149.

121. Chien, J. C. W.; Schlenoff, J. B. *Nature* **1984**, *311*, 362.

122. Park, D.; Shim, Y.; Park, S. *J. Electrochem. Soc.* **1993**, *140*, 609.

123. (A) Iseki, M.; Saito, K.; Kuhara, K.; Mizukami, A. *Synth. Met.* **1991**, *40*, 117.
(B) Iseki, M.; Saito, K.; Ikematsu, M.; Sugiyama, Y.; Kuhara, K.; Mizukami, A. *J. Electroanal. Chem.* **1993**, *358*, 221.

124. Ren, X.; Pickup, P. G. *J. Phys. Chem.* **1993**, *97*, 5356.

125. (A) Lehninger, A. L. *Principles of Biochemistry*, Worth Publishers Inc., New York, **1982**.
(B) Hoppe, W.; Lohmann, W.; Markl, H.; Ziegler, H. *Biophysics*, Springer-Verlag, Berlin, **1982**, p. 352.

126. Boyle, A.; Genies, E.; Fouletier, M. *J. Electroanal. Chem.* **1990**, *279*, 179.

127. Li, Y.; Dong, S. *J. Chem. Soc. Chem. Commun.* **1992**, 827.

128. Jorgenson, J. W.; Lukacs, K. D. *Anal. Chem.* **1981**, *53*, 1298.

129. Windholz, M. (ed.) *The Merk Index*, Merk & Co., Inc., Rahway, **1983**.

130. (A) Abruna, H. D.; Denisevich, P.; Umana, M.; Meyer, T. J.; Murray, R. W. *J. Am. Chem. Soc.* **1981**, *103*, 1.
(B) Denisevich, P.; Willman, K. W.; Murray, R. W. *J. Am. Chem. Soc.* **1981**, *103*, 4727.
(C) Willman, K. W.; Murray, R. W. *J. Electroanal. Chem.* **1982**, *133*, 211.
(D) Pickup, P. G.; Murray, R. W. *J. Am. Chem. Soc.* **1983**, *105*, 4511.
(E) Pickup, P. G.; Leidner, C. R.; Denisevich, P.; Murray, R. W. *J. Electroanal. Chem.* **1984**, *164*, 39.
(F) Leidner, C. R.; Denisevich, P.; Willman, K. W.; Murray, R. W.

J. Electroanal. Chem. **1984**, *164*, 63.
(G) Leidner, C. R.; Murray, R. W. *J. Am. Chem. Soc.* **1985**, *107*, 551.

131.(A) Murao, K.; Suzuki, K. *J. Chem. Soc. Chem. Commun.* **1984**, 238.
(B) Murao, K.; Suzuki, K. *Chem. Lett.* **1986**, 2101.

132.(A) Hillman, A. R.; Mallen, E. F. *J. Electroanal. Chem.* **1990**, *281*, 109.
(B) Torres, W.; Fox, M. A. *Chem. Mater.* **1990**, *2*, 306.

133.Downard, A. J.; Surridge, N. A.; Meyer, T. J.; Cosnier, S.; Deronzier, A.; Moutet, J.-C. *J. Electroanal. Chem.* **1988**, *246*, 321.

134.de Tacconi, N. R.; Son, Y.; Rajeshwar, K. *J. Phys. Chem.* **1993**, *97*, 1042.

135.Aizawa, M.; Shinohara, H.; Yamada, T.; Akagi, K.; Shirakawa, H. *Synth. Met.* **1987**, *18*, 711.

136.Rubinstein, I.; Rubinstein, I. *J. Phys. Chem.* **1987**, *91*, 235.

137.Shimidzu, T.; Iyoda, T.; Toyoda, H.; Fujitsuka, M.; Nakahara, R. *Synth. Met.* **1993**, *55-57*, 1335.

138.Porat, Z.; Tricot, Y.-M.; Rubinstein, I.; Zinger, B. *J. Electroanal. Chem.* **1991**, *315*, 217.

139.Prezyna, L. A.; Qiu, Y.-J.; Reynolds, J. R.; Wnek, G. E. *Macromolecules* **1991**, *24*, 5283.

BIOGRAPHICAL SKETCH

Myoungho Pyo was born on December 10, 1958 in Seoul, Korea. In the spring of 1978 he began his undergraduate education in chemistry at Seoul National University. In 1982 he began research under the supervision of Wanchul Shin. In 1984, he obtained his M.S. degree in chemistry.

Before entering the Ph.D. program at the University of Florida, he was enrolled at The University of Texas at Arlington for 2.5 years under the supervision of Professor John R. Reynolds. In the spring of 1992 he changed Ph.D. programs and transferred to the University of Florida. Mr. Pyo completed his Ph.D. in physical chemistry at the University of Florida in 1994 and will begin a postdoctoral fellowship at The University of Texas at Austin.

I certify that I have read this study and that in my opinion it conforms to acceptable standards of scholarly presentation and is fully adequate, in scope and quality, as a dissertation for the degree of Doctor of Philosophy.

John R. Reynolds, Chair
Associate Professor of Chemistry

I certify that I have read this study and that in my opinion it conforms to acceptable standards of scholarly presentation and is fully adequate, in scope and quality, as a dissertation for the degree of Doctor of Philosophy.

William Weltner, Jr.
Professor of Chemistry

I certify that I have read this study and that in my opinion it conforms to acceptable standards of scholarly presentation and is fully adequate, in scope and quality, as a dissertation for the degree of Doctor of Philosophy.

Philip J. Brucat
Associate Professor of Chemistry

I certify that I have read this study and that in my opinion it conforms to acceptable standards of scholarly presentation and is fully adequate, in scope and quality, as a dissertation for the degree of Doctor of Philosophy.

Randolph S. Duran
Assistant Professor of Chemistry

I certify that I have read this study and that in my opinion it conforms to acceptable standards of scholarly presentation and is fully adequate, in scope and quality, as a dissertation for the degree of Doctor of Philosophy.

Paul W. Chun
Professor of Biochemistry and
Molecular Biology

This dissertation was submitted to the Graduate Faculty of the Department of Chemistry in the College of Liberal Arts and Sciences and to the Graduate School and was accepted as partial fulfillment of the requirements for the degree of Doctor of Philosophy.

April 1994

_____

Dean, Graduate School